

# **For Reference**

---


**NOT TO BE TAKEN FROM THIS ROOM**



Ex LIBRIS  
UNIVERSITATIS  
ALBERTAENSIS







Digitized by the Internet Archive  
in 2022 with funding from  
University of Alberta Library

<https://archive.org/details/Eze1978>









THE UNIVERSITY OF ALBERTA

THE RELATIONSHIP BETWEEN MEMBRANE LIPID FLUIDITY AND  
PHASE STATE AND PASSIVE PERMEATION, FACILITATED DIFFUSION  
AND ACTIVE TRANSPORT PROCESSES IN ESCHERICHIA COLI

by



MICHAEL OKECHUKWU EZE

A THESIS

SUBMITTED TO THE FACULTY OF GRADUATE STUDIES AND RESEARCH  
IN PARTIAL FULFILMENT OF THE REQUIREMENTS FOR THE DEGREE  
OF DOCTOR OF PHILOSOPHY

DEPARTMENT OF BIOCHEMISTRY

EDMONTON, ALBERTA

SPRING, 1978





To my mother, Nwaku

and to my father, Ogbuefi Ezennia Nnaemeka Ezedinachi





## ABSTRACT

The role of membrane lipid fluidity and phase state on the passive permeation and facilitated diffusion of glycerol as well as on the active transport of L-glutamine and L-proline in E. coli has been investigated. Membrane lipid fatty acid composition was varied by the enrichment of the membranes of the unsaturated fatty acid (UFA) auxotroph, E. coli K1060, in one of five UFA's, linoleate (18:2c,c), palmitoleate (16:1c), oleate (18:1c), palmitelaidate (16:1t) and elaidate (18:1t). The dependence on temperature of these transport processes was studied in these cells as well as in a number of other strains which are prototrophic with respect to fatty acid metabolism. Differential thermal analysis (DTA) revealed that the relative fluidities of the membranes of the mutant K1060 decreased in the order: 18:2c,c- > 16:1c- > 18:1c- > 16:1t- > 18:1t-cells.

The rate constant ( $1/\tau$ ) for glycerol passive permeation at any temperature was highest for cells with the most fluid membranes and lowest for the least fluid. Arrhenius treatment of the data yielded straight lines for the permeation in 18:2c,c- and 16:1c-cells and biphasic linear plots for 18:1c- and 18:1t-cells. The point of intersection in each of the latter two instances was the characteristic temperature,  $T_b$ . The activation energy,  $E_a$ , for the permeation in 18:2c,c- and 16:1c-cells did not depend on UFA supplementation and was the same as that above  $T_b$  for 18:1c- and 18:1t-cells. However,  $E_a$  below  $T_b$  was higher than above it.

The  $1/\tau$  values for the facilitated diffusion of glycerol in these cells displayed a parallel behavior to the  $1/\tau$  values for the passive





permeation of this solute, being highest for the most fluid and lowest for the least fluid membranes. The  $1/\tau$  value for the facilitated diffusion was, however, higher than that for the passive permeation at any given UFA supplement and constant temperature. Arrhenius plots of the facilitated diffusion  $1/\tau$  values were single straight lines for 18:2c,c- and 16:1c-cells and biphasic for 18:1c- and 18:1t-cells. The  $E_a$  values for glycerol facilitated diffusion in 18:2c,c- and 16:1c-cells, and above  $T_b$  for 18:1c- and 18:2t-cells was constant but lower than that for the passive permeation. Below  $T_b$ , the  $E_a$  value was higher than above it. The  $T_b$  value for 18:1t-cells was constant for the facilitated diffusion and the passive permeation of glycerol while that for 18:1c-cells was lower for the facilitated diffusion than for the passive permeation of this solute. These results taken together demonstrate a profound influence of the membrane lipid fluidity and physical state on the translocation step of the passive permeation and the mediated transport of glycerol.

The  $K_m$  for  $^{14}\text{C}$ -glutamine uptake in E. coli K1060 and strain 7 remained constant, irrespective of UFA-enrichment and temperature.  $V_{\max}$  values varied with temperature for mutant K1060, only up to an upper temperature limit (UTL) above which  $V_{\max}$  started to decrease with increase in temperature. For strain 7, there was no UTL and at all temperatures, the Arrhenius plot was biphasic, displaying a  $T_b$ . For K1060, the Arrhenius plot below UTL was also biphasic, showing a  $T_b$  unique to each UFA supplement (except 18:2c,c-cells which gave a gentle curve). The  $E_a$  values were higher below  $T_b$  than above it.

The  $K_m$  for  $^{14}\text{C}$ -proline transport in mutant K1060 grown in various UFA supplements was reasonably constant as temperature varied, while





this kinetic parameter increased ten-fold in strain 7 as the temperature increased from 3°C to 45°C. No UTL was displayed for proline uptake in strain 7 and the Arrhenius plot showed a  $T_b$  as well as another break temperature at 30°C. A UTL was displayed for proline transport in K1060 and the Arrhenius plots below UTL were again biphasic (except for 18:2c,c-cells) and showed a characteristic  $T_b$  for each UFA supplement. In all instances (strain 7 and K1060)  $T_b$  was lower for proline than for glutamine uptake while for K1060, UTL was lower for proline than for glutamine uptake.

DTA results together with membrane fatty acid profiles indicate that UTL is determined by both membrane lipid acyl chain fluidity and heterogeneity, while  $T_b$  is governed by fluidity alone. Since the major difference between the glutamine and proline transport systems is in their energetics of operation, these results indicate that the possible cause of the UTL is a deficiency in energy-coupling due, possibly, to proton leakage in these cells under the experimental conditions.

It is therefore concluded that while the translocation step in a purely facilitated diffusion system responds to the fluidity and physical state of the membrane lipids, both the translocation and the energy-coupling steps are influenced by the phase state of the membrane lipids in an active transport system.



## ACKNOWLEDGEMENTS

I would like to express my deep-felt appreciation to my supervisor, Professor Ronald N. McElhaney, for his excellent supervision, guidance, encouragement and general good-natured disposition all of which made the execution of this project both a pleasure and a success.

I am indebted to Professor Peter Barton and Professor William Bridger for their encouragement, direction and many useful discussions, and to Professor Joel Weiner for invaluable discussions and advice and for the generous gift of two E. coli strains. The kind gifts of E. coli strains from Professor David Silbert and Professor William Paranchych are hereby gratefully acknowledged.

My sincere thanks are also due to Mr. John Silvius, Ms. Nanette Mak, Dr. Brian Read, Dr. Yuji Saito and Dr. David Jinks for having created an atmosphere conducive to productive work and for many stimulating discussions during the course of this investigation, to Mr. Mbanefo Ekwenchi, Dr. E. James Findlay and Dr. John Baldo for helpful suggestions, and to Ms. Nanette Mak, Mr. David Evans and Mr. Steve Cook for invaluable assistance with many of the experiments.

I do highly appreciate the contribution of Professor Neil Madsen and many other members of this department who allowed me free access to their high-priced equipment and other laboratory facilities as well as that of those who let me share their ideas and expertise.

I am grateful to Professor Agu U. Ogan for kindling my interest in biological membrane transport and to Professor Charles O. Okafor for continued interest and encouragement during the course of this study.

I should pay tribute to the entire members of this department for





having presented me with a congenial atmosphere that has contributed a great deal towards making my stay here a very worthwhile experience.

May I also thank Mr. Perry D'Obrenan and Ms. Elke Lohmeier who drew most of the figures, Mr. Roger Bradley and Mr. Ted Shehinski who did some of the photographic work and Ms. Jaclyn Dorsey for an excellent job of typing this thesis.

I am grateful to the University of Alberta for providing a graduate teaching assistantship that made this work possible.





## TABLE OF CONTENTS

	<u>Page</u>
ABSTRACT . . . . .	v
ACKNOWLEDGEMENTS . . . . .	.viii
LIST OF TABLES . . . . .	vx
LIST OF FIGURES . . . . .	.xvii
LIST OF PLATES . . . . .	xx
ABBREVIATIONS AND SYMBOLS . . . . .	xxi
 CHAPTER I: GENERAL INTRODUCTION . . . . .	 1
A. Biological Membrane Structure and Dynamics (A Review) . . .	1
1. The Fluid Mosaic Model . . . . .	1
2. Support for the Model . . . . .	4
B. The bacterial Cell Envelope and Periplasmic Space (A Review) . . . . .	13
1. Introduction . . . . .	13
2. Molecular Architecture of the Cell Wall of Bacteria . .	14
3. Implications of the Possession of a Cell Wall . . . . .	18
C. Solute Transport and Permeation Across Biomembranes (A Review) . . . . .	20
1. Introduction . . . . .	20
2. Passive Permeation . . . . .	21
3. Mediated Transport . . . . .	22
4. Energy-Dependent Transport . . . . .	25
D. Background Material Relevant to this Study . . . . .	26
1. Consequences of the Lipid Bilayer to Membrane-Bound Reactions . . . . .	26
2. Postulated Mechanisms of Mediated Membrane Transport . .	30
3. The Third Model of Transport Mechanism . . . . .	32



	<u>Page</u>
E. Objectives of this Project . . . . .	33
CHAPTER II: GENERAL MATERIALS AND METHODS . . . . .	36
A. Media and Chemicals . . . . .	36
1. Non-Radioactive Supplies . . . . .	36
2. Radioactive Supplies . . . . .	36
3. Other Chemicals . . . . .	37
B. Bacterial Strains and Growth Conditions . . . . .	37
C. Spheroplast Formation . . . . .	39
D. Inner Membrane Isolation . . . . .	40
E. Lipid Extraction and Purification . . . . .	40
F. Fatty Acid Analysis . . . . .	41
G. Protein Assay . . . . .	42
H. Paper Chromatography and Radiochromatography . . . . .	42
I. Liquid Scintillation Cocktail (Toluene-Based) . . . . .	43
J. Energy-Poisoning Methods Employed . . . . .	43
1. Method A . . . . .	43
2. Method B . . . . .	44
CHAPTER III: GLYCEROL UPTAKE IN <u>E. COLI</u> : PASSIVE PERMEATION AND FACILITATED DIFFUSION . . . . .	45
A. Introduction . . . . .	45
B. Methods . . . . .	47
1. Cell Growth and UFA Incorporation . . . . .	47
2. Preparation of Cells for Swelling Rate Assays . . . . .	47
3. Permeant Solutions . . . . .	49
4. Refractive Index Correction in Solutions . . . . .	49





	<u>Page</u>
5. Swelling Assays . . . . .	53
6. Calculation of $1/\tau \text{ sec}^{-1}$ . . . . .	54
7. Enzyme Assays . . . . .	57
8. Preparation of Mixed Inner and Outer Membranes for G3PDH Assay . . . . .	57
9. Swelling of Spheroplasts . . . . .	57
10. Differential Thermal Analysis . . . . .	58
C. Results . . . . .	61
1. Relationship between Cell Volume and Reciprocal Absorbance . . . . .	61
2. Typical Oscilloscope Trace and Calculation of $1/\tau$ . . .	62
3. Data Treated to Yield First Order Rate Constant $k \text{ sec}^{-1}$ . . . . .	62
4. The Time-Dependence of the Osmotic Response . . . . .	75
5. DTA Results . . . . .	75
6. Temperature-Dependence of Glycerol Uptake . . . . .	80
D. Discussion . . . . .	96

CHAPTER IV: ACTIVE AMINO ACID TRANSPORT IN ESCHERICHIA COLI:  
L-GLUTAMINE TRANSPORT . . . . .

A. Introduction . . . . .	102
B. Methods . . . . .	104
1. Bacterial Strains and Growth Conditions . . . . .	104
2. Preparation of Cells and $^{14}\text{C}$ -Glutamine Uptake Assays . .	104
(a) Procedure A . . . . .	104
(b) Procedure B . . . . .	105
3. Liquid Scintillation Counting . . . . .	106
C. Results . . . . .	107
1. Time Course of $^{14}\text{C}$ -Glutamine Uptake . . . . .	107



	<u>Page</u>
2. Concentration Range of L-Glutamine Employed . . . . .	107
3. Treatment of Data for $K_m$ and $V_{max}$ . . . . .	110
4. Temperature-Dependence of $K_m$ and $V_{max}$ for $^{14}C$ - Glutamine Uptake . . . . .	110
D. Discussion . . . . .	132
CHAPTER V: ACTIVE AMINO ACID TRANSPORT IN <u>ESCHERICHIA COLI</u> :	
L-PROLINE TRANSPORT AND GENERAL CONCLUSIONS . . . . .	138
L-PROLINE TRANSPORT . . . . .	138
A. Introduction . . . . .	138
B. Methods . . . . .	140
1. Bacterial Strains and Growth Conditions . . . . .	140
2. Preparation of Cells and $^{14}C$ -Proline Uptake Assays . . .	140
3. Liquid Scintillation Counting . . . . .	140
C. Results . . . . .	141
1. Time Course of $^{14}C$ -Proline Uptake . . . . .	141
2. Concentration Range of L-Proline Employed . . . . .	141
3. Treatment of Data for $V_{max}$ and $K_m$ . . . . .	149
4. Temperature-Dependence of $V_{max}$ and $K_m$ for L-Proline Uptake . . . . .	149
(i) Mutant K1060 . . . . .	149
(ii) Strain 7 . . . . .	161
D. Discussion . . . . .	161
GENERAL CONCLUSIONS . . . . .	178
SUGGESTIONS FOR FURTHER INVESTIGATIONS . . . . .	181
BIBLIOGRAPHY . . . . .	184
APPENDIX 1 <u>E. coli</u> Strains Employed in this Study . . . . .	201





	<u>Page</u>
APPENDIX 2A    Fatty Acid Profiles at Various Growth Phases of Mutant K1060 Cells Grown with 18:1c and Glycerol . . . . .	202
APPENDIX 2B    Fatty Acid Profiles at Various Growth Phases of Mutant K1060 Cells Grown with 18:1c and Glucose . . . . .	203
APPENDIX 2C    Fatty Acid Profiles at Various Growth Phases of Mutant K1060 Cells Grown with 18:1c and Xylose . . . . .	204
APPENDIX 2D    Fatty Acid Profiles at Various Growth Phases of Mutant K1060 Cells Grown with 18:1c and Succinate . . . . .	205
APPENDIX 3     Typical Fatty Acid Profiles of <u>E. coli</u> Strain 7 and Mutant K1060 Used for the Various Experiments . .	206
APPENDIX 4     Calculation of Initial Rate of Transport . . . . .	207
APPENDIX 5     Temperature Programs and Instrument Settings Used for GLC Analysis of Fatty Acid Methyl Esters . . . . .	209



# LIST OF TABLES

<u>Table</u>		<u>Page</u>
I	Membrane G3PDH Activity of <u>E. coli</u> K1060 and E15 Grown with Various Carbon and Energy Sources . . . . .	48
II	$1/\tau$ for Glycerol Passive Permeation in <u>E. coli</u> K12F <sup>-</sup> and K1060 Determined in Glycerol Solutions Either Adjusted or Not Adjusted to the Same Refractive Index with Ficoll-400 . . . . .	52
III	$1/\tau$ Values of Glycerol Passive Permeation at 25°C in <u>E. coli</u> K12F <sup>-</sup> Calculated on the Basis of $\Delta(1/A) \propto$ $\Delta\text{Volume}$ and also, for Comparison, First Order Rate Constants $k \text{ sec}^{-1}$ for the Same Process Calculated on the Basis of $\Delta A \propto \Delta\text{Volume}$ . . . . .	69
IV	Transition Ranges ( $T_l - T_h$ ) and Midpoints ( $T_m$ ) for Lipids from Whole Cells of <u>E. coli</u> K1060 and Strain 7 Grown with Various UFA Supplements . . . . .	81
V	Arrhenius Plot Break Temperatures and Activation Energies for Glycerol Permeation in <u>E. coli</u> K1060 . . . . .	94
VI	Arrhenius Plot Temperature Breaks ( $T_b$ ), Activation Energies ( $E_a$ ) and Temperatures at which $V_{\max}$ Starts to Decrease with Temperature (UTL) for L-Glutamine Transport in Relation to Membrane UFA-Enrichment (mole %) and Phase Transition Midpoint ( $T_m$ ) in <u>E. coli</u> Strain 7 and Strain K1060 . . . . .	134
VII	Mean $K_m$ Values Over the Assay Temperature Ranges for 14C-Proline Uptake in <u>E. coli</u> K1060 Grown with Different UFA Supplements . . . . .	144
VIII	Dependence of $K_m$ and $V_{\max}$ for the Transport of L- Glutamine (L-Gln) and L-Proline (L-Pro) in <u>E. coli</u> Strain 7 on Assay Temperature . . . . .	150
IX	Arrhenius Plot Temperature Breaks ( $T_b$ ), Activation Energies ( $E_a$ ) and Temperatures at which $V_{\max}$ Starts to Decrease with Temperature (UTL) for L-Proline Transport in Relation to Membrane UFA-Enrichment (mole %) and Phase Transition Midpoint ( $T_m$ ) in <u>E. coli</u> K1060 and Strain 7 . . . . .	160
X	Activation Energies ( $E_a$ ) for L-Glutamine (L-Gln) and L-Proline (L-Pro) Transport in <u>E. coli</u> Strain 7 and <u>E. coli</u> K1060 . . . . .	169





<u>Table</u>	<u>Page</u>
XI	Arrhenius Plot Temperature Breaks ( $T_b$ ) and Temperatures at which $V_{max}$ Starts to Decrease with Temperature (UTL) for L-Glutamine (Gln) and L-Proline (Pro) Transport in <u>E. coli</u> Strain 7 and <u>E. coli</u> K1060 . . . . . 170
XII	Arrhenius Plot Break Temperatures ( $T_b$ ) for L-Proline Uptake $V_{max}$ Values in <u>E. coli</u> K1060 Compared with the Same Parameter for L-Proline "Initial Rate" of Uptake in Other <u>E. coli</u> UFA Auxotrophs Reported in References 71 and 76 . . . . . 176
XIII	Activation Energies ( $E_a$ ) Below and Above $T_b$ for L-Proline Uptake $V_{max}$ in K1060 Compared with the Same Parameter for L-Proline "Initial Rate" of Uptake Reported in Reference 76 for Another <u>E. coli</u> UFA Auxotroph . . . . . 177



# LIST OF FIGURES

<u>Figure</u>		<u>Page</u>
1	Refractive index correction curves . . . . .	51
2	Double reciprocal plot showing the relationship between cell volume ( $1/A_{650}$ ) and reciprocal tonicity using Ficoll correction for n . . . . .	56
3A - C	Relationship between millimolar and milliosmolal concentrations of aqueous solutions of glycerol and sucrose . . . . .	60
4	Typical oscilloscope trace . . . . .	64
5	Typical calculation of $1/\tau \text{ sec}^{-1}$ . . . . .	66
6	Data treated to yield first order rate constant $k \text{ sec}^{-1}$ for passive glycerol permeation in <u>E. coli</u> K12F <sup>-</sup> . . . . .	68
7A	Dependence of initial swelling rates of <u>E. coli</u> K1060 on glycerol concentration, as measured by conventional spectrophotometry . . . . .	72
7B & C	Dependence of initial swelling rates of <u>E. coli</u> K1060 on glycerol or erythritol concentration, as measured by conventional spectrophotometry . . . . .	74
8A	Differential thermal analysis of lipids from whole cells of <u>E. coli</u> K1060 grown with 16:1t- and 18:1c-supplements, as well as lipids from inner membranes of 16:1t-grown K1060 . . . . .	77
8B	Differential thermal analysis of lipids from whole cells of strain K1060 grown in 16:1c and 18:2c,c and of lipids from strain 7 . . . . .	79
9	The influence of temperature on the $1/\tau$ values for glycerol passive permeation and facilitated diffusion in <u>E. coli</u> K1060 grown with various UFA's . . . . .	83
10A	Arrhenius plots of $1/\tau$ for glycerol passive permeation (top panel) and facilitated diffusion (lower panel) in <u>E. coli</u> K1060 cells enriched in 18:1c . . . . .	86
10B	Arrhenius plots of $1/\tau$ for glycerol passive permeation (top panel) and facilitated diffusion (lower panel) in <u>E. coli</u> K1060 cells enriched in 18:1t . . . . .	88
10C	Arrhenius plots of $1/\tau$ for glycerol passive permeation (top panel) and facilitated diffusion (lower panel) in <u>E. coli</u> K1060 cells enriched in 18:2c,c . . . . .	90





<u>Figure</u>		<u>Page</u>
10D	Arrhenius plots of $1/\tau$ for glycerol passive permeation (top panel) and facilitated diffusion (lower panel) in <u>E. coli</u> K1060 cells enriched in 16:1c . . . . .	92
11	Time course of L-glutamine uptake in <u>E. coli</u> strain 7 at 14.2°C . . . . .	109
12	Lineweaver-Burk plot of the variation of initial rates of $^{14}\text{C}$ -glutamine uptake with glutamine concentration in <u>E. coli</u> strain 7 at 21°C . . . . .	112
13A	Hanes' treatment of data for the calculation of $K_m$ and $V_{\max}$ values for $^{14}\text{C}$ -glutamine uptake at various temperatures in 16:1c-enriched K1060 cells . . . . .	114
13B	Hanes' treatment of data for the calculation of $K_m$ and $V_{\max}$ values for $^{14}\text{C}$ -glutamine uptake at various temperatures in 18:2c,c-enriched K1060 cells . . . . .	116
13C	Hanes' treatment of data for the calculation of $K_m$ and $V_{\max}$ values for $^{14}\text{C}$ -glutamine uptake at various temperatures in 18:1c-enriched K1060 cells . . . . .	118
14A	Arrhenius plot of $V_{\max}$ values for L-glutamine uptake in <u>E. coli</u> strain 7 . . . . .	121
14B	Arrhenius plot of $V_{\max}$ values for L-glutamine uptake in <u>E. coli</u> K1060 enriched in 18:1t . . . . .	123
14C	Arrhenius plot of $V_{\max}$ values for L-glutamine uptake in <u>E. coli</u> K1060 enriched in 16:1t . . . . .	125
14D	Arrhenius plot of $V_{\max}$ values for L-glutamine uptake in <u>E. coli</u> K1060 enriched in 18:1c . . . . .	127
14E	Arrhenius plot of $V_{\max}$ values for L-glutamine uptake in <u>E. coli</u> K1060 enriched in 16:1c . . . . .	129
14F	Arrhenius plot of $V_{\max}$ values for L-glutamine uptake in <u>E. coli</u> K1060 enriched in 18:2c,c . . . . .	131
15	Lineweaver-Burk plot of the variation of initial rates of $^{14}\text{C}$ -proline uptake with L-proline concentration in <u>E. coli</u> K1060 enriched in 16:1t . . . . .	143
16A	Hanes' treatment of data for the calculation of $K_m$ and $V_{\max}$ values for $^{14}\text{C}$ -proline uptake at various temperatures in 18:1c-enriched K1060 cells . . . . .	146
16B	Hanes' treatment of data for the calculation of $K_m$ and $V_{\max}$ values for $^{14}\text{C}$ -proline uptake at various temperatures in 16:1c-enriched K1060 cells . . . . .	148



<u>Figure</u>		<u>Page</u>
17A	Arrhenius plot of $V_{\max}$ values for L-proline uptake in <u>E. coli</u> K1060 enriched in 16:1t . . . . .	153
17B	Arrhenius plot of $V_{\max}$ values for L-proline uptake in <u>E. coli</u> K1060 enriched in 16:1c . . . . .	155
17C	Arrhenius plot of $V_{\max}$ values for L-proline uptake in <u>E. coli</u> K1060 enriched in 18:1c . . . . .	157
17D	Arrhenius plot of $V_{\max}$ values for L-proline uptake in <u>E. coli</u> K1060 enriched in 18:2c,c . . . . .	159
18	Arrhenius plot of $V_{\max}$ values for L-proline uptake in <u>E. coli</u> strain 7 . . . . .	163
19	Van't Hoff plot of $K_m$ values for L-proline uptake in <u>E. coli</u> strain 7 . . . . .	165





# LIST OF PLATES

<u>Plate</u>		<u>Page</u>
1	The Fluid Mosaic Model of Biological Membrane Structure (taken from ref. 1) . . . . .	2
2	A Schematic Representation of the Gel to Liquid Crystalline Lipid Phase Transition (modified from ref. 30) . . . . .	6
3	Structure of Gram-Positive Cell Wall (taken from ref. 134 . . . . .	15
4	Structure of Gram-Negative Cell Wall (taken from ref. 134 . . . . .	17



## ABBREVIATIONS AND SYMBOLS

### ABBREVIATIONS

A	absorbance (optical density)
<u>A. laidlawii</u>	<u>Acholeplasma laidlawii</u>
ATP	adenosine-5'-triphosphate
B <sub>1</sub>	(same as <u>thi</u> ) gene symbol for vitamin B <sub>1</sub> (thiamine) synthesis
C°	centigrade degrees
°C	degrees centigrade
CE	counting efficiency
cm	centimeter
cpm	counts per minute
DH	dehydrogenase
DSC	differential scanning calorimetry
DTA	differential thermal analysis
Ea	activation energy
<u>E. coli</u>	<u>Escherichia coli</u>
EDTA	ethylenediaminetetraacetate
EM	electron microscopy
ESR	electron spin resonance
<u>et al.</u>	<u>et alii</u> (and others)
F	gene symbol for F-pilus
<u>fab</u>	gene symbol for fatty acid biosynthesis (ref. 319)
<u>fabB</u>	gene symbol for $\beta$ -ketoacyl acyl carrier protein synthetase (ref. 319)
<u>fad</u>	gene symbol for fatty acid degradation (same as <u>old</u> ) (ref. 319)



<u>fadE</u>	gene symbol (possibly electron transport flavoprotein for acyl-coenzyme A dehydrogenase; see also <u>old E</u> )
g	grams or gravitational acceleration
GLC	gas-liquid chromatography
Glp	denoting <u>glp</u> gene phenotypic function
<u>glp</u>	gene symbol for the glycerophosphate regulon (ref. 317)
<u>glpA</u>	gene symbol for the anaerobic G3P dehydrogenase (ref. 317)
<u>glpD</u>	gene symbol for the aerobic G3P dehydrogenase (ref. 317)
<u>glpF</u>	gene symbol for the glycerol facilitator (ref 317)
<u>glpK</u>	gene symbol for the glycerol kinase (ref. 317)
<u>glpR</u>	gene symbol for the regulator (repressor) (ref. 317)
<u>glpT</u>	gene symbol for the G3P transport system (ref. 317)
G3P	glycerol-3-phosphate (L- $\alpha$ -glycerophosphate)
G3PDH	glycerol-3-phosphate dehydrogenase
G6P	D-glucose-6-phosphate
G6PDH	D-glucose-6-phosphate dehydrogenase
hr	hour
hsec	hecto-seconds (1 hsec = 100 sec)
k	first order rate constant
kg	kilogram
$K_m$	Michaelis constant
lac	gene symbol for the lactose operon
LSC	liquid scintillation counter
M	molar concentration (i.e., moles of solute per liter of solution)
mg	milligram
$\alpha$ MG	methyl- $\alpha$ -D-glucoside





min	minute
ml	milliliter
mm	millimeter
mM	millimolar
mosM	milliosmolar (i.e., milliosmoles of solute per liter of solution)
mV	millivolts
MTT	3(4,5-dimethylthiazolyl-1-2)2,5-diphenyltetrazolium bromide
n	refractive index
NADH	reduced nicotinamide adeninedinucleotide
NMR	nuclear magnetic resonance
<u>old</u>	gene symbol for oleate degradation (same as <u>fad</u> )
<u>old</u> E	gene symbol (possibly electron transport flavoprotein for acyl-coenzyme A dehydrogenase; see also <u>fad</u> E)
PBP	periplasmic binding protein
PEP	phosphoenolpyruvate
PC	phosphatidylcholine
<u>phoA</u>	symbol for structural gene for alkaline phosphatase
PTS	phosphotransferase system
SA	specific activity
SD	standard deviation
sec	second
T	temperature
$T_b$	Arrhenius plot break temperature
$T_c$	transition temperature
$T_h$	upper boundary of a phase transition range
<u>thi</u>	(same as $B_1$ ) gene symbol for vitamin $B_1$ (thiamine) synthesis



$T_1$	lower boundary of a phase transition range
$T_m$	transition midpoint
$T_{30}$	Arrhenius plot break at 30°C
Tris	tris(hydroxymethyl)aminomethane
UFA	unsaturated fatty acid
$\mu M$	micro-molar
$V_{max}$	maximum velocity
vol	volume

#### SYMBOLS

16:0	palmitate
16:1c	palmitoleate
16:1t	palmitelaidate
18:1c	oleate
18:1t	elaaidate
18:2c,c	linoleate
18:3c,c,c	linolenate
Cp17	<u>cis</u> -9,10-methylenehexadecanoate
Cp19	<u>cis</u> -9,10-methyleneoctadecanoate or <u>cis</u> -11,12-methyleneoctadecanoate
$\tau$	relaxation time
$1/\tau$	reciprocal relaxation time
$\Delta\psi$	membrane potential
$\Delta\bar{\mu}_{H^+}$	electrochemical gradient of protons



# CHAPTER I

## GENERAL INTRODUCTION

### A. BIOLOGICAL MEMBRANE STRUCTURE AND DYNAMICS (A REVIEW)

#### 1. The Fluid Mosaic Model

It now appears generally accepted that the biological membrane consists of a lipid bilayer matrix (fluid under physiological conditions) (1 - 5) in which are embedded largely globular protein molecules. This model (see plate 1), presented by Singer and Nicolson in 1972 as "the Fluid Mosaic Model of the Structure of Cell Membranes", views membranes as two-dimensional solutions of oriented globular proteins and lipids (1, see also 3, 4, 6, 7 for reviews). It serves as a useful conception to explain an enormous variety of physical, chemical and biological data on membrane structure (4) and was born as a synthesis of the earlier models presented by Gorter and Grendel, 1925 (8), Danielli and Davson, 1935 (9), Robertson, 1959 (10) and Benson, 1966 (11).

The formulation of this model was based on extensive theoretical thermodynamic considerations, coupled with the knowledge that the major constituents of biological membranes are lipids, proteins and oligosaccharides (12), together with available evidence on lipid and protein structure, organization and lateral mobility (1, 3, 4, 6, 7, 13 - 15). These thermodynamic principles, which have been extensively documented by Benson and Singer (16), Singer (12, 17), and Singer and Nicolson (1), deal with the noncovalent interactions that hold the membrane components together to yield the stable structure (12) in which are maximized the lowest free energy environments of the membrane lipids, proteins and saccharides (6, 12).





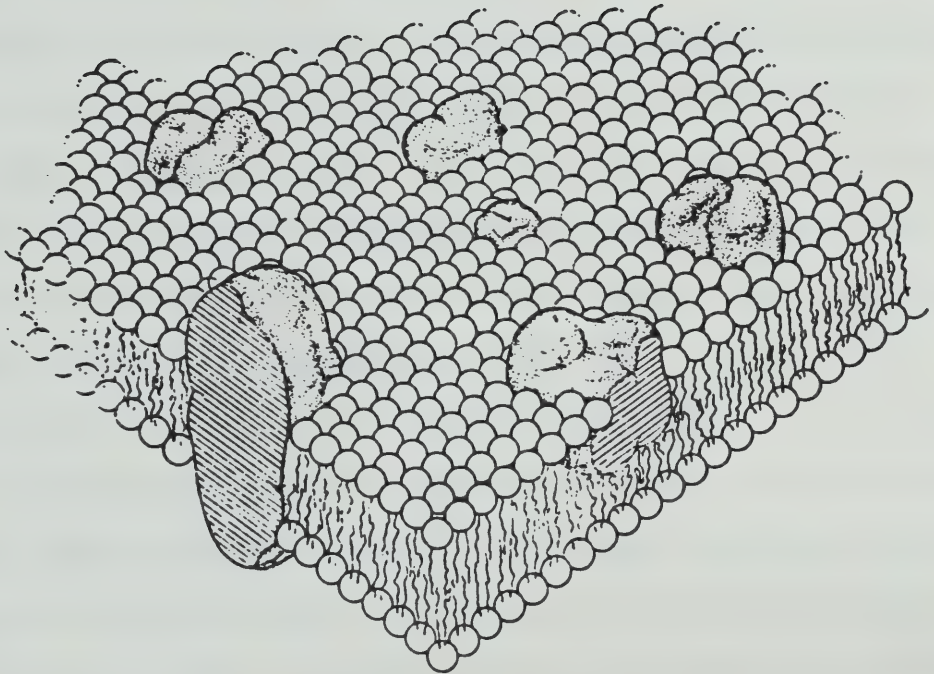


PLATE 1. The Fluid Mosaic Model of Biological Membrane Structure  
(ref. 1)



Some membrane proteins ["integral" (1, 12) or "intrinsic" (18) proteins] either are partially buried within or span the lipid bilayer, and require drastic conditions like detergents, chaotropic agents or organic solvents for solubilization (1, 12, 15). Other membrane proteins ["peripheral" (1, 12) or "extrinsic" (18) proteins] are loosely associated with the surface of the membrane mainly by electrostatic interactions with the polar head groups of the membrane phospholipids and/or exposed hydrophilic ends of specific integral or peripheral membrane proteins (15). This latter class of proteins, exemplified by cytochrome c of mitochondrial membranes and spectrin of erythrocyte ghosts (19), are easily solubilized from membranes by mild aqueous treatment, e.g., high ionic strength and chelating agents, and their removal normally does not destroy the integrity of the lipid bilayer (1, 6, 12, 15).

The structurally important membrane components are the phospholipids and integral membrane proteins. The integral proteins, like the phospholipids, are considered to be amphipathic in their interactions with water (1, 4, 6, 12). These proteins may, in particular instances, be attached to oligosaccharides to form glycoproteins or be interacting strongly with specific lipids to form lipoproteins. The phospholipid bilayer is arranged with the hydrocarbon chains being on the average perpendicular to the plane of the membrane and sequestered into the interior of the bilayer (region of least contact with water) and stabilized mainly by hydrophobic interactions, while their ionic and polar head groups (hydrophilic portions) interact with each other and with the aqueous phase (1, 3, 4, 6, 12, 15).

Some integral proteins span the entire bilayer and possess two hydrophilic ends, one exposed to the internal environment and the other



in contact with the external aqueous phase. The central hydrophobic portions of such proteins are stabilized by hydrophobic interaction with the fatty acyl chains of the phospholipids of the bilayer. These proteins are said to be trimodal. Other integral proteins have only one polar and one hydrophobic portion and are described as bimodal. These bimodal proteins can be only partially buried in the bilayer (1, 3, 4, 6, 15, 20). Evidence is now accumulating that integral proteins are in oligomeric associations within the membrane (21, 22).

## 2. Support for the Model

The bilayer configuration of membrane amphipathic lipids has been supported by a vast body of experimental evidence derived by the use of various physical techniques.

Phospholipid bilayers (liposomes or myelin forms consisting of concentric tubes of bimolecular leaflets) usually form spontaneously in excess water as the configuration of lowest free energy when amphipathic phospholipid molecules come in contact with water above their transition temperatures (3, 12, 23 - 27). The hydrocarbon chains tend to sequester into a region of least contact with water while the polar heads are in the aqueous phase. The width of the bilayer varies with the fatty acyl chains of the phospholipids, being small for short chain fatty acids and increasing with chain length (28).

The distinguishing characteristic which has been exploited in establishing the bilayer nature of membrane structure is the fact that some membranes (like the artificial bilayers, liposomes) exhibit reversible, cooperative, thermotropic gel  $\rightleftharpoons$  liquid crystalline phase transitions (14, 27, 29, 30). This order  $\rightleftharpoons$  disorder transition takes place at a definite temperature ( $T_c$ ) for any particular single phospholipid mole-





cular species (26, 31, 32). During the transition, the bilayer structure is essentially maintained (30). In the gel state, below  $T_c$ , the phospholipid hydrocarbon chains are fully extended (i.e. in the all-trans configuration), rigid, highly ordered and closely packed in a hexagonal array. The bilayer thickness is larger and the cross-sectional area per lipid molecule is small. There is also restricted lateral diffusion within the plane of the bilayer and permeability is low. In the liquid crystalline state, above  $T_c$ , the hydrocarbon chains possess a number of gauche conformers, are loosely packed, fluid and flexible. They are highly disordered in the two-dimensional lattice, this resulting in an overall decrease of bilayer thickness and an increase in cross-sectional area of each phospholipid molecule (see plate 2). Despite the fact that there is only a small net increase in volume per lipid molecule, a substantial lateral expansion in the plane of the membrane occurs (14, 26, 28, 31, 32). The fluid state ( $T > T_c$ ) permits rapid lateral diffusion in the plane of the membrane of the lipid molecules (14, 33 - 37) and other membrane components (3, 4, 6, 7, 12, 15, 36 - 41), and a marked increase in permeability (30). Since this transition is highly cooperative, a relatively large number of lipid molecules in a continuous phase is a prerequisite for its occurrence (14).

$T_c$  varies with the phospholipid head group (26) and for a particular class (head group) of phospholipids containing saturated fatty acyl chains,  $T_c$  also varies with phospholipid acyl chain length (26, 29, 30, 32, 42), being higher the longer the chain length. The enthalpy of transition also increases with chain length (42). Unsaturation or branching of the acyl chains decreases  $T_c$  (26, 29, 43). The presence



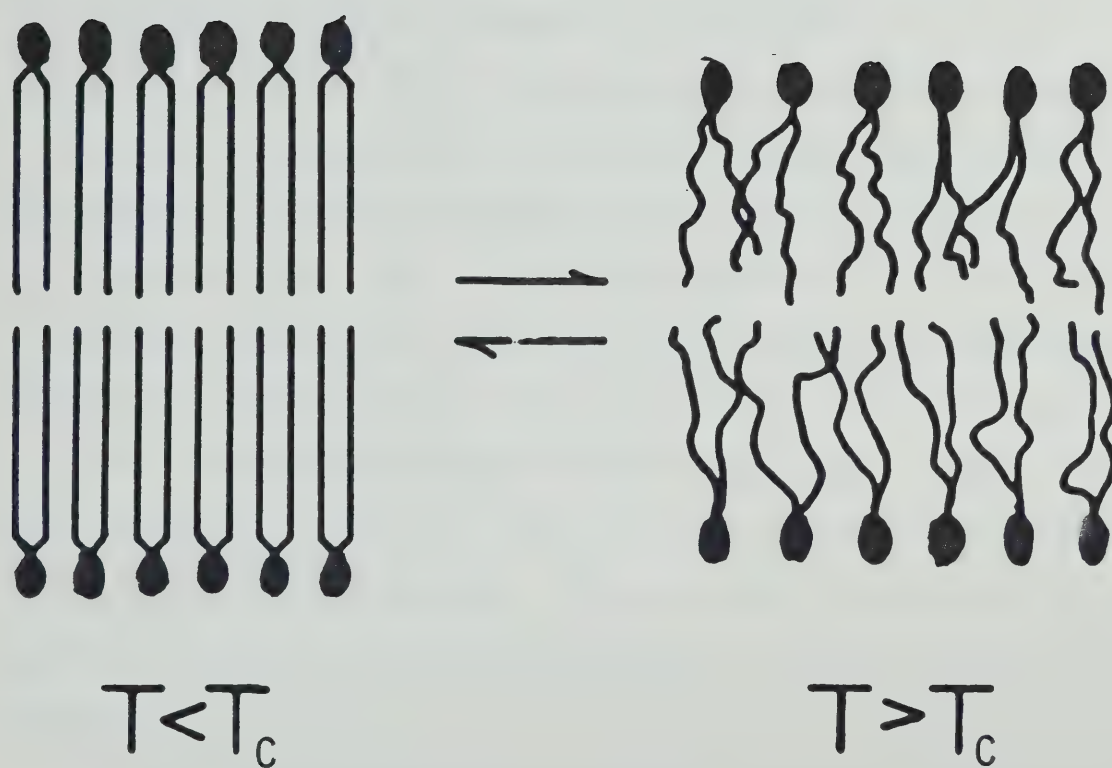


PLATE 2. A Schematic Representation of the Gel to Liquid Crystalline Lipid Phase Transition (ref. 30).



of other molecules like cholesterol or anesthetics affects the transition by altering the normal packing of the fatty acid chains (320). Cholesterol disrupts the ordered array of hydrocarbon chains in the gel state. Thus the thermotropic transition is broadened and its enthalpy decreased in the presence of cholesterol. This effect progressively increases as the cholesterol concentration increases and the transition is completely obliterated at 33 mole% cholesterol (26, 44 - 52).

Cholesterol also inhibits lipid chain motion above  $T_c$  (53). Thus, at a particular temperature, the presence of cholesterol keeps the hydrocarbon chains of differing phospholipid molecules in an "intermediate fluid" condition (48). The anesthetic methoxyfluorane has been shown to decrease the midpoint of transition ( $T_m$ ) as well as the temperatures marking the onset ( $T_l$ ) and end ( $T_h$ ) of the transition in mixed dipalmitoyl- and dimyristoylphosphatidyl choline bilayers (54). Protein (55) and peptides, e.g. gramicidin A (55, 56) and alamethicin (57), also remove the cooperative component of the transition (i.e. broaden it) without affecting  $T_m$  and, at high concentrations, eventually abolish the transition.

Data from various physical techniques (see for reviews 13, 27, 43, 58, 59) have established that biological membranes which are not rich in cholesterol do exhibit this gel  $\rightleftharpoons$  liquid crystalline cooperative, thermotropic phase transition. In this case, it is not a sharp transition because of heterogeneity in the polar head groups and fatty acyl chains of the membrane lipids. There is therefore a transition range marked by a lower boundary, i.e., the onset of the melt ( $T_l$ ), an upper boundary, i.e., the end of the melt ( $T_h$ ), and a transition midpoint ( $T_m$ ), at which 50% of the lipids are liquid crystalline in





coexistence with 50% gelled lipid. In the temperature range  $T_l$  to  $T_h$ , varying proportions of fluid and gel phase lipid coexist. The percent gel phase lipid is highest just above  $T_l$  and lowest just below  $T_h$ . Above  $T_h$  all the lipid is in the liquid crystalline phase as against the situation below  $T_l$  when 100% of the lipids are in the gel state. The broad phase transition is thus a progressive lateral phase separation in which domains of gel and liquid crystalline phases exist simultaneously (30).

Melchior and Steim (27) have reported that the inner membrane transition in whole cells of E. coli wild type and unsaturated fatty acid (UFA) auxotrophs can be resolved from that of the outer membrane using differential scanning calorimetry (DSC). Thus both the outer and inner membrane lipids are in the bilayer form. However, other results obtained with the same technique and employing similar auxotrophs (60, 61) have demonstrated that preparations of E. coli whole cells display phase transitions similar to those of the isolated plasma membranes as well as to those of the aqueous dispersions of the extracted lipids (i.e. derived liposomes), showing similar  $T_l$ ,  $T_h$  and  $T_m$  values. Moreover, fluorescence probing (14, 62) and wide angle X-ray diffraction studies (62) have shown that the isolated outer and inner membranes do exhibit similar  $T_l$ ,  $T_h$  and  $T_m$ , but that a higher proportion (60-80%) of the inner membrane lipids than the outer (25-40%) take part in the transition, i.e., are in bilayer form hydrophobically uninfluenced by the presence of protein. These data are consistent with electron spin resonance (ESR) results (63). The progress of phase transitions has also been followed in UFA auxotrophs by monitoring the partitioning between the polar aqueous phase and the hydrophobic membrane core of the



ESR probe 2,2,6,6-tetramethylpiperidine-1-oxyl (TEMPO) (60, 64 - 66). Data from wide angle X-ray diffraction studies (67, 68) corroborate these findings and reveal that  $T_m$  depends on the UFA-enrichment of the membrane. Investigations employing DSC (27, 29, 69, 70) and differential thermal analysis (DTA) (2, 55, 71 - 77) demonstrate that for a wide variety of membranes from other sources, the transition is also similar in membranes and derived liposomes [and also in whole cells in some cases (29, 70)], thus indicating that the common denominator among all these various membranes is the lipid bilayer. The phase transition can also be followed in these membranes using X-ray diffraction (28, 44, 78 - 81), ESR (18, 82 - 97), nuclear magnetic resonance (NMR) (83) and Raman (98) spectroscopy. In these studies, the sharpness of the transition gives an idea of its cooperative nature. From values of the transition enthalpy and the proportion of the total membrane lipid participating in the transition, it has been calculated using fluorescence spectroscopy (62, 99) and X-ray diffraction (62) that in the E. coli isolated inner membrane, as much as 70% or more of the membrane lipids are in the bilayer state, hydrophobically uninfluenced by the presence of proteins. By contrast, only 25-40% of the lipids in the isolated outer membrane exists as a bilayer hydrophobically uninfluenced by protein (62). In membranes from eukaryotes and other prokaryotes, ESR (93) and calorimetry (29) have also demonstrated the existence of ~70% lipid bilayer, uninfluenced by membrane proteins.

These physical techniques have thus helped to establish that membrane phospholipids are arranged in an interrupted bilayer as a result of the intercalated proteins in the lipid bilayer matrix. The



acyl chains of the phospholipid molecules show a fluidity gradient (30) which is detectable in lobster walking leg nerve fibre membranes by ESR (84) and in artificial lipid bilayers by NMR (100) spectroscopy, being least fluid near the ester bond and most fluid at the methyl terminus.

Jost and associates (18, 97) used the ESR spectra of spin-labeled fatty acids incorporated into cytochrome oxidase vesicles to demonstrate the presence of boundary lipid associated with this membrane enzyme complex isolated from beef heart mitochondria. They showed that spectra for immobilized lipid only were discernible below a phospholipid:protein weight ratio of 0.2 and above this, additional ESR spectra were obtained indicative of mobile lipid. Thus about 0.2 mg phospholipid/mg protein is in close association with the protein and its properties are modified with respect to bulk membrane lipid. Calculations reveal that this amount of lipid is sufficient to form a halo of immobilized lipid a single molecule thick, thus "insulating" the hydrophobic protein from adjacent fluid bilayer in this membrane model. This bound lipid is required for maximal cytochrome oxidase activity and apparently plays a role in maintaining the thermal stability of the enzyme complex. Essentially the same phenomenon has been shown by the same technique for the interaction of dipalmitoyllecithin (DPL) with  $\text{Ca}^{2+}$ ,  $\text{Mg}^{2+}$ -dependent ATPase from sarcoplasmic reticulum (101). "Boundary" lipid has been termed variously "annular" (101) and "intimate" (85) lipid.

The technique of freeze-fracture electron microscopy (EM) (82, 102 - 104; also for reviews, see 3, 4, 6) has revealed that E. coli cells and isolated membranes maintained at a temperature above  $T_h$  before freeze-fracture show a near random distribution of particles believed to be membrane proteins (55, 66, 68, 105). However, progressive





aggregation was noted as the temperature at which the sample was maintained before freeze-fracture was reduced. The same observation was made for membranes from other sources (2, 5, 72, 106, 107). Thus this technique gives evidence for the fluid lipid bilayer matrix of the biological membrane and the free lateral mobility of proteins within the plane of this bilayer above the lipid phase transition temperature. It is also possible to discern the heterogeneity of the membrane lipids and also estimate the percent bilayer from these studies using an E. coli UFA auxotroph (68).

Under physiological conditions, when the lipid bilayer matrix is fluid, most if not all membrane lipids diffuse laterally rather freely in the plane of the membrane. This has been demonstrated by the use of fluorescence spectroscopy in E. coli (14, 33) membranes and membranes from eukaryotic sources (34 - 37). The diffusion coefficient for this lateral motion is of the order of  $D \approx 10^{-8} \text{ cm}^2 \cdot \text{sec}^{-1}$  (36, 37, and reviews 4, 6). Membrane integral proteins also diffuse laterally with  $D = 10^{-10}$  to  $10^{-9} \text{ cm}^2 \cdot \text{sec}^{-1}$  (36 - 41, and for reviews see 3, 4, 6, 7). These membrane components are also capable of exhibiting rotational diffusion about an axis perpendicular to the surface (108, 109). There is, however, no evidence for free movement of either the amphipathic (glyco- and phospho-) lipids (88, 94, 110 - 112) or the amphipathic integral proteins (3, 4, 6, 113, 115, 116) from one half of the bilayer to the other (flip-flop). This flip-flop rate is extremely low (see 15 for review).

Evidence from chemical and enzymatic labelling and enzymatic modification studies on inside-out and right side out vesicles, and electron microscopy of samples labeled with fluorescent antibody (see



15 for review) support the asymmetric distribution of membrane lipids (88, 94, 111, 112, 114, 117 - 119), membrane proteins (36, 110, 113, 115, 116, 119 - 125), cholesterol (111, 126) and carbohydrates (127) in various kinds of membranes.

The role of lipid asymmetry in maintaining certain physiological functions is not clear. However, asymmetric lipid composition could regulate differential membrane fluidity in each half of the bilayer (58). Alternatively, the higher proportion of anionic phospholipids on the inner portion of the bilayer may facilitate ionic interactions (through, say,  $\text{Ca}^{2+}$ ) with membrane associated and peripheral membrane components (4, 15).

Asymmetric distributions (and orientations) of proteins within the membrane confer obvious advantages to the efficient functioning of the cell. By exposing the antigenic determinants and receptors at the correct surface, it is possible for the cell to react to its environment, e.g. cell recognition (128). Moreover, compartmentation of enzyme reactions within a cell can only be meaningful and efficient if the required enzymes are fixed in the right disposition within the membrane. In addition, as extensively reviewed by Coleman (129), multienzyme sequences (e.g. redox sequences of the electron transport chain) can only function efficiently with the assistance of the membrane which holds the different members of the enzyme complex in the right disposition with regard to a common metabolite. Vectorial reactions which result in the separation of substrates from products on two sides of the membrane are rendered feasible and efficient by the asymmetric distribution and orientation of the required enzymes in the membrane, as exemplified by group translocation reactions, the sucrase reaction of



mammalian gut, which involves a sequential action of an enzyme with a closely linked transport system for its product (glucose), and mitochondrial electron transport and oxidative phosphorylation. Thus, it is important that the inherent asymmetric distribution of the membrane constituents between the two halves of the bilayer be preserved by the absence of flip-flop (3, 4, 128, 130).

## B. THE BACTERIAL CELL ENVELOPE AND PERIPLASMIC SPACE (A REVIEW)

### 1. Introduction

The cytoplasm of the bacterial cell (both gram positive and gram negative) is bounded by a cytoplasmic membrane (true plasma membrane), which is in turn surrounded by the cell wall (see plates 3 and 4). The plasma membrane together with the cell wall constitute the cell envelope (see reviews 131-136). The cell wall is a complex, partly inelastic structure which protects the cell from osmotic swelling and lysis and also conditions the microenvironment of the cytoplasmic membrane. Between the plasma membrane and the cell wall is the periplasmic space (131 - 136), as defined by Mitchell (137). The composite cell envelope regulates the complicated molecular traffic between the cell and its environment, since it serves both as an ion exchange resin (being predominantly negatively charged) and a molecular sieve (because it excludes large molecules) (133 - 137). The cytoplasmic membrane has a relatively consistent chemical composition and molecular architecture and available evidence (131 - 136) indicates that it can be adequately described by the fluid mosaic membrane model (1, 15). It is the major permeability barrier of the cell (132, 138) and contains enzyme systems related to electron transport (132, 139 - 144),





active transport of solutes (132, 143 - 145) and phospholipid biosynthesis (143, 144, 146, 147). The cell walls of bacteria, however, vary widely between the chemically simple walls of some gram-positive species, e.g. Micrococcus lysodeikticus (148), and the very complex multilayered walls of smooth strains of gram-negative bacteria (131 - 136, 149 - 151).

## 2. Molecular Architecture of the Cell Wall of Bacteria

Both gram-positive and gram-negative bacterial cell walls have as a common feature a peptidoglycan (murein) layer, which is an inelastic, sac-like, macromolecule (133, 134, 136, 152, 153). This is composed of glycan strands interconnected through short peptide chains. The glycan strand is made up of interconnecting  $\beta$ -1,4-linked N-acetylglucosamine and N-acetylmuramic acid residues. The peptide subunit, linked to the lactyl group of N-acetylmuramic acid, is normally a tetrapeptide composed of L- and D-amino acids, but in some cases a tri- or pentapeptide occurs (152, 153). Peptidoglycan can thus be regarded as a derivative of chitin (153). Variations in the detailed structure of the peptide can occur both between and within the two groups of bacteria (gram-positive and gram-negative). A great proportion of the peptides are cross-linked (152).

The gram-positive cell wall consists mainly of a thick fibrous layer of this murein [up to 10 nm thick (154)] against which the cytoplasmic membrane is adpressed (see plate 3). Other molecules such as teichoic acids (155, also see 156 for review), teichuronic acids, and lipids are interspersed with the basic peptidoglycan structure, but these do not form coherent or continuous structures within the cell wall (133, 134, 157). The periplasmic space is taken to include the



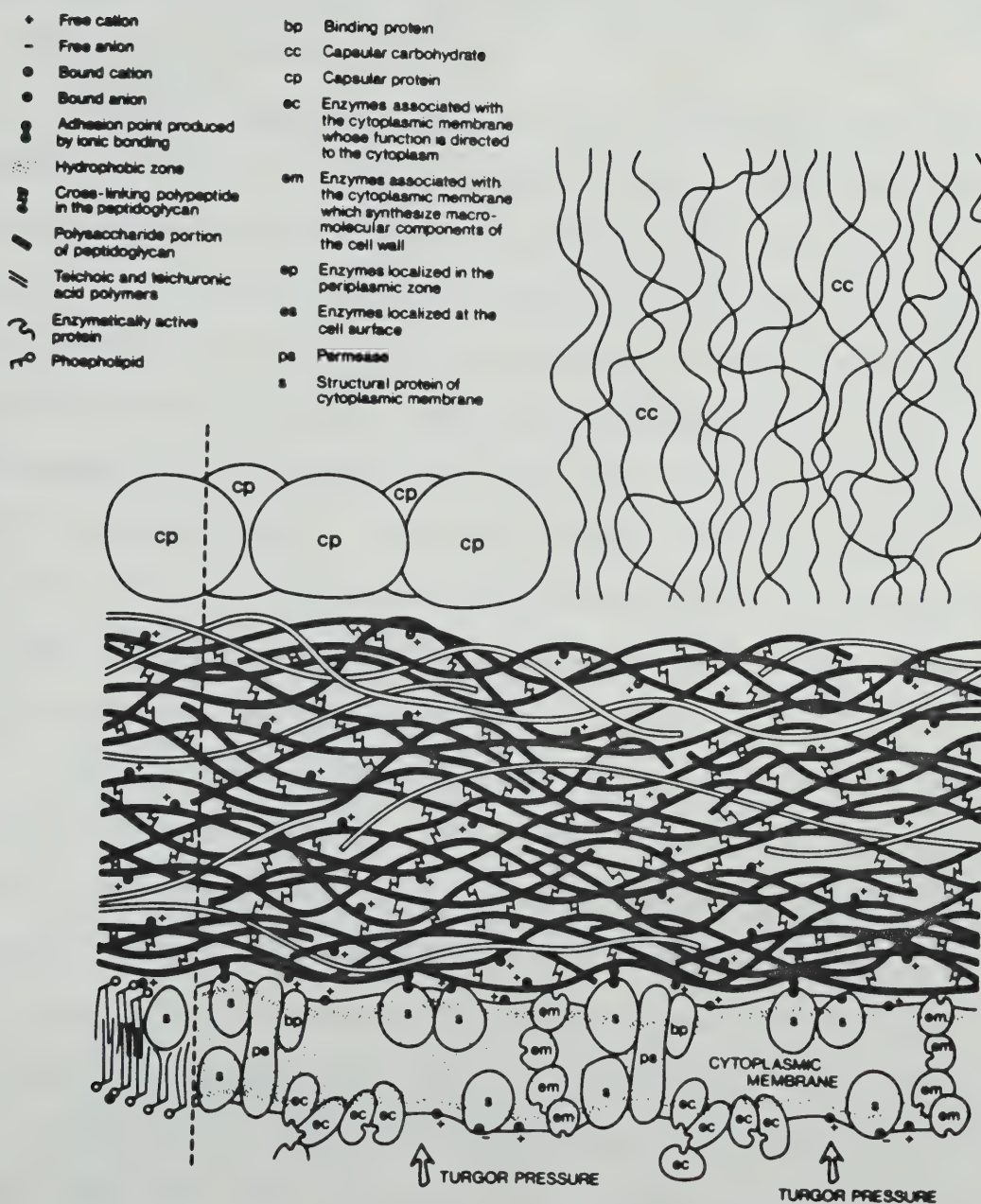


PLATE 3. Structure of Gram-Positive Cell Wall (ref. 134).



space between the cytoplasmic membrane and the murein layer as well as the space within the fibrous murein network. At their outermost surface, these bacteria may bear globular protein coats or very extensive fibrillar carbohydrate capsules (134).

The gram-negative cell wall is a very complex structure whose innermost element is the rigid peptidoglycan layer to which the cytoplasmic membrane is both addressed and adherent (133 - 136) (see plate 4). The peptidoglycan layer, which can be 0.8 nm to 30 nm thick, does not contain integrated polymers similar to teichoic acids, but is covalently linked to elongate lipoprotein molecules (133, 134, 136). These extend outward in bundles and their lipid moieties associate with an outer membrane, which is composed of phospholipids and protein (131-136, 158). The peptidoglycan-lipoprotein complex thus maintains, and partly occupies, a well-defined periplasmic space between the inner (i.e. cytoplasmic) and outer membranes.

There is evidence that the outer membrane is basically a lipid bilayer with integral lipoproteins (131-136, 158, 159) but the fraction of the bilayer that takes part in the gel  $\rightleftharpoons$  liquid crystalline phase transition is small (62, 63). The presence of lipopolysaccharide as a major membrane component is a unique feature of this outer membrane (133-135, 160). The function of this outer membrane is obscure (158) but it may serve as a molecular sieve, excluding molecules above 700 daltons (161, 162). Thus, penetration of antibiotic molecules could be prevented while hydrophilic small molecules like sugars could be let into and out of the periplasmic space (133-135) through water-filled channels presumably formed by the lipoproteins (158, 159, 161-163). This permeation could be affected by pH, ionic strength and cations (164,





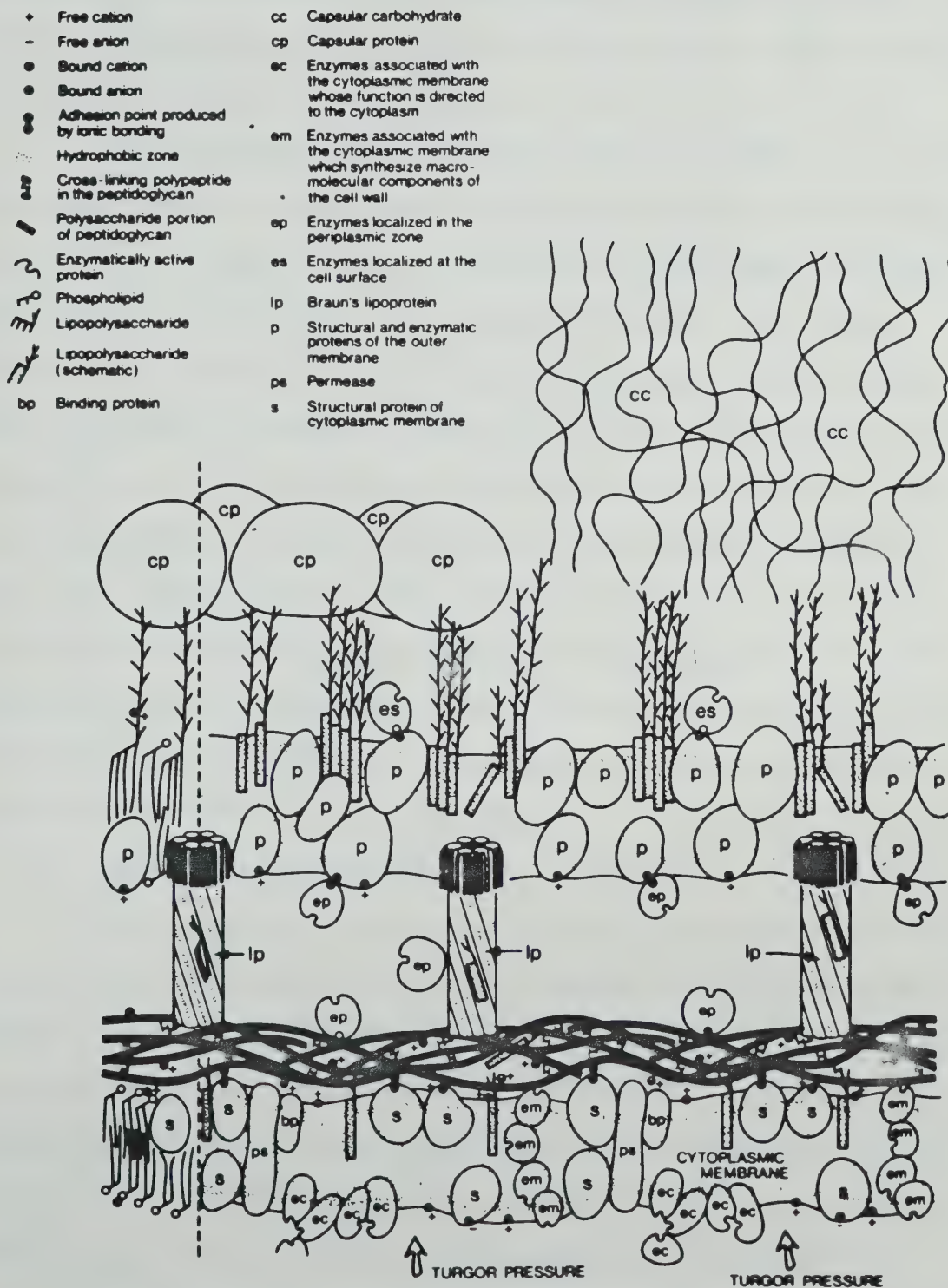


PLATE 4. Structure of Gram-Negative Cell Wall (ref. 134).





165). An endogenous phospholipase A activity is the only enzyme detectable in this membrane (166). The external surface of the outer membrane is shielded probably by long carbohydrate chains of the lipopolysaccharide molecules (133-135, 166).

The periplasmic space of bacteria contains a number of proteins which are released on mild osmotic shock as described by Neu and Heppel (167). Some of these proteins are hydrolytic enzymes such as alkaline phosphatase, 5'-nucleotidase and  $\beta$ -lactamase (133, 134, 168), while others are specific transport binding proteins, e.g., for L-glutamine in E. coli (169). Synthesis of the cell wall and periplasmic space components occurs in the cytoplasmic membrane and the molecules are extruded through the periplasmic space to their final destinations (133 - 136, 170). Methods are now available for the separation of the inner and outer membranes of E. coli, Salmonella typhimurium and other gram-negative bacteria (139) based on sucrose gradient centrifugation (171) of these membranes obtained after degradation of peptidoglycan using lysozyme-EDTA treatment (143, 172, 173).

### 3. Implications of the Possession of a Cell Wall

The functions of the bacterial cell wall and its components are not yet fully understood (144, 174-177). Being a molecular sieve and an ion exchange bed, cell walls have been implicated in antibiotic resistance and general restriction of molecules which get into, and out of, the periplasmic space. Hence, periplasmic binding proteins and enzymes are not lost to the external medium. They have also been implicated in the success of some of these bacteria as pathogens (133-135).

Some aspects of the kinetics of transport in gram-negative bacteria could also be altered as a result of the possession of a cell



wall. Carrier mediated efflux\* studies of the lactose transport system in E. coli, performed in the conventional way of preloading cells with radioactive substrate, diluting into warm substrate-free medium and sampling at convenient times, yielded only 10-15% of the expected efflux. This was due to a "recapture" phenomenon. That is, within the periplasmic space, substrate molecules which have left the cell do not readily mix with the bulk of the extracellular fluid. Thus, after exit, substrate molecules in this space have a high probability of being recaptured by the carrier and net efflux from the cell is significantly reduced. The "accelerative exchange diffusion" which characterizes facilitated diffusion systems is found to operate faster than expected for exit and slower than expected for entry in energy-uncoupled lactose transport in E. coli as a consequence of the recapture problem. The kinetics of "counterflow", a phenomenon which is also characteristic of facilitated diffusion systems, have eluded quantitative analysis due to the recapture event. In a number of cases, it has been possible to devise adequate experimental modifications in order to circumvent this recapture problem (178). In addition, passive permeation of glycerol and erythritol assayed by optical means does not give a linear concentration dependence of rate (174). However, for other aspects of transport studies, these problems do not seem to exist. For instance, it has been reported (179) that the  $K_m$  for L-proline transport, in membrane vesicles prepared from E. coli according to the method described by Kaback (180), corresponds closely to  $K_m$  obtained with whole cells (181). Also, Kaback et al. (182) have reported that in many cases these membrane vesicles

---

\*The terms "flux", "efflux" and "influx" are used in this report to mean, respectively, "rate of flow", "rate of exit" and "rate of entry", as defined by Halvor Christensen (see reference 128).



transport metabolites at rates that are comparable to those of the parent intact cells.

## C. SOLUTE TRANSPORT AND PERMEATION ACROSS BIOMEMBRANES (A REVIEW)

### 1. Introduction

The membrane of the cell or organelle constitutes an effective barrier separating the intracellular (or intraorganelle) constituents from the external environment as well as separating the various compartments within the cell or organelle. In order to ensure its normal functioning and continued existence, therefore, adequate transport systems are mandatory. Biological membranes are thus highly selective permeability barriers and the flow of molecules and ions between the cell (or organelle) and its environment is precisely regulated by specific transport systems. Transport processes have a number of important roles (183, 128), among which are: (i) to maintain correct osmotic balance and thus regulate cell volume; (ii) to maintain intracellular pH and ionic composition ( $\text{Ca}^{2+}$ ,  $\text{Mg}^{2+}$ ,  $\text{K}^+$ ,  $\text{Na}^+$ , etc.) within a narrow range, in order to provide a favorable environment for enzyme activity. The cell indeed maintains within itself a great variety of internal environments carrying out a vast number of chemical reactions that are inherently incompatible with one another; (iii) to extract and concentrate metabolic fuels and building blocks (amino acids, nucleosides and nucleotides) from the environment and to extrude toxic substances; (iv) to generate ion gradients that are essential for neurotransmission, muscle contraction (and related phenomena), and transduction of energy from chemical to other forms. For instance, proton extrusion in E. coli during ATP hydrolysis by  $(\text{Ca}^{2+}, \text{Mg}^{2+})\text{ATPase}$ , or substrate oxidation and subsequent





electron transport, generates a proton motive force (PMF or  $\Delta\bar{\mu}_{H^+}$ ) which in turn can drive active transport of solutes. Reversal of this process under appropriate conditions can generate chemical bond energy (ATP).

Solute uptake in cells and organelles occurs by either non-energy-dependent (passive permeation and facilitated diffusion) or energy-dependent (active transport and group translocation) processes (13, 128, 184, 185). Passive permeation of solute through the membrane occurs by simple diffusion driven down a concentration gradient of solute until equilibrium is established across the membrane, i.e., there is no accumulation of permeant. Facilitated diffusion is protein-mediated but since it is not energy-coupled, results in equilibration just like passive permeation. Its rate is, however, generally much faster than the passive permeation rate for hydrophilic nonelectrolytes and ions. In common with energy-dependent transport, facilitated diffusion systems are protein-mediated. The activation energy,  $E_a$ , for mediated transport has been observed to be lower than that for the passive permeation of the same permeant molecule through liposomes (71).

## 2. Passive Permeation

The kinetics of passive permeation can be described using Fick's first law of diffusion in free solution (128, 184, 185) while applying the following considerations: (i) The biological membrane exerts an effective barrier action and therefore the diffusion constant is smaller than for the diffusion of solute in free solution; (ii) Since the membrane is thin, the concentration difference can be treated as though it occurred abruptly. The initial rate of flow in one direction (unidirectional flux) can then be expressed as:



$$V_{\text{initial}} = J = PC \quad [1]$$

where C is the concentration of solute in the phase of its origin and P is the permeability coefficient under unit area. Passive flux thus increases linearly with applied concentration of solute. P is governed by the following factors: (i) solute size: for small molecular weight (MW) solutes (MW <100), P decreases as (MW)<sup>1/2</sup> increases since the product P(MW)<sup>1/2</sup> should remain constant if other conditions are constant; (ii) solubility of the solute in the lipid phase as compared to its solubility in the aqueous phase (oil/water partition coefficient): this is largely determined by the number of exposed -CH<sub>2</sub>- groups as well as the number of hydrogen bonds (with water) to be broken.

### 3. Mediated Transport

Facilitated diffusion and the energy-dependent transport systems are mediated by some component of the membrane (believed to be protein) which is in limited supply. Thus, the substrate (S) is transiently bound by this membrane-bound mediating structure (M). The kinetics of these mediated transport processes do not therefore conform with Fick's first law and can be described, like classical enzyme kinetics (186), by the Michaelis-Menten equation (128, 184, 185). Thus,

$$\text{Initial rate} = v = \frac{V_{\text{max}} \cdot [S]}{K_m + [S]} \quad [2]$$

where [S] is the substrate concentration,  $V_{\text{max}}$  is the maximum transport rate attainable at saturation and  $K_m$  is the substrate concentration which results in  $1/2 V_{\text{max}}$ . Mediated transport thus comprises a number of steps, viz.: substrate recognition, substrate binding, translocation, substrate release and recovery of the mediator. Then another cycle can be repeated.



Inherent in the Michaelis-Menten formulation for transport are the following facts: (i) Mediated transport is a saturable process yielding a hyperbolic dependence of initial rate with substrate concentration. (ii) Transport systems exhibit specificity for their substrates. This can be highly restricted to a single substrate, e.g., the system for L-glutamine and that for L-proline in E. coli, or general, e.g., the systems for some other amino acids in E. coli. In most cases, stereospecificity is exerted whereby only one optical isomer can be transported by a system, as exemplified by the L-glutamine and L-proline systems mentioned above and the glucose carrier in the human red blood cell, which transports only D-glucose. (iii) Substrate analogs exert competitive inhibition. (iv) Transport rate is specifically reduced by the presence (even in small amounts) of substances differing chemically from the substrate, these inhibitors being chemical agents also active as enzyme poisons, e.g., sulfhydryl reagents. (v) Each of the following phenomena, "competitive exchange diffusion", "counterflow" and accelerative exchange diffusion, can be demonstrated (128, 178, 184) as a characteristic of facilitated diffusion, or an active transport system from which the energy link has been broken (energy-uncoupled active transport) which then operates as a facilitated diffusion. These phenomena are both a consequence of, and a test for, mediation.

Competitive exchange diffusion and counterflow require the operation of a transport carrier in the presence of two substrates (analogues) transportable by the carrier (184). The outward and inward flows should not interfere with each other. Competitive exchange diffusion [or cis-inhibition (128)] will be found in any situation where a facilitated diffusion system (e.g., that for glucose in the human





erythrocyte) is originally at or near saturation (with glucose in this case) at both faces of the membrane and a second substrate (e.g., galactose) sharing the same system is added (in substantial concentration in relation to its  $K_m$ ) to one face of the membrane. The originally low net flux will be converted into a high unidirectional flux by cis- inhibition, i.e., inhibition of glucose binding at the galactose-rich face, which then prevents re-entry of the glucose leaving the cell as galactose enters. Thus, addition of galactose to the external face effectively leads to a high efflux of glucose from the cell.

Counterflow also refers to a special type of competitive inhibition (178). In counterflow experiments, a transient accumulation against a concentration gradient may be demonstrated in a system which carries out facilitated diffusion. If cells are preloaded with a high internal concentration of (unlabelled) substrate A, centrifuged, and then resuspended in a low concentration of (labelled) substrate B, there is a transient accumulation of B within cells. This is due to competition for outflow between preloaded molecules of substrate A at high internal concentration, and newly entering molecules of substrate B, which are at a low internal concentration. For the control, cells are not preloaded and it is observed that B would not accumulate but would reach an internal concentration equal to that in the external medium due to simple facilitated diffusion.

Accelerative exchange diffusion is also known as trans- stimulation (120). It refers to the observation that the entry or exit of substrate may be stimulated by the presence of substrate on the opposite face of the membrane. This has been explained by assuming that the carrier-substrate complex traverses the membrane more rapidly than the free





carrier. Thus the rate-limiting step in entry or exit would be the return (or recovery) of the empty carrier, and this may be accelerated if the carrier returns combined with a substrate molecule (128, 178, 184). Thus, it was found that for the transport of  $^{14}\text{C}$ -glucose into red blood cells, the rate of entry was higher the higher the internal level of unlabeled (preloaded) glucose (184).

#### 4. Energy-Dependent Transport

Energy-dependent transport systems require input of metabolic energy and result in the accumulation of solute against its electrochemical potential. The introduction of energy results in an asymmetry such that solute gradients are established. Thus the symmetrical carrier in the facilitated diffusion system, which transports solute across the membrane in both directions with equivalent kinetics, differs from the carrier in the presence of energy coupling (187). For the E. coli lactose carrier, for instance, it has been found (178, 188) that energy-coupling reduced the affinity of the carrier for its substrate on the inner surface of the plasma membrane. Uncoupling the energy input by the use of metabolic inhibitors reduced the  $K_m$  for exit about two orders of magnitude, whereas the  $K_m$  for entry remained constant.

In bacteria, three different broad classes of energy-dependent transport systems are known. In two of these, the energized membrane-dependent transport and the periplasmic binding protein-dependent transport systems (189-192), substrate is accumulated without modification. The former (shock-resistant) type is driven by an electrochemical potential of protons (proton motive force) as defined by Mitchell's chemiosmotic theory (193 - 200). It does not require the presence of ATP or a related compound per se and is retained after cold osmotic



shock (167) and also in membrane vesicles (180). The proline transport system and the lactose transport system in E. coli are examples. This group includes, in addition, the recently discovered  $\text{Na}^+$ -gradient-driven accumulation of amino acids in Halobacterium halobium envelope vesicles (201-203) and glutamate accumulation in membrane vesicles (206) and intact cells (204, 205) of E. coli strain 29-78, a mutant strain of E. coli B. In these cases, a proton motive force generated by light, respiration or ATP hydrolysis (187) creates (by antiport, i.e., simultaneous movement of two solutes in opposite directions mediated presumably by the same carrier) a chemical gradient of sodium ions (201, 206). The substrate is transported as a ternary complex on the carrier with the co-ion,  $\text{Na}^+$ , (i.e., by symport).

The periplasmic binding protein-dependent (shock-sensitive) type is lost after cold osmotic shock and is absent in membrane vesicles. It requires the presence of ATP per se or a related compound. The L-glutamine transport system in E. coli is a good example.

The third type of energy-dependent transport is the group translocation system exemplified by the phosphoenol pyruvate (PEP)-dependent phosphotransferase system (PTS) (207, 208), which catalyzes the vectorial phosphorylation of sugars in E. coli. This covalent modification of the substrate thus prevents exit via the same solute-specific carrier.

#### D. BACKGROUND MATERIAL RELEVANT TO THIS STUDY

##### 1. Consequences of the Lipid Bilayer to Membrane-Bound Reactions

Implicit in the fluid mosaic model of membrane structure are the following facts:

- (i) Since the lipid bilayer constitutes the major permeability



barrier of the membrane, the permeant molecule would interact directly with the hydrophobic core of the membrane during passive permeation. In the case of a protein mediated transport (or a membrane-bound enzyme reaction), the substrate may also experience the hydrophobic environment, either directly or indirectly (in association with the mediating protein), during the overall process.

(ii) The physical state of the membrane lipid fatty acyl chains should affect the rate of these processes if some movement within the lipid bilayer is part of the rate limiting step, the reaction being faster the higher the fluidity of the membrane hydrophobic core, while a change in the gel  $\rightleftharpoons$  liquid crystalline phase condition of this zone would result in a change in activation energy,  $E_a$ .

(iii) Protein mediators and enzymes involved in these processes may require some lipid obligatorily and this lipid requirement may be very specific in some cases.

(iv) Flip-flop rates for membrane amphipathic lipids and integral proteins are at a minimum since flip-flop is energetically expensive. However, lateral and rotational diffusion within the plane of the membrane are relatively fast for these components. It is thus likely that no step in these processes would involve transmembrane diffusion of these amphipathic components.

The following are some experimental evidence in support of each of these facts:

(i) De Gier et al. (209) and McElhaney et al. (74) observed that the activation energy for the passive permeation of a number of polyols in liposomes and in pig and rabbit erythrocytes, as well as through A. laidlawii B membranes was dependent on the number of hydrogen





bonds broken between the polyol and water (i.e., dehydration) before the permeation process. This energy parameter was dependent neither on the degree of unsaturation of the membrane or liposome phospholipid fatty acyl chains nor on the presence of cholesterol within the bilayer hydrophobic core. It was therefore inferred that both the lipid bilayers and the biological membranes are penetrated by single, fully dehydrated molecules. This observation, coupled with the dependence of the rate of permeation on the fluidity and phase state of the membrane lipids (see (ii) below) suggests that these molecules pass through the hydrophobic core of the membrane. Sprott et al. (210) have recently demonstrated that under sub-maximally energized conditions, the active transport rate of a vast number of amino acids belonging to different active transport types increased with the hydrophobic nature of the amino acid. These results suggest that a common rate-limiting step among the amino acid transport systems is the transfer of the substrate from an aqueous to an apolar environment.

(ii) The rate of glycerol or erythritol passive permeation in liposomes as well as in intact cells of A. laidlawii B increased with increasing fluidity of the membrane phospholipid fatty acyl chains. The presence of fatty acyl chains of reduced chain length or containing double bonds or branched chains increased permeability in both liposomes and cells while introduction of cholesterol in the bilayer decreased the rate (74, 209, 211). A decrease in the passive permeation of glycerol, erythritol and organic acids has also been observed in porcine and bovine erythrocytes up to a cholesterol/lipid ratio of 0.6 (212). Glycerol permeation in human erythrocytes containing cholesterol to varying levels, which occurs by facilitated diffusion (213) increased with



cholesterol depletion (214). In addition, the passive permeation of glycerol and erythritol in A. laidlawii B cells and liposomes assayed by the swelling rate method responded to the membrane physical state. Normal swelling occurred at high temperatures but at temperatures where most of the membrane lipids were determined by DTA to exist in the gel state, spontaneous lysis occurred during the assay (74). A gross membrane phenomenon like the growth of these cells (72, 73) and of wild type and temperature-sensitive strains of Bacillus stearothermophilus (75) also responded to the gel  $\rightleftharpoons$  liquid crystalline phase state of the membrane. Growth of A. laidlawii B (72, 73) ceased only when the phase transition was approximately complete (<10% fluid). Membrane fluidity and physical state are also known to control the rate of active transport of solutes in A. laidlawii B (71), E. coli UFA auxotrophs (14, 58, 67, 215-219; see also 194, 220 for reviews) and mammalian cultured cells (221) as well as membrane-bound enzyme reactions in a variety of cell membrane types (67, 77, 78, 106, 107, 222-233).

(iii) The requirement for lipid in a host of membrane transport and enzyme reactions has been extensively documented (18, 222, 224, 225, 234-255; see also 129, 144 for reviews). In many cases (224, 245-254) this requirement is restricted to one or two specific phospholipid types. The fluid state of the lipid is a prerequisite for normal function. It has been demonstrated that some membrane enzymes require and possess a layer of lipid one molecule thick whose properties are modified with respect to bulk membrane lipids (18, 101). This is an immobilized lipid layer and has been termed "boundary" lipid (18), "annular" lipid (101) or "intimate" lipid (85).

(iv) Experiments specifically designed to probe the possible



contribution of flip-flop to transport mechanism (i.e., rotating or mobile carrier mechanism) have so far indicated that transmembrane rotation of the transport carrier protein does not contribute to the translocation step (122, 123, 125). Specific antibodies were bound to purified canine renal ( $\text{Na}^+, \text{K}^+$ )ATPase (122) or to purified  $\text{Ca}^{2+}$ -ATPase from rabbit sarcoplasmic reticulum (125). These antibodies inhibited neither the ATPase nor the specific ion transport associated with the system, even though the binding of the antibody would have completely prevented transmembrane rotation.

## 2. Postulated Mechanisms of Mediated Membrane Transport

Little information is so far available, at the molecular level, on the translocation mechanism of mediated biological membrane transport (187). Until recently, the two most favoured models depicting the mechanism of this translocation step were (i) the classical "pore" or "channel" model in which lipid-insoluble substances, e.g., ions, are supposed to permeate the membrane through water-filled channels penetrating the membrane, i.e., through a hydrophilic environment, and (ii) the "mobile" (or "rotating") carrier model which postulates that transport occurs by the attachment of the substrate to a component of the membrane, a "carrier", which shuttles between opposite faces of the membrane (184, 185).

Model systems which operate by these two possible mechanisms have been designed using the ionophoric antibiotics. They are, respectively, the pore former antibiotic-mediated ion transport, e.g., gramicidin A-mediated  $\text{K}^+$  transport, and the mobile carrier antibiotic, e.g., nonactin- or valinomycin-mediated  $\text{K}^+$  transport in lipid bilayers (256, see also 257 for review). Light was shed on the mechanism of operation of these two antibiotic types by Krasne et al. (258) who reported that





there was a profound effect of the membrane physical state on ion transport by the mobile carrier, nonactin, but there was no such effect on the pore-former, gramicidin A. Cooling the bilayer to the gel state eliminated conduction by nonactin but not by gramicidin A. In addition, valinomycin-induced  $K^+$  efflux in intact cells of A. laidlawii B has been shown to decrease gradually with temperature and become zero below the gel  $\rightleftharpoons$  liquid crystalline phase transition (259).

These results looked very attractive because the influence of cell membrane lipid fluidity and phase state could be used in a similar manner to differentiate between transport by a pore-former mechanism from that by a mobile carrier mechanism. Indeed, there are many reports in the literature on the influence of membrane lipid fluidity (71, 74, 209, 211, 212, 214, 218; see also 43 for review) and phase state (14, 33, 64, 65, 68, 71, 74, 209, 215-218, 260-264; see also 43, 58, 144, 220 for reviews) on biological membrane passive permeation and mediated transport of solute in microorganisms and in animal cells (221). The phase state effects were discerned by correlating temperature breaks in Arrhenius-type plots of temperature-dependence of rate with points within the gel  $\rightleftharpoons$  liquid crystalline phase transition. However, sufficient as these studies seemed in answering a few isolated questions about mediated biological membrane transport mechanism, they suffered from the following shortcomings:

(i) In some studies on energy-dependent transport, the contributions to the observed results by the response of the energy coupling mechanisms to the membrane lipid fluidity and physical state were not adequately considered (68, 221, 262, 263) and only the translocation step was assumed to have been affected. Interpretations based on such





studies may be invalid since in the simplest sense, one can consider solute active transport systems as composed of two distinct elements, a solute-specific membrane carrier which provides solute recognition and translocation and a system for energy coupling (187).

(ii) Not all the different transport system types have been studied in detail. For instance, among the gram-negative bacteria, efforts have so far concentrated on the proton motive force-driven transport of  $\beta$ -galactosides and L-proline as well as the PEP-dependent PTS for  $\beta$ -glucosides in E. coli. The only study reported of the membrane lipid phase state dependence of a periplasmic binding protein-dependent transport system was done over a small temperature range and a limited number of temperature points were obtained (265). This would limit the amount of information obtainable from these data (85). Moreover, most of the transport system types studied were done in isolation from one another and in different cell types. Any general model built from such data would suffer from the fact that species differences could introduce different characteristics in these systems.

(iii) In many studies (14, 33, 64, 65, 68, 215 - 217, 260, 262 - 264) only a single substrate concentration was used. However, Sullivan et al. (218) have shown that the sharp breaks in Arrhenius plots of initial rates of transport at a fixed concentration of substrate might be due to sharp temperature-dependent changes in  $K_m$  which cause the substrate to become less saturating at temperatures above the transition point. This has recently been corroborated by Silvius et al. (266).

### 3. The Third Model of Transport Mechanism

It is noteworthy that while the valinomycin or nonactin molecule



complexes a  $K^+$  ion and exposes an entirely hydrophobic surface to the membrane hydrocarbon core (267), the integral membrane proteins presumed to catalyze transport are amphipathic and are unlikely to expose an entirely hydrophobic surface on binding substrate as these antibiotics do. The classical mobile carrier, as exemplified by the valinomycin or non-actin model, may therefore not apply directly to the biological membrane "carrier". A third model for mediated transport translocation step mechanism has therefore been proposed by Singer and associates from a consideration of thermodynamic principles similar to those which underlie the fluid mosaic membrane model. It is called the "aggregate rearrangement" model (12, 15) and is mechanistically a hybrid of the pore-former and the mobile carrier models, but it is expected to respond like the mobile carrier model with respect to membrane lipid fluidity and phase state. As previously discussed, the two transport systems specifically probed,  $(Na^+ + K^+)ATPase$  and  $Ca^{2+}-ATPase$ , did not give evidence of a mobile carrier mechanism. Nonetheless, the activities of these enzymes from the same or different sources do show breaks in Arrhenius plots (78, 224, 225, 227, 230, 268). It has been postulated (1, 12) and experimentally shown (4, 21, 22, 123) that membrane proteins may exist as oligomers. These aggregates with associated water-filled channels form good candidates for potential transport carriers whose topological dispositions and channel dimensions could change on binding substrate, thus leading to transmembrane "haulage" of substrate.

#### E. OBJECTIVES OF THIS PROJECT

The objective of this study therefore was to undertake detailed investigations of the temperature-dependence of a representative number



of the known transport system types in a single strain, a UFA auxotrophic mutant of E. coli, in the light of the foregoing discussion. Data from these studies on the influence of membrane lipid fluidity and phase state on the transport systems would be amenable to analysis with regard to the possible mechanism(s) of the translocation step in mediated transport. Contributions to the results by the effects of membrane lipid alteration on the energy coupling system itself would also be easily seen.

Since group translocation results in covalent alteration of the solute, it seems to involve a rather more complicated mechanism and does not fit the strict definition of active transport which requires that solute be accumulated unaltered (187). It was therefore thought better to investigate the first two energy-dependent transport systems together with a facilitated diffusion system, in conjunction with passive permeation.

It would have been ideal to study the systems in as simple a form as possible in order to make interpretations much easier and less equivocal. To this end, the study of an active transport system as well as the same system with its energy coupling step poisoned would have ensured the investigation of the same carrier protein(s) in the presence or absence of energy coupling. With such data, it would have been easy to discern the contribution due to the energy coupling reaction(s). However, treatment of cells during energy-poisoning could result in deleterious effects (178, 187, 190). In this case, the integrity of the transport carrier may be affected and so interpretation of data from the system would be difficult. Fortunately, however, glycerol is thought to penetrate the E. coli membrane either by passive permeation





in glucose-grown (GlpF-noninduced) cells or by facilitated diffusion in GlpF-induced cells, i.e., cells grown in the presence of glycerol or sn-glycerol-3-phosphate (269, 270; see 271 for review). This is the only known facilitated diffusion system in E. coli (271) and may be considered a prototype of carrier-mediated transport. It was then seen as an advantage to investigate this prototypical facilitated diffusion system for glycerol as well as the passive permeation of the same molecule in noninduced cells.

For an osmotic shock-sensitive transport system, the L-glutamine transport system in E. coli was a particularly good one to study because it has been well characterized, is highly specific (169, 272) and does not operate via multiple systems. The L-proline transport system was investigated as a typical proton motive force-driven transport system.

Membrane lipid composition was altered by preferential enrichment of the membranes of E. coli K1060, a UFA auxotroph in one of a number of UFA's which were included in the defined growth media. This auxotroph is deficient in UFA biosynthesis and degradation. It is therefore very suitable for manipulation. Other strains of E. coli used as controls under various circumstances were K12F<sup>-</sup>, E15 and strain 7.



## CHAPTER II

### GENERAL MATERIALS AND METHODS

#### A. MEDIA AND CHEMICALS

##### 1. Non-Radioactive Supplies

The following were purchased from J.T. Baker Chemical Co., Phillipsburg, New Jersey, U.S.A.: glucose, anhydrous dextrose,  $[\alpha]_D^{25} = 52.9^\circ$ , Baker Analysed Reagent; sucrose, crystalline,  $[\alpha]_D^{25} = 66.6^\circ$ , Baker Analysed Reagent; D(+)-xylose,  $[\alpha]_D^{20} = +17^\circ$  to  $+20^\circ$ ; glycerol, anhydrous, 99.5% pure, Baker Analysed Reagent; tris(hydroxymethyl)aminomethane (Tris buffer), Baker grade; meso-erythritol, 99%. L-proline (hydroxy-L-proline free), L-glutamine (crystalline, grade III, 99-100% pure), chloramphenicol (crystalline), imidazole, glucose-6-phosphate dehydrogenase and glucose-6-phosphate were from Sigma Chemical Co., St. Louis, Missouri, U.S.A. Difco supplied vitamin-free casamino acids and trypticase soy broth. Ficoll-400 was supplied by Pharmacia (Canada) Ltd., Dorval, Quebec. Salt-free egg white lysozyme (11,500 u/mg and 13,200 u/mg) was purchased from Worthington Biochemical Corporation, Freehold, New Jersey, U.S.A. NuChek Prep Inc., Elysian, Minnesota, U.S.A. supplied all the unsaturated fatty acids, elaidate (18:1t), palmitelaidate (16:1t), oleate (18:1c), palmitoleate (16:1c) and linoleate (18:2c,c), each at >99% purity.

All chemicals were used without further purification.

##### 2. Radioactive Supplies

Uniformly labeled  $^{14}\text{C}$ -proline {Proline, L- $^{14}\text{C}(\text{U})$ }-} and  $^{14}\text{C}$ -glutamine {Glutamine, L- $^{14}\text{C}(\text{U})$ }-} were purchased from New England Nuclear Corporation, Boston, Massachusetts, U.S.A. The  $^{14}\text{C}$ -proline came



in three batches: batch #1, used for preliminary experiments, had a specific activity (SA) of 261 mCi/mmol and was 99% pure according to its radiochemical specifications, while batch #'s 2 and 3, used for the main experiments, had an SA of 255.0 mCi/mmol and were each 99.2% pure. The  $^{14}\text{C}$ -glutamine was supplied in four batches: batch #1, used for preliminary experiments, had an SA of 213.4 mCi/mmol and was specified as 98.2% pure, while batch #'s 2 to 4 each had an SA of 251.4 mCi/mmol and a radiochemical purity of 98.8%.

$^{14}\text{C}$ -glutamine batch #'s 2 and 3 were checked by paper chromatography with authentic L-glutamine and L-glutamic acid standards in two different solvent systems (see later). This was followed by paper radiochromatography as detailed later. The purity of these two  $^{14}\text{C}$ -glutamine batches was found to conform to the radiochemical specifications by these procedures. These and the other radiochemicals were used without further purification.

### 3. Other Chemicals

All other standard chemicals were of the highest purity available and were purchased from standard sources. They were used without further purification.

## B. BACTERIAL STRAINS AND GROWTH CONDITIONS

Four E. coli strains were employed for this study (see Appendix 1). Escherichia coli K1060, an unsaturated fatty acid auxotrophic mutant, was the generous gift of Dr. David Silbert; wild type E. coli K12F<sup>-</sup> was kindly donated to us by Dr. William Paranchych, while the two alkaline phosphatase-deficient strains, strain 7 (constitutive for the glp regulon) and strain E15 (inducible in glp regulon), were the kind gifts





of Dr. Joel Weiner. Strain K1060 was always grown in medium 63 (M63) (273) in the presence of unsaturated fatty acid (UFA) ( $75 \mu\text{g}/\text{ml}^{-1}$ ) solubilized with 0.12% (w/v) polyoxyethylene [20] cetyether (Brij 58), thiamine ( $1 \mu\text{g}/\text{ml}^{-1}$ ), 0.3% (w/v) casamino acids and 0.4% (w/v) glycerol or 0.23% (w/v) xylose or 0.54% (w/v) glucose or 1% succinate titrated to 7.0 with KOH as carbon and energy source. Strains E15 and 7 were grown in medium 9 (M9) (274), or M63 with or without UFA/Brij 58, and supplemented with nutrients as described for strain K1060. Strain K12F<sup>-</sup> was grown on trypticase soy broth (TSB) without supplementation, M63 (273) or M9 (274) with carbon source, casamino acids and thiamine, but with or without UFA/Brij 58.

Routinely, cells were grown at 37°C (or 39°C when elaidate-supplemented medium was used) with rapid shaking (approximately 170 rev/min) in a New Brunswick Scientific Co. gyrotary shaker bath, or for large volumes, in a warm room using a New Brunswick Scientific Co. gyrotary shaker.

For the experiments on glycerol passive permeation and facilitated diffusion, cells were first grown overnight in a small volume (starter culture). This overnight culture was diluted 100-fold in fresh medium and the shaking continued till mid-exponential phase ( $A_{550} = 0.35 - 0.5$ , read on a Baush & Lomb Spectronic 20 spectrometer), when the cells were harvested by centrifugation at 4°C and 6000 x g for 10 min in a Sorval RC-2B centrifuge. Cells had to be harvested within exponential phase because growth experiments revealed that incorporation of the exogenously supplied unsaturated fatty acid (UFA) in strain K1060 was optimal at this phase and metabolic conversion of cis-unsaturates to cyclopropane derivatives was minimal (Appendix 2A to D).



For the amino acid transport experiments (and also for the isolation of inner membranes used for DTA), an initial ~24-hr starter culture was diluted ~10-fold to form the final starter, which was then grown for another ~12 hr. The working culture was a 50-fold dilution of the final starter. For transport experiments, this working culture was typically ~300 ml in a 2-litre Erlenmeyer flask. For inner membrane isolation, however, much larger culture volumes were employed and these were grown in 1-litre batches, each contained in a 4-litre Erlenmeyer flask. The cells were harvested within the exponential phase ( $A_{550} = 0.45 - 0.6$  as read on a Bausch & Lomb Spectronic 20 spectrometer).

#### C. SPHEROPLAST FORMATION

Spheroplasts of E. coli K12F<sup>-</sup> used for swelling rate assays were formed essentially as described by Osborn and Munson (139) but using tris(hydroxymethyl)aminomethane hydrochloride (tris·HCl) rather than tris·acetate. However, spheroplasts of mutant K1060 could not be formed under the ice-cold conditions recommended by these authors due to extensive lysis during the dilution stage. Some modifications, therefore, had to be employed in which the cells were harvested by centrifugation at 4°C but all subsequent spheroplasting operations were carried out at room temperature. In addition, the dilution step, after plasmolysis in 0.75 M sucrose and treatment with lysozyme, was done with 1.25 volumes of 1.8 mM ethylenediaminetetraacetate (EDTA). These modifications ensured as high as 98-100% spheroplasting efficiency as measured by the ratio of the number of spheroplasts per field of view to the total number of spheroplasts plus intact cells in the same field of view



of a phase contrast microscope.

For swelling rate assays, this spheroplast suspension was mixed with a spheroplast-stabilizing solution of total osmolality of 1020 milliosmolal (584 mM sucrose, 20 mM  $\text{MgCl}_2$  in 100 mM tris·HCl, pH 7.5) at the rate of 60 ml of spheroplast suspension to 20 ml of this stabilizing solution and the mixture centrifuged at  $8,700 \times g$  for 10 min in a Sorval RC-2B centrifuge. The spheroplast pellet thus recovered was washed once with the stabilizing solution and spun down again as above. It was then finally suspended in a small volume of the spheroplast stabilizing solution, ready for swelling assays.

#### D. INNER MEMBRANE ISOLATION

The spheroplasts (without treatment with the spheroplast stabilizing solution) were lysed by dilution in 4 volumes of ice-cold water and the resulting membranes separated on sucrose density gradients as described by Osborn and Munson (139). The only difference was that sucrose solutions were made up in tris·HCl rather than in tris·acetate.

#### E. LIPID EXTRACTION AND PURIFICATION

E. coli whole-cell and membrane lipids were extracted by the method of Bligh and Dyer (275). A whole cell pellet from 200 ml of culture at  $A_{550} = 0.35 - 0.6$  (or inner membrane pellet from  $\sim 1$  litre of culture) was suspended in a total of 8 ml of water by tituration. A 20-ml aliquot of methanol was then first added with swirling before 10 ml of chloroform was added and the mixture swirled further. This suspension was centrifuged at  $13,000 \times g$  for 20 min at room temperature. The supernatant was saved and the resulting pellet extracted once more in the





same manner, this second supernatant being pooled with the first. To this 76 ml of pooled supernatant in a screw-cap bottle were added, in order, 20 ml chloroform, 20 ml water and 40 ml more chloroform with vigorous shaking after each addition. The resultant milky mixture was centrifuged again at  $13,000 \times g$  for 20 min at room temperature, producing two liquid phases separated by a protein interphase. The upper (aqueous) phase together with the particulate protein interphase were removed by aspiration and discarded. The lower (chloroform) phase was evaporated to a small volume on a rotary evaporator and then applied to a column of  $\sim 2$  g of Bio-sil A (200 - 400 mesh, Bio-Rad Labs, Richmond, California, U.S.A.) silicic acid in chloroform. The column was eluted with 50 ml of methanol, thus recovering all the lipid material while protein and other non-lipid contaminants were retained on the column. This lipid extract was then used for differential thermal analysis and/or fatty acid analysis.

#### F. FATTY ACID ANALYSES

Methyl esters of the fatty acids present in the extracted lipids were formed by acid-catalyzed transesterification. The volume of the silicic acid-purified lipid solution was reduced on a rotary evaporator. This sample was taken to complete dryness under a stream of nitrogen gas in a screw cap tube (of dimensions, 100 mm by 13 mm) with a teflon cap liner, and then 1 ml of anhydrous methanol and 1 drop of concentrated sulfuric acid were added. This tube was tightly capped and incubated for 2 hr at  $60 - 70^{\circ}\text{C}$ . To the cooled contents of the screw cap tube was added 1 ml of water. The tube contents were then extracted twice with 0.5 ml of hexane each time (while still in the screw cap



tube), retaining the upper organic solvent layer and discarding the aqueous bottom layer after the second extraction. The pooled hexane phase was then dried over anhydrous  $\text{MgSO}_4$  and centrifuged at moderate speed for 3 min in a clinical centrifuge.

The fatty acid methyl esters thus made were analyzed by gas-liquid chromatography (GLC) on a 6 ft by 1/4 in column of 10% diethyleneglycol succinate (DEGS) on Anakrom 60/70 AS mesh, installed in a Hewlett Packard Gas Chromatograph Model 5700A. This instrument was equipped with a Hewlett Packard Integrator Model 3370B and Strip Chart Recorder Model 7128A. Before analysis by GLC, the solution of the lipid sample was first taken to dryness under a stream of nitrogen gas and then taken up in ~10  $\mu\text{l}$  of hexane. Usually, 3  $\mu\text{l}$  of this 10  $\mu\text{l}$  hexane solution was applied onto the GLC column and the analysis was carried out using any of the temperature programs shown in Appendix 5.

#### G. PROTEIN ASSAY

Protein was assayed essentially according to the method of Lowry et al. (276) with bovine serum albumin as standard.

#### H. PAPER CHROMATOGRAPHY AND RADIOCHROMATOGRAPHY

The purity of radioactive  $^{14}\text{C}$ -glutamine was checked by a combination of paper chromatography and paper radiochromatography. Whatman #1 filter paper spotted with  $^{14}\text{C}$ -L-glutamine and authentic standards of L-glutamine and L-glutamate was developed in the ascending mode in one of two solvent systems. Solvent system I was a mixture of 100 g phenol and 39 ml water with 0.04% 8-hydroxyquinoline (as recommended by the New England Nuclear quality control brochure, Boston, Massachusetts)



and solvent system II was n-butanol-acetic acid-water (12:3:5 v/v) (277). After development, the paper was dried and cut into longitudinal strips, each representing one original spot. The strips containing the authentic standards were sprayed with ninhydrin and heated for ~5 min in an oven at ~100°C.

Radiochromatography of the paper strips containing the  $^{14}\text{C}$ -glutamine spots was performed on a Nuclear Chicago Actigraph III Paper Radiochromatograph equipped with a chart recorder. In order to assist in aligning the paper chromatogram strip with the peak(s) recorded on the chart, an extra strip of Whatman #1 paper carrying a colored marker radioactive spot was attached to each end of the paper chromatogram strip before a scan was run on the radiochromatograph.

#### I. LIQUID SCINTILLATION COCKTAIL (TOLUENE-BASED)

This was prepared by stirring overnight a mixture of 15.748 g of 2,5-diphenyloxazol (PPO) and 0.210 g of 1,4-bis[2-(4-methyl-5-phenyloxazolyl)]benzene (POPOP) in 4 litres of toluene (169).

#### J. ENERGY-POISONING METHODS EMPLOYED

##### 1. Method A

A suspension of K1060 cells grown in the presence of 18:1c was made 30 mM in  $\text{NaN}_3$  and 1 mM in iodoacetate ( $\text{Na}^+$  salt) (188). Chloramphenicol was added to a final concentration of 80  $\mu\text{g}/\text{ml}$  and the mixture was incubated at room temperature for 30 min. These cells were used as controls during glutamine transport assay without any further centrifugation (Chapter IV).





## 2. Method B

A suspension of K1060 cells grown as for method A above was made 40 mM in  $\text{NaN}_3$  and 20 mM in  $\alpha$ -methyl glucoside (278). Chloramphenicol was added as in method A above. The suspension was then incubated at 37°C for 60 min. These energy-poisoned cells were used as controls during glutamine transport assay without further centrifugation (Chapter IV).



## CHAPTER III

### GLYCEROL UPTAKE IN E. coli: PASSIVE PERMEATION AND FACILITATED DIFFUSION

#### A. INTRODUCTION

Nonelectrolyte permeation in cells and phospholipid multilamellar vesicles (liposomes) is easily measured by the swelling rate assay. In this technique, uptake of the permeant molecules induces water influx and the resulting change in volume is monitored spectrophotometrically as a change in the absorbance of the suspension. This technique has been used for the study of the swelling of erythrocytes in glycerol (279), E. coli in lactose (280) and erythritol (281), and liposomes in various nonelectrolytes (282, 283). Nonelectrolyte permeation in Acholeplasma laidlawii B and derived liposomes suspended in sucrose solution has been studied by measuring initial swelling rates following addition of permeant solution at the same tonicity as the sucrose solution (71, 74, 209, 211, 284). A. laidlawii B behaves as an ideal osmometer over a considerable range of permeant concentrations and the initial swelling rate is linearly proportional to permeant concentration, as expected for a passive diffusional process. Results from this technique have given ample indication that the nonelectrolyte molecules permeating passively through artificial or biological membranes interact directly with the apolar core of the bilayer, sensing its fluidity and physical state (74, 209, 211). It has, therefore, been considered advantageous to extend this approach to E. coli where, due to the rather small cell water volume and the rapid efflux of low molecular weight nonelectrolytes from this organism, many technical problems attend the use of, for example,



radio-labelled glycerol to study initial rates of uptake (178). It is not practical to make E. coli suspensions isotonic with the permeant solution since, under such conditions, the swelling amplitude is small. This may be due to the restraining effect of the cell wall on the swelling of the inner membrane. In practice, therefore, the cells are suspended in dilute buffer (270, 274) and then mixed with hypertonic permeant solution made up in the same buffer. Thus, plasmolysis first occurs due to water efflux followed by permeant entry and swelling. Conventional spectrophotometry, however, can be used to measure only the passive process and not the facilitated diffusion, which is much too fast for this technique.

Alemohammad & Knowles (274) have described a stopped-flow spectrophotometric assay which can purportedly be used to measure the passive permeation of glycerol in noninduced E. coli as well as the facilitated diffusion of glycerol into induced cells. The swelling resulting from permeant entry leads to an increase in transmittance which is displayed on the screen of a storage oscilloscope. The reciprocal relaxation time  $[1/\tau]$ , corresponding to  $k$  of Alemohammad & Knowles (274) for the permeation is calculated from this trace. An inherent limitation in this technique, however, is that at low effective glycerol concentrations (below approx. 70 mM in our hands) swelling cannot be measured (274). It is thus not possible to derive  $V_{\max}$  and  $K_m$  values for the facilitated diffusion system. The experiments on the temperature-dependence of glycerol permeation reported herein, therefore, have been performed at 400 mM effective glycerol concentration. This concentration was assumed to be saturating for the facilitated diffusion system since its  $K_m$  would not be expected to exceed 10 mM (274).





## B. METHODS

### 1. Cell Growth and UFA Incorporation

It was found that mutant K1060 incorporates less exogenous UFA due to metabolic compensation when grown on glucose than when grown on glycerol as carbon and energy source (see Appendix 2A & B). Since glucose is the classical catabolite repressor of the glp regulon (269, 270), glucose-grown cells were used for the investigations on the variation of  $1/\tau$  (and initial swelling rate for conventional spectrophotometry) with effective glycerol (or erythritol) concentration. However, in order to generate comparable fatty acid compositions at each UFA supplementation in both induced (glycerol-grown) and non-induced cells (for the temperature-dependence experiments on glycerol facilitated diffusion and passive permeation, respectively), a carbon and energy source other than glucose was mandatory for the non-induced cells. Xylose proved to be a suitable one by the following criteria: (i) the fatty acid composition of the cells grown on xylose was comparable to that of glycerol-grown cells with each UFA supplement tested (Appendix 2A & C); (ii) aerobic glycerol-3-phosphate dehydrogenase (G3PDH) activity was absent in the membranes of xylose-grown strain K1060 cells, just as in glucose-grown cells of strain K1060 and strain E15 (Table I), suggesting that glpF was not induced by growth on xylose (174, 269, 270).

### 2. Preparation of Cells for Swelling Rate Assays

The cells were washed 3 times at 4°C in either 10 mM imidazole hydrochloride, pH 7.0, or 5 mM tris·HCl, pH 7.5, containing 1 mM  $\text{MgCl}_2$  (1 mM  $\text{MgCl}_2$  was found to be essential for the stability of cells of strain K1060 suspended in dilute tris buffer). The final pellet was suspended to an  $A_{550}$  of 0.35 for stopped-flow measurements. It was found, however,



TABLE I

Membrane G3PDH Activity of E. coli K1060 and E15  
Grown with Various Carbon and Energy Sources

<u>E. coli</u> strain:	K1060			E15	
Carbon and energy source:	Glycerol	Glucose	Xylose	Glycerol	Glucose
Membrane G3PDH (SA $\mu\text{M}\cdot\text{MTT}/\text{min}/\text{mg}$ cell protein) $\pm$ SD	2.07 $\pm$ 0.56	Nil	Nil	1.37 $\pm$ 0.04	Nil

Cultures were grown in M63 supplemented with the indicated carbon and energy source and harvested as detailed in Chapter II. Mixed inner and outer membranes were prepared and G3PDH assay carried out as given in "Methods".



that using either one-half or twice this cell concentration made no difference whatsoever in the values of  $1/\tau$  obtained. The suspension was then left for at least 8 h at room temperature (21° - 23°C) for restoration of maximum osmotic sensitivity before use. For the complementary initial swelling rate assays employing the Zeiss PMQII spectrophotometer, the cell suspension was made about 10 times more concentrated.

### 3. Permeant Solutions

Glycerol and erythritol solutions were made up in the same buffer in which the cells were suspended.

### 4. Refractive Index Correction in Solutions

The synthetic high polymer Ficoll-400 has a high refractive index ( $n$ ) but, since it also has a very high molecular weight, has little effect on the osmotic pressure of the medium (274, 285). When Ficoll was used, the appropriate amount was added to each permeant (or sucrose) solution, as well as to the suspension of E. coli, to bring the refractive index of each of these to the same value; refractive indices were determined with an Abbe 3-L Bausch and Lomb refractometer. The refractive index ( $n$ ) at room temperature of an aqueous solution of Ficoll-400 or sucrose or glycerol varied linearly with concentration within the range used. With  $n = 1.3332$  for water, the refractive index increments,  $\Delta n$ , were  $1.48 \times 10^{-3} \cdot (\text{gm}\%)^{-1}$  Ficoll-400,  $5.0 \times 10^{-5} \cdot \text{mM}^{-1}$  sucrose and  $1.043 \times 10^{-5} \cdot \text{mM}^{-1}$  glycerol (see Fig. 1). The osmolality of each solution was read from an Osmette S osmometer (Precision Systems, Waltham, Massachusetts, U.S.A.) and within the range we used (Table II), showed no significant difference when Ficoll-400 was present. Data on temperature-dependence of glycerol permeation reported here were therefore obtained without Ficoll correction for  $n$ .







FIGURE 1. Refractive index correction curves. These solutes are in aqueous solution.

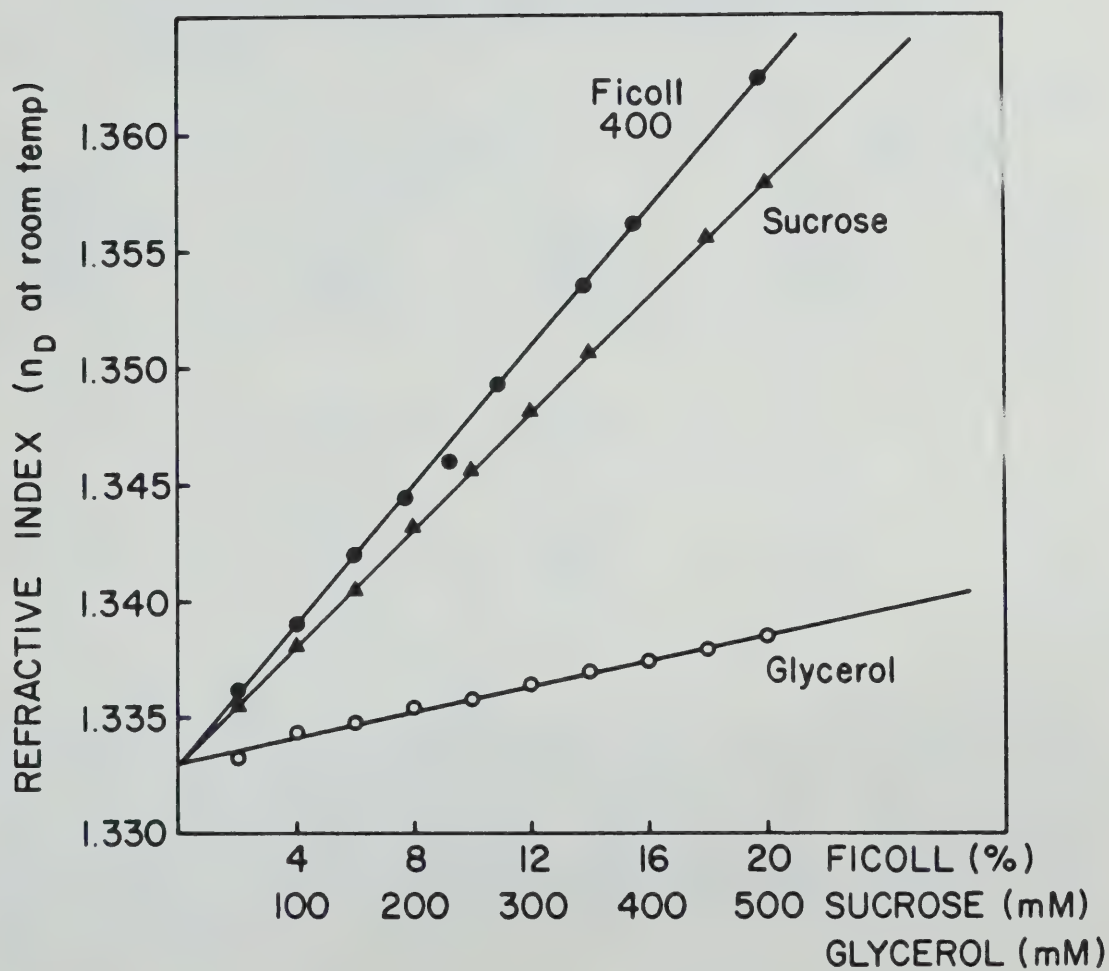




TABLE II

1/τ for Glycerol Passive Permeation in E. coli K12F<sup>-</sup> and K1060  
 Determined in Glycerol Solutions Either Adjusted or Not  
 Adjusted to the Same Refractive Index with Ficoll-400

Effective glycerol concentration (mM)	<u>E. coli</u> K12F <sup>-</sup> 1/τ(sec <sup>-1</sup> ) at 25°C		<u>E. coli</u> K1060 1/τ(sec <sup>-1</sup> ) at 26.2°C	
	Ficoll present	Ficoll absent	Ficoll present	Ficoll absent
100	-	-	0.073	0.073
150	0.111	0.109	-	-
200	0.099	0.093	0.048	0.048
300	0.077	0.071	0.036	0.036
400	0.062	0.059	0.029	0.029

E. coli K12F<sup>-</sup> and K1060 were each grown in M63 plus glucose and oleic acid. The cells were harvested, washed three times (the former strain with 10 mM imidazole·HCl, pH 7.0, and the latter with 5 mM tris·HCl, pH 7.5, plus 1 mM MgCl<sub>2</sub>) and suspended to A<sub>550</sub> of 0.35 in the same buffer. Equilibration was allowed before use (see "Methods"). The refractive index of each of one set of glycerol solutions (in the appropriate buffer) was adjusted with Ficoll-400 to that of the highest glycerol concentration used.



## 5. Swelling Assays

The swelling in glycerol of E. coli grown in the presence of glycerol, glucose or xylose was measured in a Durrum-Gibson stopped-flow spectrophotometer (Durrum Instrument Corporation, Palo Alto, California U.S.A.), while the initial swelling rates in erythritol, and also of glucose-grown cells in glycerol, were measured by conventional spectrophotometry using a Zeiss PMQII spectrophotometer. This was set up as described by McElhaney et al. (74). During the latter assay, 500  $\mu$ l of E. coli suspension was pipetted into 4.0 ml of hypertonic permeant solution in the water-jacketted cuvette containing a high-speed stirring bar.

The Durrum-Gibson stopped-flow spectrophotometer was set up essentially as described by Alemohammad and Knowles (274), except that the stop syringe assembly in the original apparatus described by Gibson & Milnes (286) was retained. This stop syringe activated a microswitch as soon as the suspension of E. coli from one drive syringe and the hypertonic glycerol solution from the other drive syringe entered the cuvette. The initial fast decrease in transmittance at 550 nm resulting from plasmolysis of the cells, and the subsequent increase in transmittance as glycerol entered the cells, resulted in a trace displayed on the screen of a storage oscilloscope. This second phase transmittance increase was allowed to continue to an asymptote, whereupon relaxation kinetic treatment (287, 288) was applied to calculate  $1/\tau \text{ sec}^{-1}$  for glycerol permeation from a photograph of this trace, after having converted transmittance to absorbance using the Lambert-Beer law. The modification made by Alemohammad and Knowles (274), which excluded the stop syringe in order to prevent the artifactual volume changes, was





not necessary in our apparatus since this would only affect the  $1/\tau$  for the first phase (transmittance decrease) due to water efflux and not the  $1/\tau$  for glycerol entry in which we were interested and which occurred in the second phase (transmittance increase). Experiments were done at 550 nm except where otherwise stated.

## 6. Calculation of $1/\tau \text{ sec}^{-1}$

Since cell volume is linearly related to reciprocal absorbance (74, 282, and Fig. 2 here), within the range of about 200 milliosmolal to at least 400 milliosmolal, change in volume ( $\Delta\text{vol}$ ) is directly proportional to change in reciprocal absorbance,  $\Delta(1/A)$  during the swelling of the cells. This has been applied in the calculation of  $1/\tau$  given below. However, Alemohammad and Knowles (274) calculated the rate constant  $k \text{ sec}^{-1}$  for glycerol permeation with the assumption that change in volume ( $\Delta\text{vol}$ ) was proportional to change in absorbance ( $\Delta A$ ). We have therefore used this assumed relationship for some calculations (where indicated) in order to be able to compare our data with those presented by these authors.

As stated above, we applied relaxation kinetics to calculate  $1/\tau \text{ sec}^{-1}$  (287, 288) which, for the passive permeation process, has the same value as the first order rate constant  $k \text{ sec}^{-1}$  calculated by Alemohammad and Knowles (274). Thus:

$$\Delta\text{vol}_t = \Delta\text{vol}_{\text{max}} \cdot e^{-t/\tau}$$

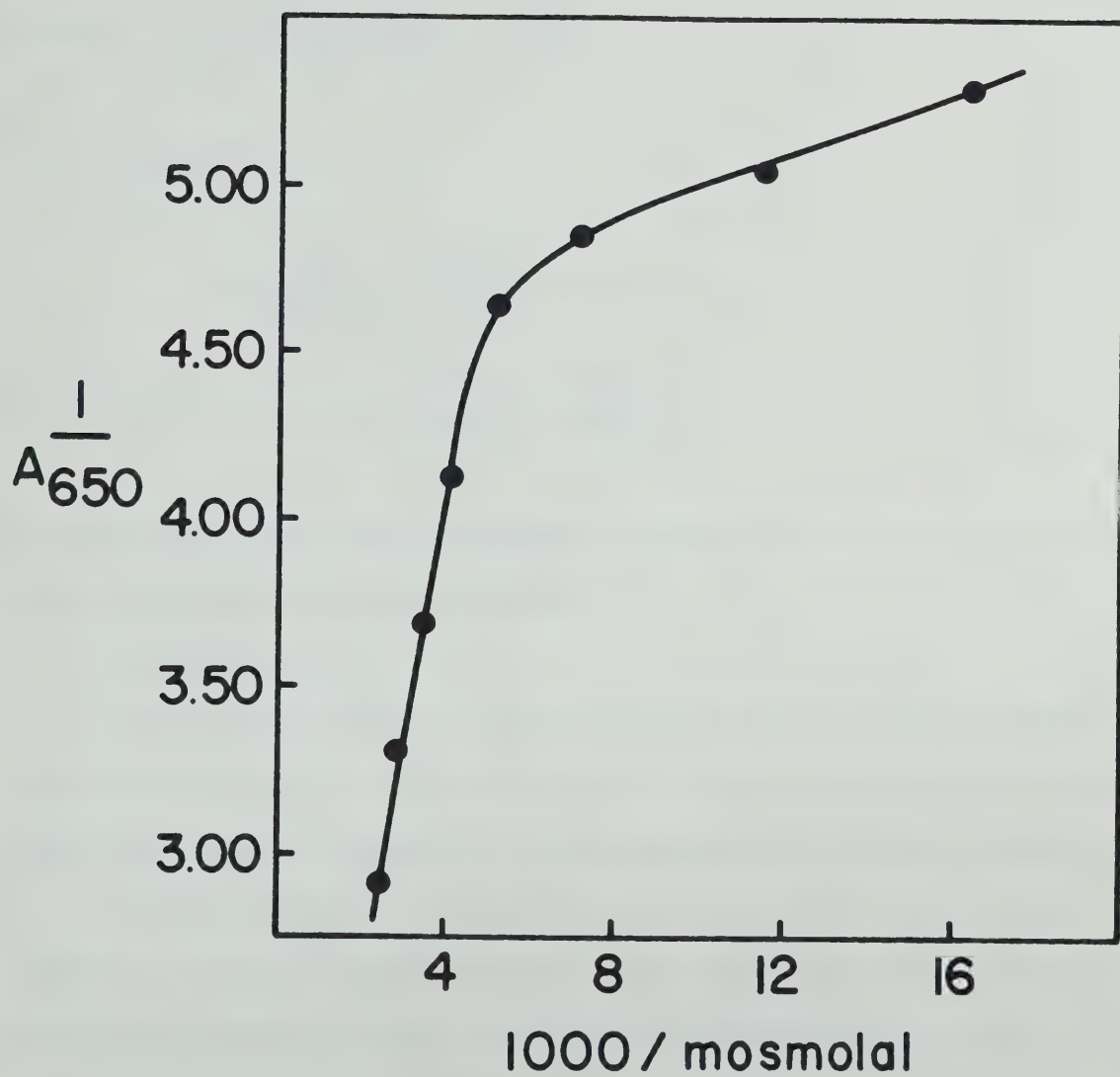
$$\text{i.e.} \quad (\text{vol}_t - \text{vol}_\infty) = (\text{vol}_0 - \text{vol}_\infty) \cdot e^{-t/\tau}$$

where  $\text{vol}_0$  = volume at a chosen zero point on the second phase





FIGURE 2. Double reciprocal plot showing the relationship between cell volume ( $1/A_{650}$ ) and reciprocal tonicity using Ficoll correction for  $n$ . E. coli K1060 was grown in xylose medium (Chapter II) with oleic acid-supplementation. The cells were harvested at mid-exponential phase, washed once with 250 mM sucrose containing 3.365% w/v Ficoll-400, and resuspended in the same solution. Samples (50  $\mu$ l) of this thick suspension were mixed with 3.75 ml of sucrose solutions of various concentrations, the refractive indices of which had been adjusted to that of the 250 mM sucrose plus 3.365% Ficoll solution. These suspensions were equilibrated for 2 min at room temperature and the absorbance at 650 nm determined. The osmolal concentration of each of the sucrose solutions was also determined.







of the trace (increasing transmittance)

$\text{vol}_t$  = vol at time  $t$  sec relative to the chosen zero

$\text{vol}_\infty$  = volume of the cells at equilibrium (asymptote).

Hence, 
$$\ln \left[ \frac{\text{vol}_t - \text{vol}_\infty}{\text{vol}_0 - \text{vol}_\infty} \right] = \frac{-t}{\tau}$$

and since  $\text{vol} \propto 1/A$ ,

$$\ln \left[ \frac{(1/A)_t - (1/A)_\infty}{(1/A)_0 - (1/A)_\infty} \right] = \frac{-t}{\tau}$$

The slope of a plot of  $\ln \left[ \frac{(1/A)_t - (1/A)_\infty}{(1/A)_0 - (1/A)_\infty} \right]$  vs.  $t$  is  $-1/\tau$ .

For calculating  $k$ , first order kinetic treatment was applied as reported by Alemohammad and Knowles (274).

## 7. Enzyme Assays

Glucose-6-phosphate dehydrogenase (D-glucose-6-phosphate:NADP<sup>+</sup> oxidoreductase [EC 1.1.1.49]) was assayed as described by Langdon (289), using a Beckman DBG T spectrophotometer equipped with a chart recorder.

Aerobic glycerol-3-phosphate dehydrogenase (EC 1.1.99.5) was assayed in membranes (mixed inner plus outer membranes) as well as in whole cells, by the procedure described by Schryvers et al. (244).

## 8. Preparation of Mixed Inner and Outer Membranes for G3PDH Assay

This was done as described by Schryvers et al. (244).

## 9. Swelling of Spheroplasts

In some initial experiments, spheroplasts prepared from non-induced cells were employed for the swelling rate assay using the Zeiss PMQII spectrophotometer. This was done in an attempt to find ways of



averting the possible problems that could arise as a consequence of the presence of the cell wall when whole cells were used (174). However, in order to keep the fragile spheroplasts stable, a suspending solution of non-penetrant sucrose in 100 mM tris HCl pH 7.5 containing 20 mM  $\text{MgCl}_2$  of about 1000 milliosmolal total concentration was required. The swelling experiments therefore had to be performed in glycerol solutions in the same tris buffer made isotonic with respect to this suspending medium by the addition of the appropriate amounts of sucrose (see Fig. 3A - C). These conditions were grossly inadequate for these experiments because of the very high viscosity of these solutions. All the experiments reported here therefore were performed with whole cells for this reason.

#### 10. Differential Thermal Analysis

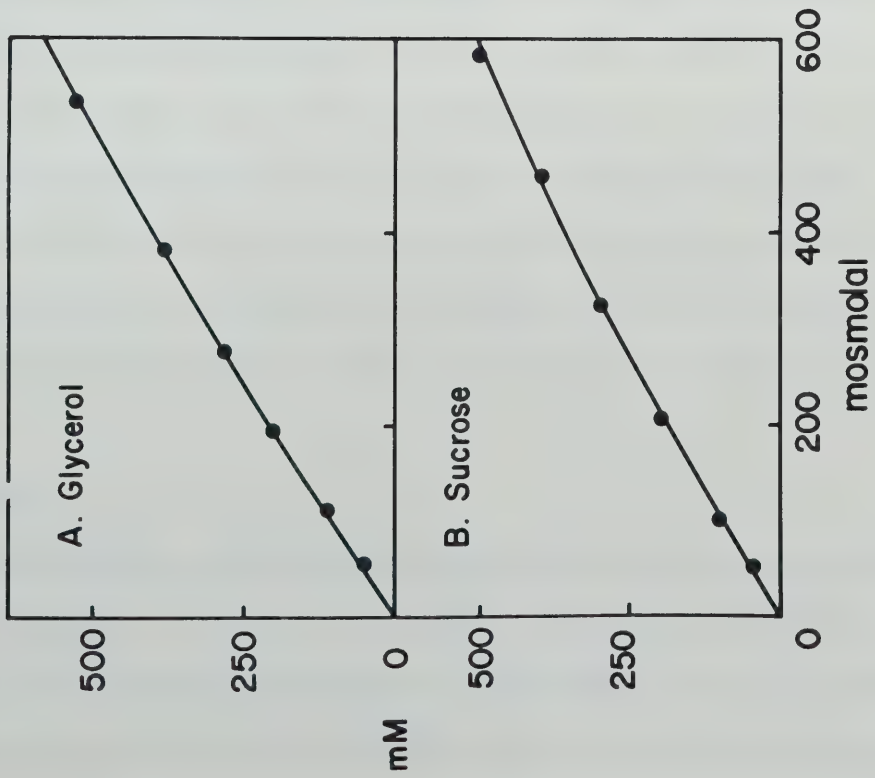
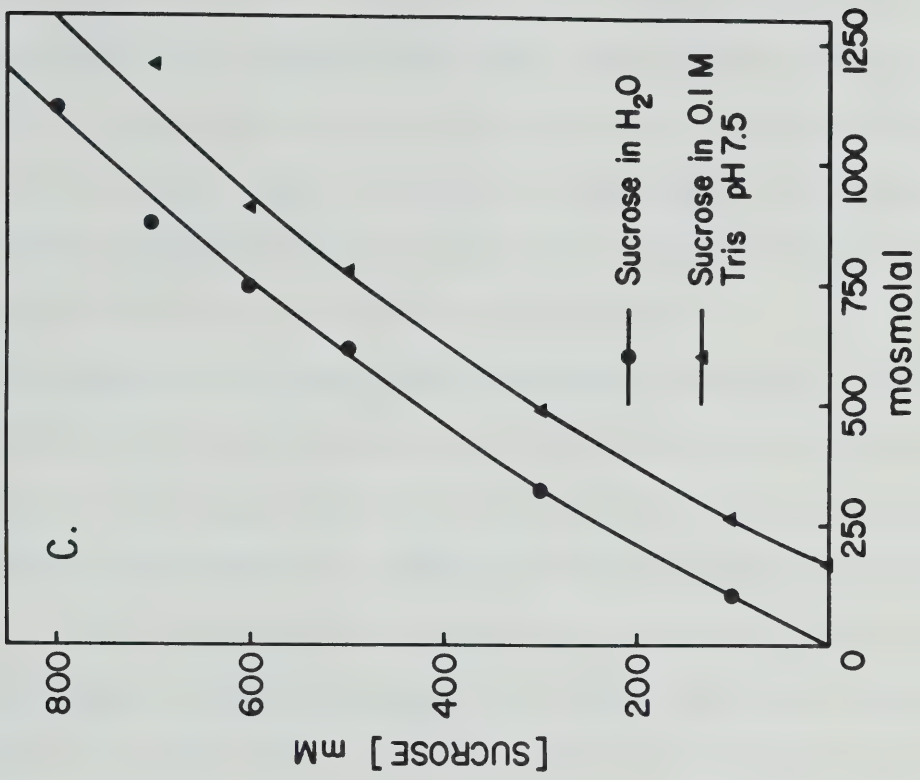
It has been demonstrated by Jackson and Sturtevant (61) that the DSC scans of whole cells and derived lipids of E. coli K1060 grown in the presence of 18:1t are similar. Baldassare et al. (60) have also shown that such scans for E. coli inner membranes are in agreement with those for the derived lipids. For these reasons, in addition to the fact that DTA thermograms obtained from inner membranes using macro sample tubes were not cooperative enough to detect, the DTA thermograms reported here were obtained from either inner membrane lipids or whole cell lipids. In order to avoid the large endotherm for water, these lipid samples were dispersed in 50% v/v ethylene glycol, since it has been reported (60, 290) that this glycol does not adversely affect the DSC scans of E. coli membranes and lipids. Thus, the DTA thermograms presented here reflect those of the lipids in situ (60).

The DTA curves were obtained from a DuPont 900 Thermal Analyzer





FIGURE 3A - C. Relationship between millimolar and milliosmolal (i.e. milliosmoles/Kg of H<sub>2</sub>O) concentrations of aqueous solutions of (A) glycerol, (B) sucrose, (C) higher concentrations of sucrose (-●-●-) and sucrose in 0.1 M Tris pH 7.5 (-▲-▲-).







using glass micro tubes with glass beads as a reference material. Analyses were done at the highest instrumental sensitivity at heating rates of 5 or 10 centigrade degrees (C°) per minute. Cooling rates of up to 10 C° per minute could be obtained by circulation of nitrogen gas, chilled by passage through a copper coil immersed in liquid nitrogen, through the differential thermal analysis cell.

The isolation of E. coli inner membranes, and lipid extraction from whole cells or inner membranes were done as detailed in Chapter II. The solution of the lipid extract was evaporated to dryness on a rotary evaporator and then taken up in a minimum volume of chloroform:methanol (2:1 v/v). This lipid solution was carefully transferred into the DTA micro sample tube using a very-fine-tip micropipet and evaporating off the solvent after each small aliquot was added to the sample micro tube. The last traces of solvent were removed over  $P_2O_5$  in a vacuum oven at room temperature overnight. (The sample could be stored frozen at this stage, if the need arose, after the tube had been sealed over a flame.) Hydration was effected with 50% v/v ethylene glycol added at 2  $\mu$ l/mg lipids and centrifuging in the clinical centrifuge at top speed. This ensured expulsion of air bubbles and tight-packing of the pellet, but to ensure efficient solvation, it was necessary to seal the tube and spin to pack the pellet at each end of the tube alternately.

## C. RESULTS

### 1. Relationship between Cell Volume and Reciprocal Absorbance

Figure 2 relates the variation of reciprocal absorbance at 650 nm to the reciprocal osmolality of suspensions of E. coli strain K1060 in non-permeant sucrose solutions whose refractive indices (n)



had been adjusted to the same value with Ficoll-400 as described in the legend to this figure. Since it has earlier been demonstrated in other systems (74) that cell volume ( $1/A$ ) is linearly dependent on the reciprocal tonicity of non-penetrant solute, we surmise that these cells behave as ideal osmometers in the concentration range 200 milliosmolal to at least 400 milliosmolal, obeying the Boyle-Mariotte-van't Hoff law (285) under these conditions. It is noteworthy that the correction for refractive index was essential here where absolute absorbance values were measured. In the swelling experiments where changes in absorbance were monitored, however, we found that this correction for  $n$  was not necessary (Table II).

## 2. Typical Oscilloscope Trace and Calculation of $1/\tau$

From a typical oscilloscope trace (Fig. 4) a  $1/\tau$  value of  $0.095 \text{ sec}^{-1}$  has been calculated (Fig. 5). The fact that the plot from which  $1/\tau$  was calculated was always a single straight line passing through the origin showed that there was no lysis of the cells during swelling. This conclusion was supported by the failure to detect glucose-6-phosphate dehydrogenase activity in E. coli suspended in hypertonic glycerol, unless the suspension was first treated with toluene (273).

## 3. Data Treated to Yield First Order Rate Constant $k \text{ sec}^{-1}$

Oscilloscope traces at  $25^\circ\text{C}$  and varying effective glycerol concentrations were used to yield the first order rate constant  $k \text{ sec}^{-1}$  (Fig. 6). It is obvious that  $k$  decreases in value as the permeant concentration increases between 75 mM and 500 mM.

Neither the reciprocal relaxation time ( $1/\tau \text{ sec}^{-1}$ ) nor the first order rate constant ( $k \text{ sec}^{-1}$ ) is constant for the passive permeation of glycerol in noninduced cells (Tables II and III). The same trend, i.e.,





Figure 1. Relationship between the number of people and the number of people per room.

FIGURE 4. Typical oscilloscope trace. E. coli K1060 was grown in M63 supplemented with oleic acid and glycerol (see Chapter II) and prepared as detailed in Methods. The trace shown here was generated on treating these cells with 200 mM glycerol at 27.8°C.



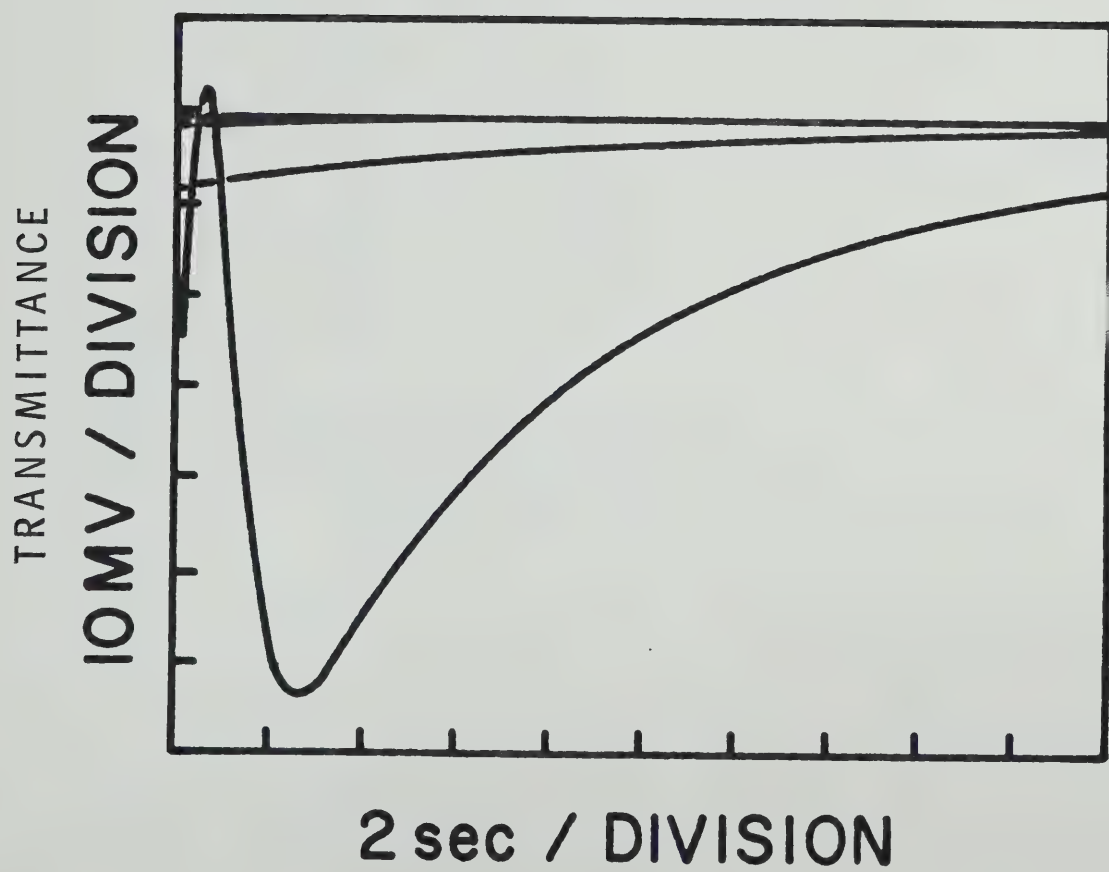






FIGURE 5. Typical calculation of  $1/\tau \text{ sec}^{-1}$ . Points were taken from the second phase (transmittance increase) of Fig. 4. Transmittance was converted to absorbance using Lambert-Beer Law and the calculation effected as described in Methods.

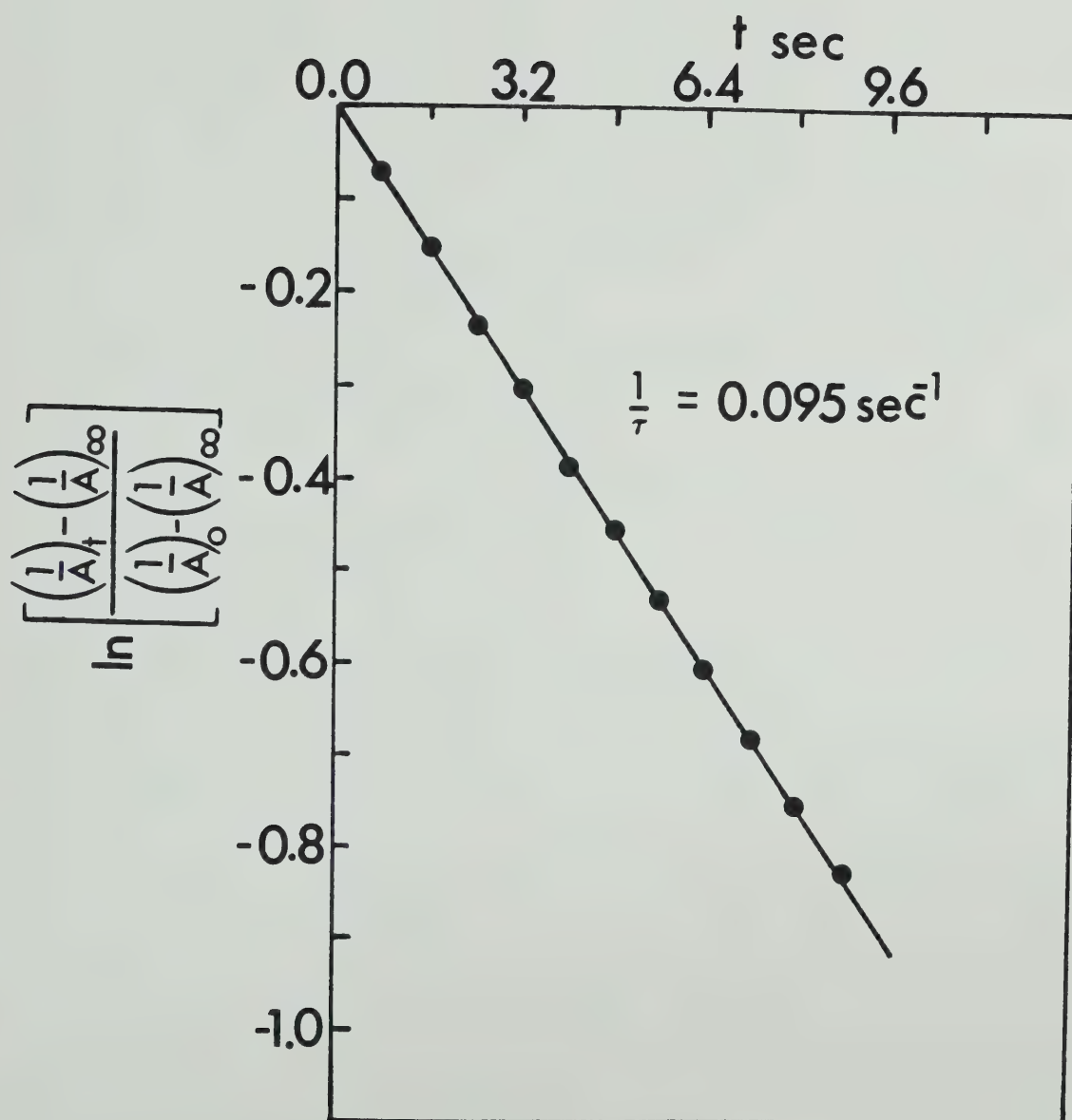








FIGURE 6. Data treated to yield first order rate constant  $k \text{ sec}^{-1}$  for passive glycerol permeation in E. coli K12F<sup>-</sup>. E. coli K12F<sup>-</sup> was grown, harvested, washed and resuspended as described in Table II. The stopped-flow traces were then treated to yield  $k \text{ sec}^{-1}$  for the passive glycerol permeation, with the assumption that  $\Delta A_{550} \propto \Delta \text{volume}$ .

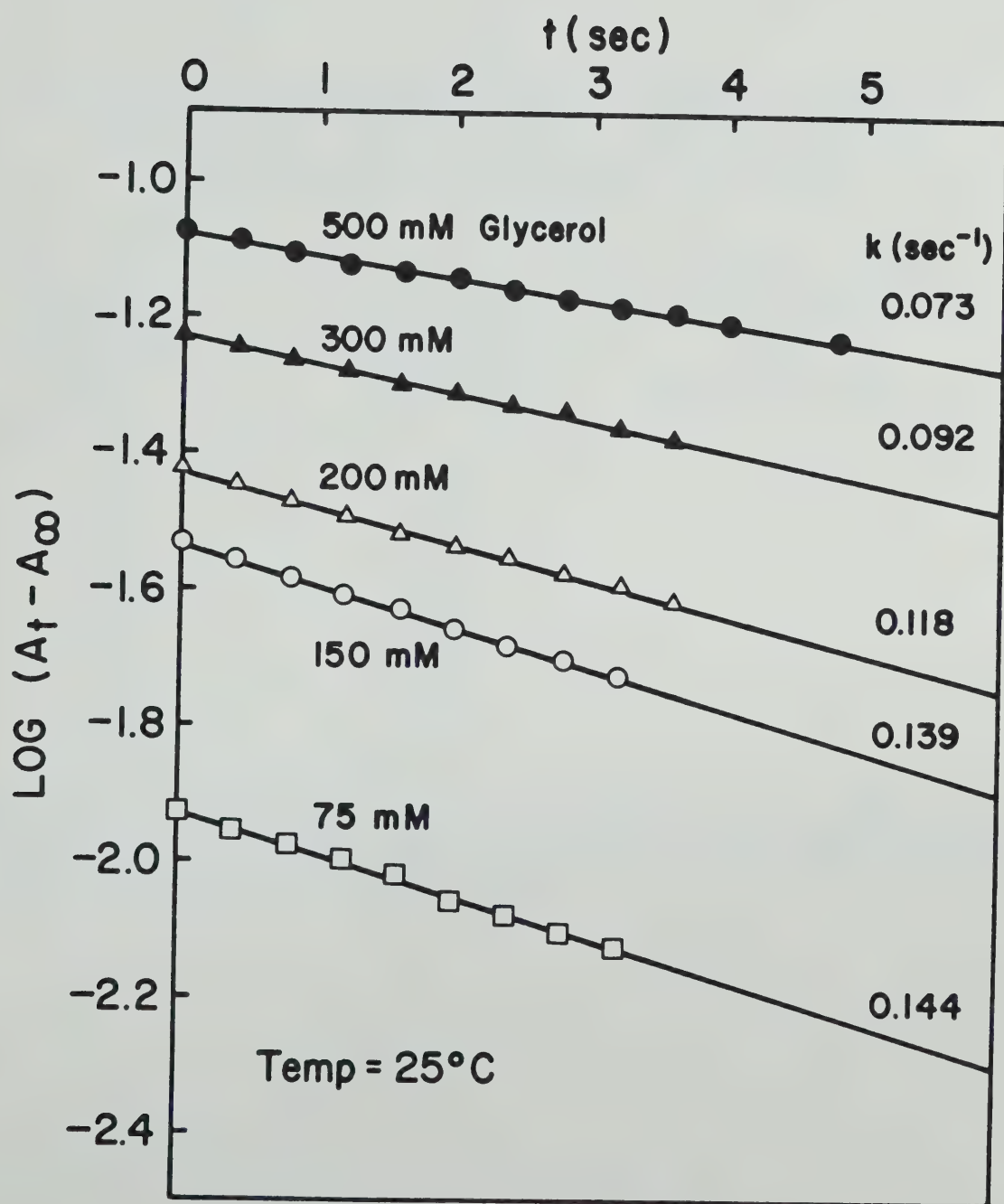




TABLE III

$1/\tau$  Values of Glycerol Passive Permeation at 25°C in *E. coli* K12F<sup>-</sup>  
 Calculated on the Basis of  $\Delta(1/A) \propto \Delta\text{Volume}$  and also, for  
 Comparison, First Order Rate Constants  $k \text{ sec}^{-1}$  for the Same  
 Process Calculated on the Basis of  $\Delta A \propto \Delta\text{Volume}$

Effective glycerol concentration (mM)	$1/\tau(\text{sec}^{-1})$ at 25°C calculated on the basis of $\Delta(1/A) \propto \Delta\text{vol}$	$k(\text{sec}^{-1})$ at 25°C calculated on the basis of $\Delta A \propto \Delta\text{vol}$ (Data taken from Fig. 6)
75	0.141	0.144
150	0.121	0.139
200	0.108	0.118
300	0.077	0.092
500	0.056	0.073

*E. coli* K12F<sup>-</sup> was grown in M9 plus glucose medium without UFA/Brij 58 as described in "Methods". The cells were washed three times in 10 mM imidazole·HCl pH 7.0, suspended to A<sub>550</sub> of 0.35 in the same buffer and then equilibrated for 12 hr before use.



a decrease in  $1/\tau$  (or  $k$ ), is observed irrespective of which parameter was measured for change in volume,  $\Delta(1/A)$  or  $\Delta A$ . In addition, this deviation from constancy is not a result of refractive index differences since the same values were obtained from the same batch of cells (Table II) whether or not refractive index was corrected for.

As indicated by Fig. 7(A)(i), the deviation from linearity seen in the dependence of initial swelling rates on glycerol concentration could not be due to the presence of a saturable component contributed by some residual level of the glycerol facilitator. Stein (291) reported that  $10^{-7}$  M  $\text{Cu}^{2+}$  is a potent inhibitor of the glycerol facilitator in erythrocytes. Glycerol facilitated diffusion was completely inhibited by  $5 \times 10^{-7}$  M  $\text{CuCl}_2$  in E. coli K1060 grown in the presence of glycerol, but  $\text{CuCl}_2$  did not eliminate the anomalous behavior in question. The cells used for these experiments on the dependence of passive permeation rate on glycerol concentration were grown in the presence of glucose. Glucose is known to repress the permeability of E. coli to glycerol (269), probably by catabolite-repression of the synthesis of the facilitator protein. Aerobic glycerol-3-phosphate dehydrogenase (EC 1.1.99.5) activity could not be detected in cells grown in the presence of glucose or xylose (Table I). This result supports the notion that glucose-grown cells were noninduced for Glp function, since it has been suggested (269) that the system for glycerol facilitated diffusion in E. coli belongs to the L- $\alpha$ -glycerophosphate regulon described by Cozzarelli, Freedberg and Lin (292) to which the aerobic glycerol-3-phosphate dehydrogenase also belongs. It should be noted that the same trends in variation of  $1/\tau$  with concentration of glycerol were observed with induced cells although the values obtained were much higher.







FIGURE 7A. Dependence of initial swelling rates of E. coli K1060 on glycerol concentration, as measured by conventional spectrophotometry. The cell was grown in M63 plus glucose and oleic acid and washed and prepared as described in Methods. (i) Initial swelling rates  $\{[(1/A)(d(1/A)/dt)]\text{hctosec}^{-1}\}^*$  at 20°C in glycerol in the presence of  $5 \times 10^{-7}$  M  $\text{CuCl}_2$ . Calculation of initial rates was done on the basis of  $\Delta(1/A) \propto \Delta\text{volume}$ . (ii) Same as (i) but initial swelling rates  $(dA/dt)\text{min}^{-1}$  at 20°C were calculated on the basis of  $\Delta A \propto \Delta\text{volume}$ . \*hctosec = 100 sec.

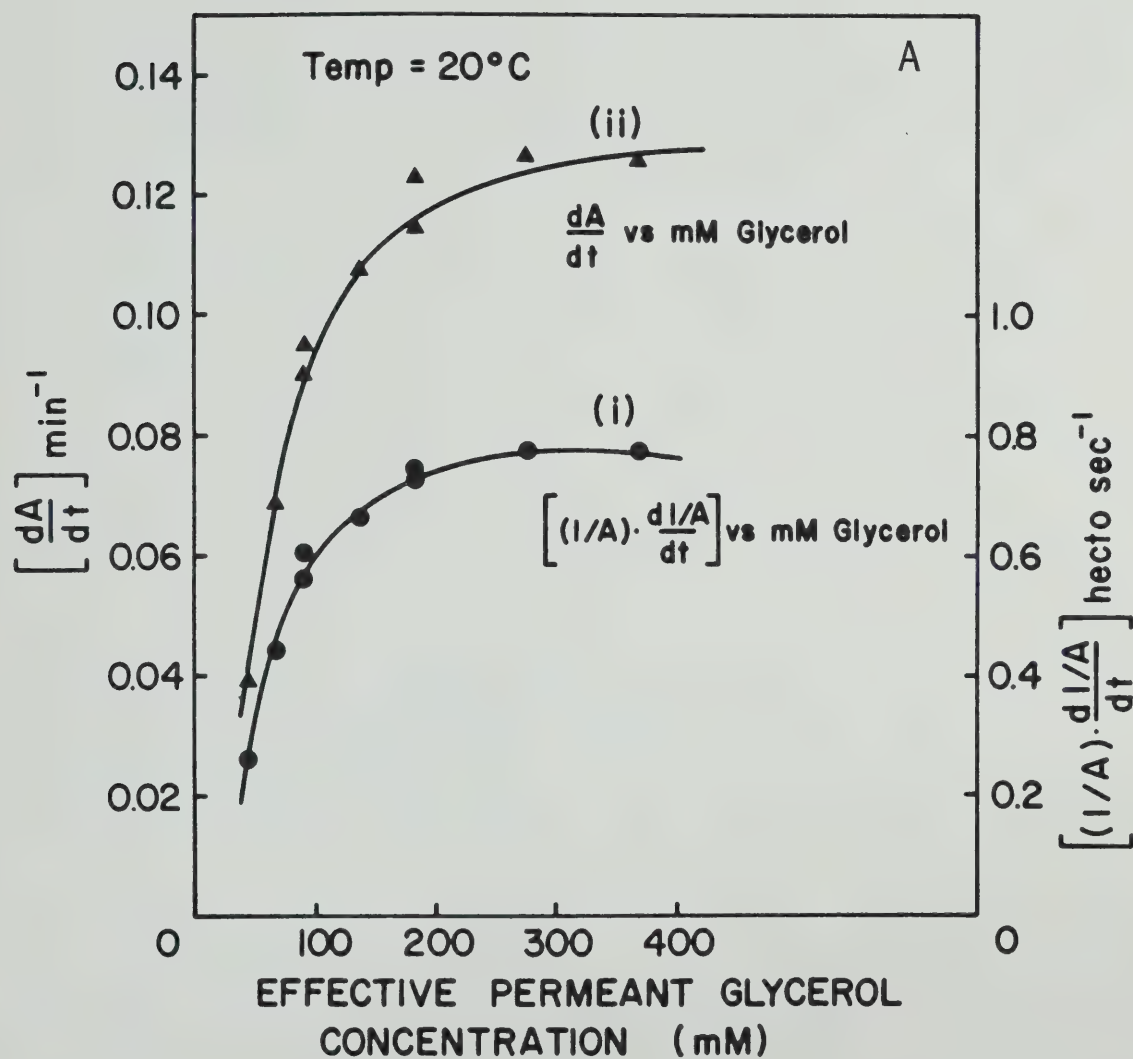






FIGURE 7B & C. Dependence of initial swelling rates of E. coli K1060 on glycerol or erythritol concentration, as measured by conventional spectrophotometry. (B) Initial swelling rates at 25°C in glycerol solutions the refractive indices of which were adjusted to the same value with Ficoll-400. (C) Initial swelling rates in erythritol at 30°C.

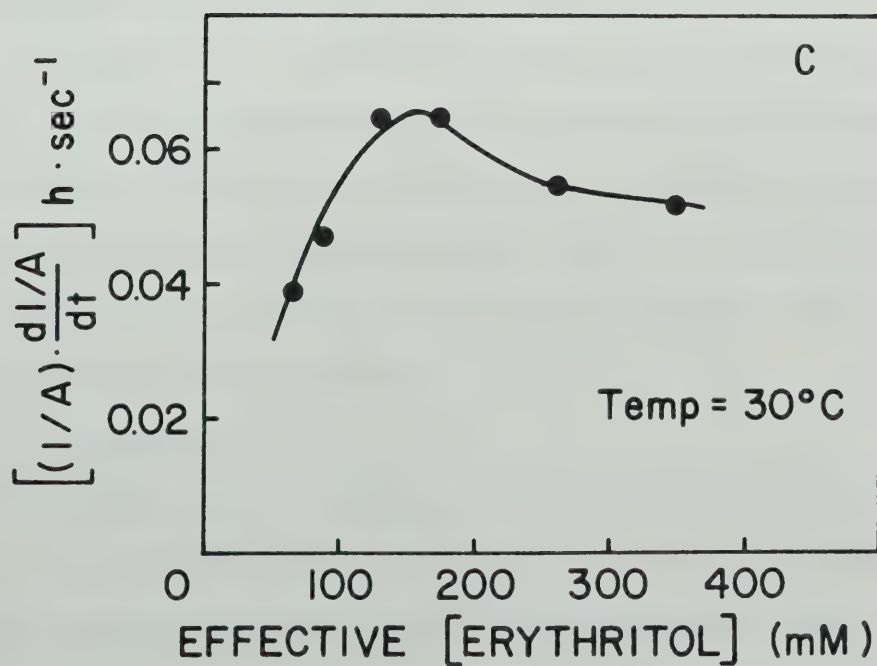
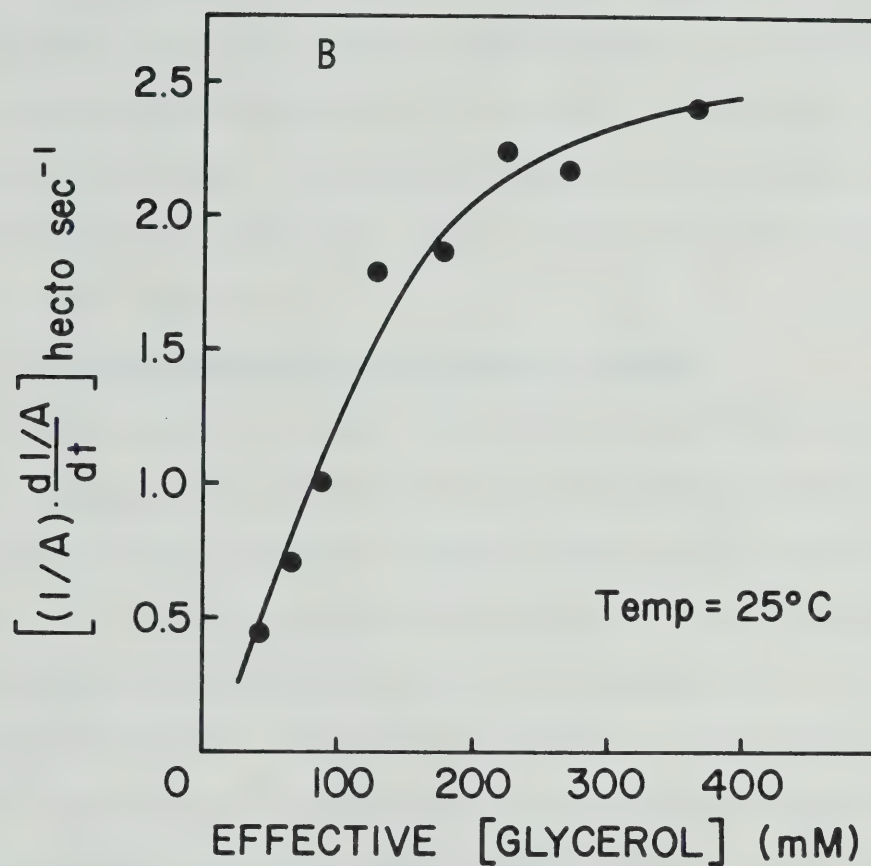






Figure 7B represents the variation of initial swelling rates (of non-induced K1060 cells) with glycerol concentration at 25°C in solutions whose  $n$  values were adjusted with Ficoll-400. In Figure 7C, the concentration-dependence of initial swelling rates of noninduced K1060 in erythritol at 30°C is reported. The non-linearity in the curves is obvious in both these cases.

#### 4. The Time-Dependence of the Osmotic Response

Alemohammad and Knowles (274) did not specify the time of incubation of E. coli in the dilute buffer before injection of the cells into the hypertonic solution of permeant compound. We have observed, however, that all four E. coli strains tested were not osmotically sensitive immediately after washing with, and suspension in, dilute buffer. Irrespective of whether the cells were induced or noninduced for the glycerol facilitator, they required at least 8 h incubation at room temperature before adequate osmotic sensitivity was restored. If swelling experiments were done soon after suspension of the cells in dilute buffer, the amplitude of swelling was small and  $1/\tau$  values calculated from the data were abnormally high. The absence of glucose-6-phosphate dehydrogenase in the suspending medium after suspension attested to the integrity of the inner membrane at this stage. The inner membrane could, nonetheless, be sufficiently leaky to small molecules like glycerol to prevent normal swelling.

#### 5. DTA Results

The differential thermograms obtained for the aqueous dispersions of the extracted lipids from whole cells and inner membranes of E. coli are given in Figure 8A and B. The thermograms from lipids from whole cells and inner membranes of mutant K1060 grown in the presence





FIGURE 8A. Differential Thermal Analysis of lipids from whole cells of E. coli K1060 grown with 16:1t- and 18:1c-supplements, as well as lipids from inner membranes of 16:1t-grown K1060. All the thermograms were obtained with lipids dispersed in the presence of 50% ethylene glycol as stated in the text (see Methods).  $T_l$  was established from the cooling curve while  $T_h$  was established from the heating curve and  $T_m^*$  was obtained by comparison of areas under the curves (see ref. 72).

\* $T_m$  is used here as an operational definition for the midpoint of the broad phase transition when 50% gel phase lipid co-exists with 50% liquid crystalline lipid. This definition assumes that the enthalpies of all the phospholipid species are the same.

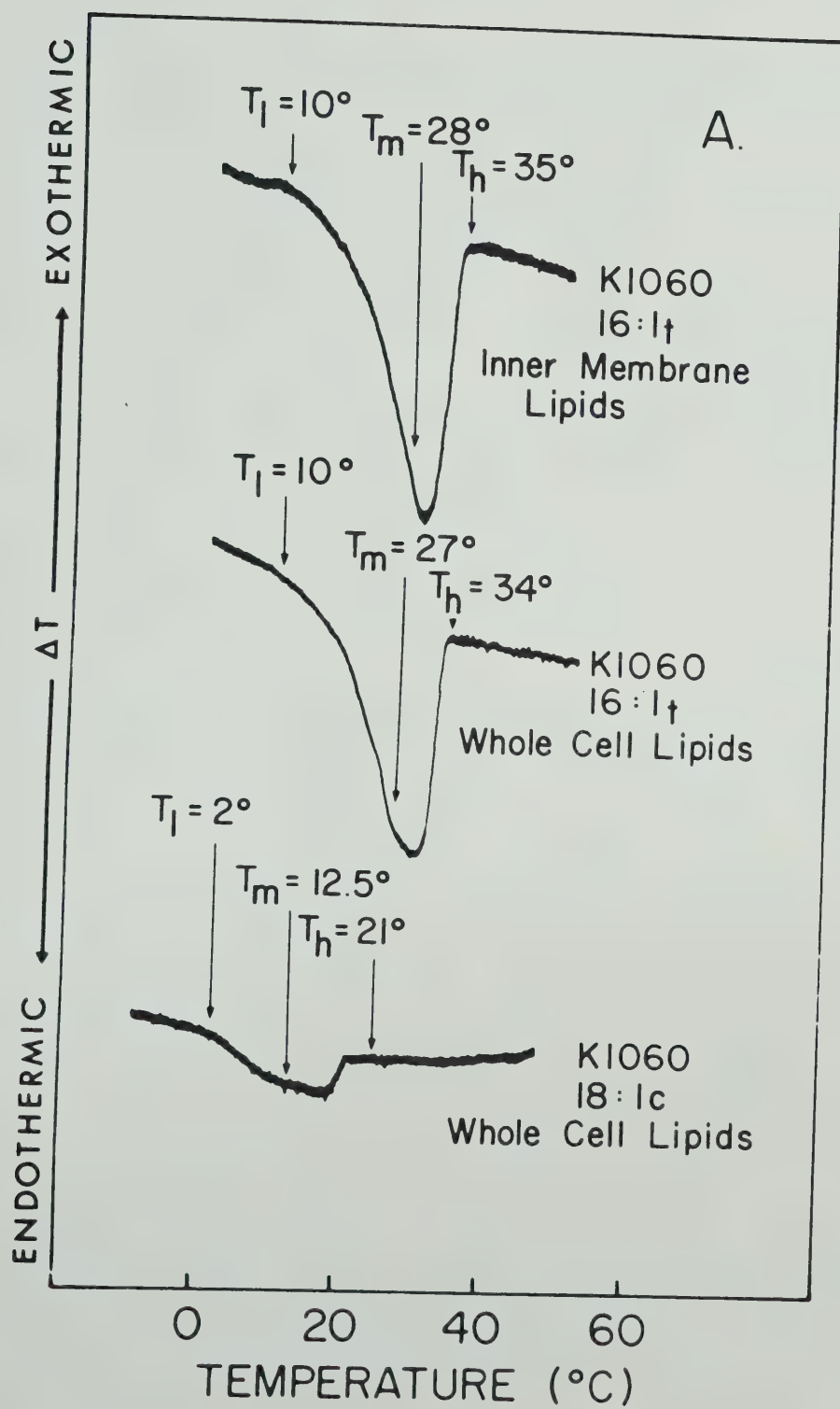
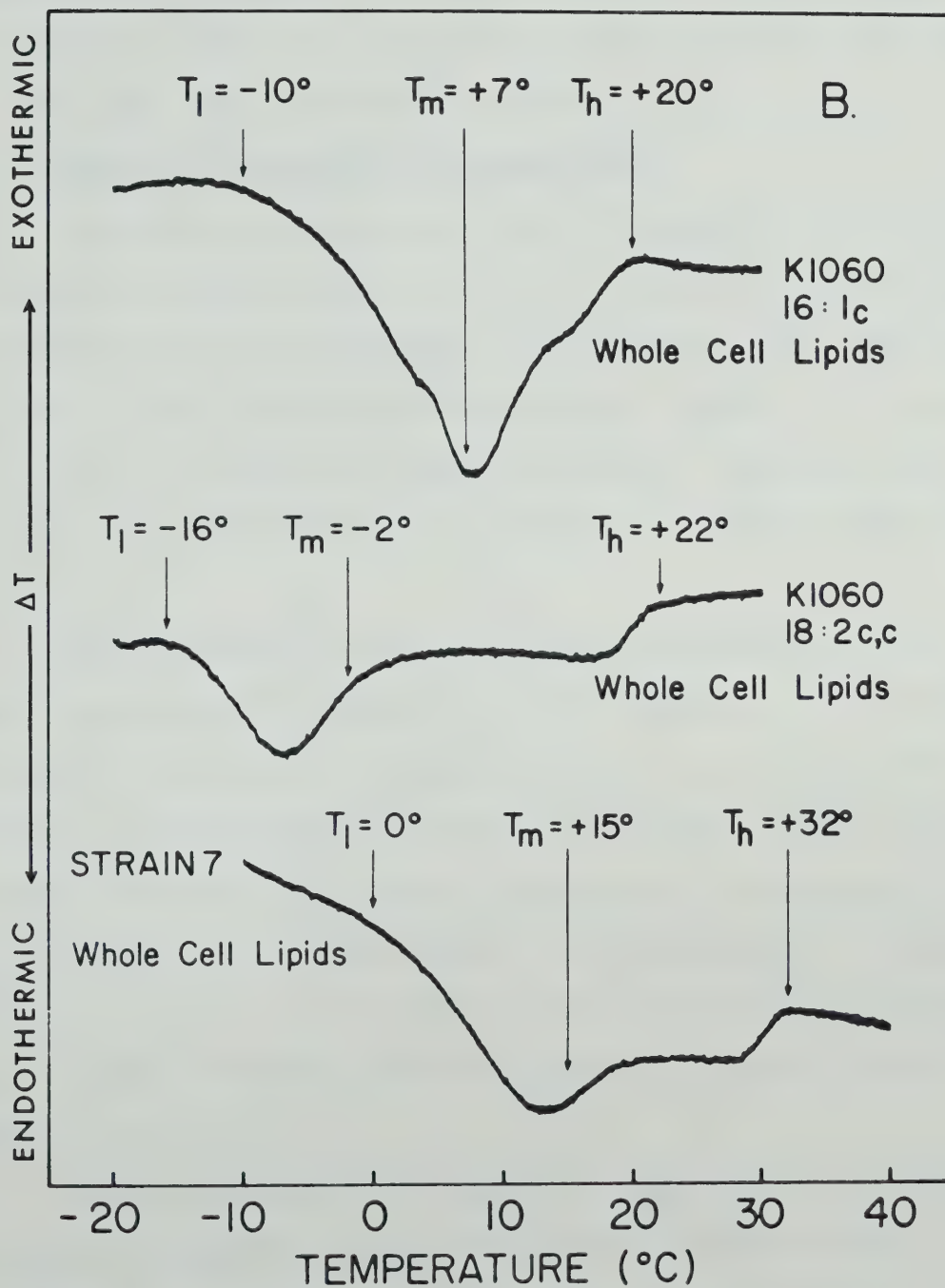








FIGURE 8B. Differential Thermal Analyses of lipids from whole cells of strain K1060 grown in 16:1c and 18:2c,c and of lipids from strain 7. Thermograms were obtained as for Fig. 8A.





of 16:1t (Fig. 8A) demonstrate the similarity between these two lipid samples and confirm earlier DSC data (61). The phase transition boundaries ( $T_l$  and  $T_h$ ) and midpoints ( $T_m$ ) derived from these thermograms are collected in Table IV. The values for 18:1t grown K1060 cells given in this table have been taken from reference 61.

#### 6. Temperature-Dependence of Glycerol Uptake

The foregoing results suggest that the permeation of glycerol in noninduced E. coli is complicated, possibly due to the presence of the cell wall and periplasmic space in this bacterium (174). The precise basis of this complex behavior is unknown. However, it is assumed that if it is a consequence of some perturbation of either the inner membrane or cell wall (or both), it should not be markedly temperature-sensitive.

With this assumption, the temperature dependence of both the passive permeation and facilitated diffusion of glycerol in mutant K1060 grown under a variety of UFA regimes was studied by the stopped flow technique at 400 mM effective glycerol concentration. Similar experiments with 200 mM effective glycerol concentration gave essentially similar Arrhenius plots to those obtained at 400 mM glycerol, but the absolute values of  $1/\tau$  were a bit higher at the lower glycerol concentration. Technical limitations, however, prevented the use of the lower glycerol concentrations.

The data obtained on the temperature dependence of the passive permeation of glycerol in E. coli K1060 reveal a marked influence of the fluidity and physical state of the membrane lipids on the rate constant for this process. In Figure 9, the plot of  $1/\tau$  for passive permeation against temperature shifts to higher temperatures for cells



TABLE IV

Transition Ranges ( $T_1 - T_h$ ) and Midpoints ( $T_m$ ) for Lipids from Whole Cells of *E. coli* K1060 and Strain 7 Grown with Various UFA Supplements

Cells	UFA Supplement	Transition Range ( $T_1$ to $T_h$ ) (°C)		Temperature at which 50% of mem- brane lipids are liquid crystalline $T_m$
K1060	18:1t*	+30° (approx.)	+40° (approx.)	+38° (approx.)
	16:1t	+10°	+34°	+27°
	16:1c	-10°	+20°	+7°
	18:2c,c	-16°	+22°	-2°
	18:1c	+2°	+21°	+12.5°
Str 7	-	0	+32°	+15°

Data taken from Fig. 8A and B.

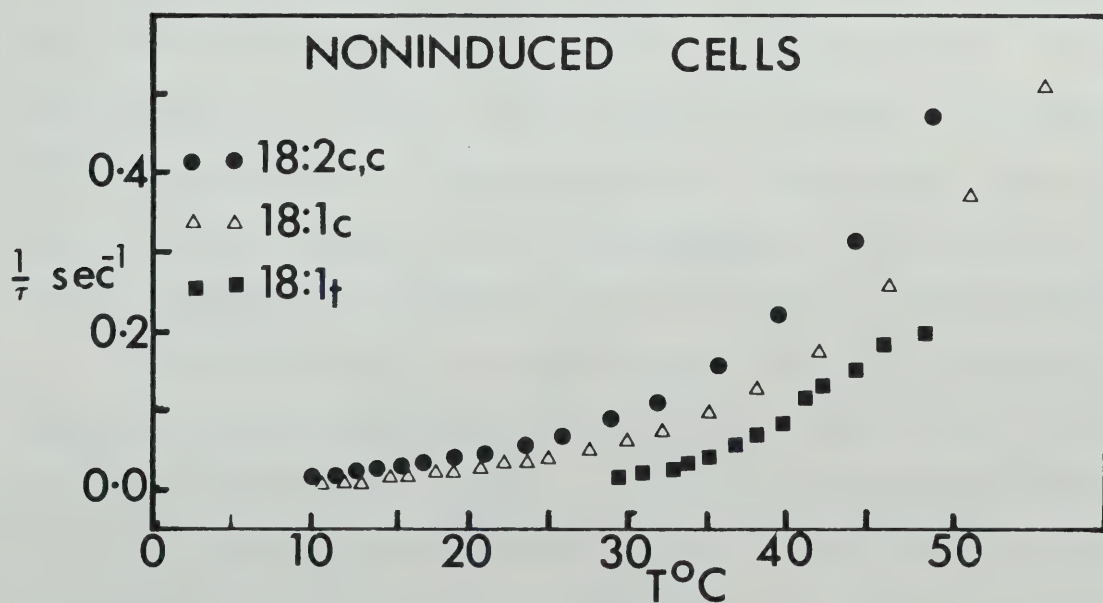
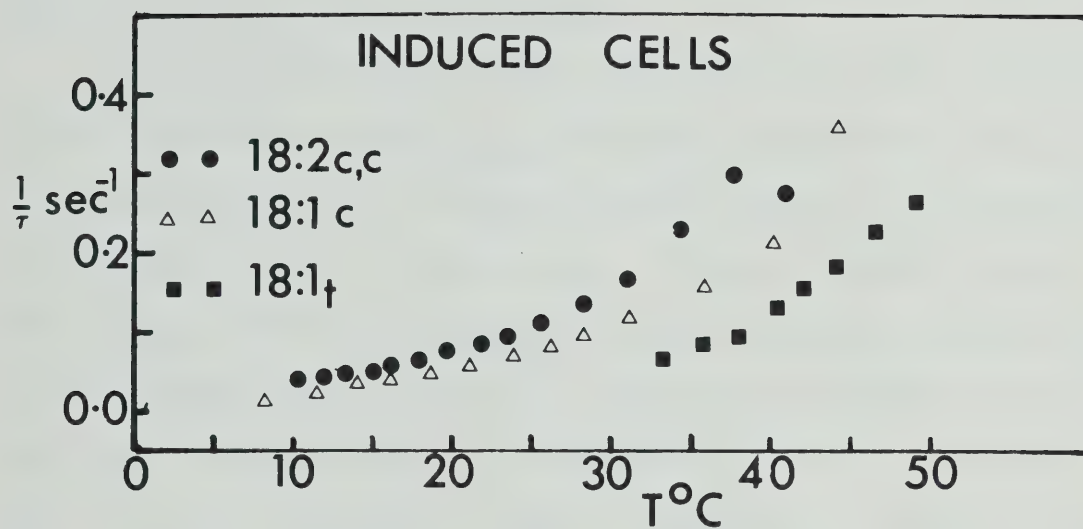
\*Values given here for 18:1t-enriched K1060 were taken from DSC scan in Figure 1 of ref. 61 [Jackson & Sturtevant, J. Biol. Chem. 252 (1977) 4749-4751].







FIGURE 9. The influence of temperature on the  $1/\tau$  values for glycerol passive permeation (lower panel) and facilitated diffusion (top panel) in E. coli K1060 grown with various UFA's. Cultures were grown in M63 in the presence of either glycerol (induced cells) or glucose (noninduced cells) together with the UFA. Cells were prepared and  $1/\tau$  values for glycerol permeation obtained with the stopped flow spectrophotometric assay procedure as given in Methods.





enriched in 18:1t and to lower temperatures for 18:2c,c-rich cells. Oleate- and palmitoleate-grown cells form an intermediate class. Thus, passive permeation of glycerol is more rapid when most (or all) of the membrane lipid is in the liquid crystalline state than when most (or all) of the lipid is in the gel state.

Differential thermal analysis (DTA) (Fig. 8A and B) and DSC of lipids from 18:1t-enriched E. coli K1060 (61) together with the fatty acid profiles (Appendix 3) indicate that the fluidity of the membranes should decrease in the following order: 18:2c,c- > 16:1c- > 18:1c- > 18:1t-cells, which is the order of decreasing transition midpoints ( $T_m$ ) for these cells (Tables IV and VI). This order of fluidity is consistent with previous reports on the membranes of other UFA auxotrophs (67, 68). It is also precisely the order of decreasing  $1/\tau$  values for glycerol passive permeation in these cells. This is therefore a demonstration that the permeating glycerol molecules sense the fluidity of the apolar core of the membrane. These results are completely in agreement with the increase in the passive permeation of glycerol and other non-electrolytes previously reported in A. laidlawii B cells (74, 211) as well as in phospholipid vesicles (209), as membrane fluidity increases.

In the Arrhenius plots shown in Figure 10C and D, no break is observed for the passive permeation rate constant in linoleate- and palmitoleate enriched cells. However, the corresponding Arrhenius plots for oleate and elaidate cells (Fig. 10A and B) display biphasic slopes intersecting at a characteristic temperature,  $T_b$ . A comparison of the areas of the DTA thermograms (Fig. 8A and B) shows that  $T_b$  for noninduced 18:1c-cells occurs when 70% of the membrane lipids are in the liquid crystalline state. However,  $T_b$  for noninduced 18:1t-cells occurs







FIGURE 10A. Arrhenius plots of  $1/\tau$  for glycerol passive permeation (top panel) and facilitated diffusion (lower panel) in E. coli K1060 cells enriched in 18:1c. Cells were prepared and glycerol permeation assayed as given in the legend for Fig. 9.

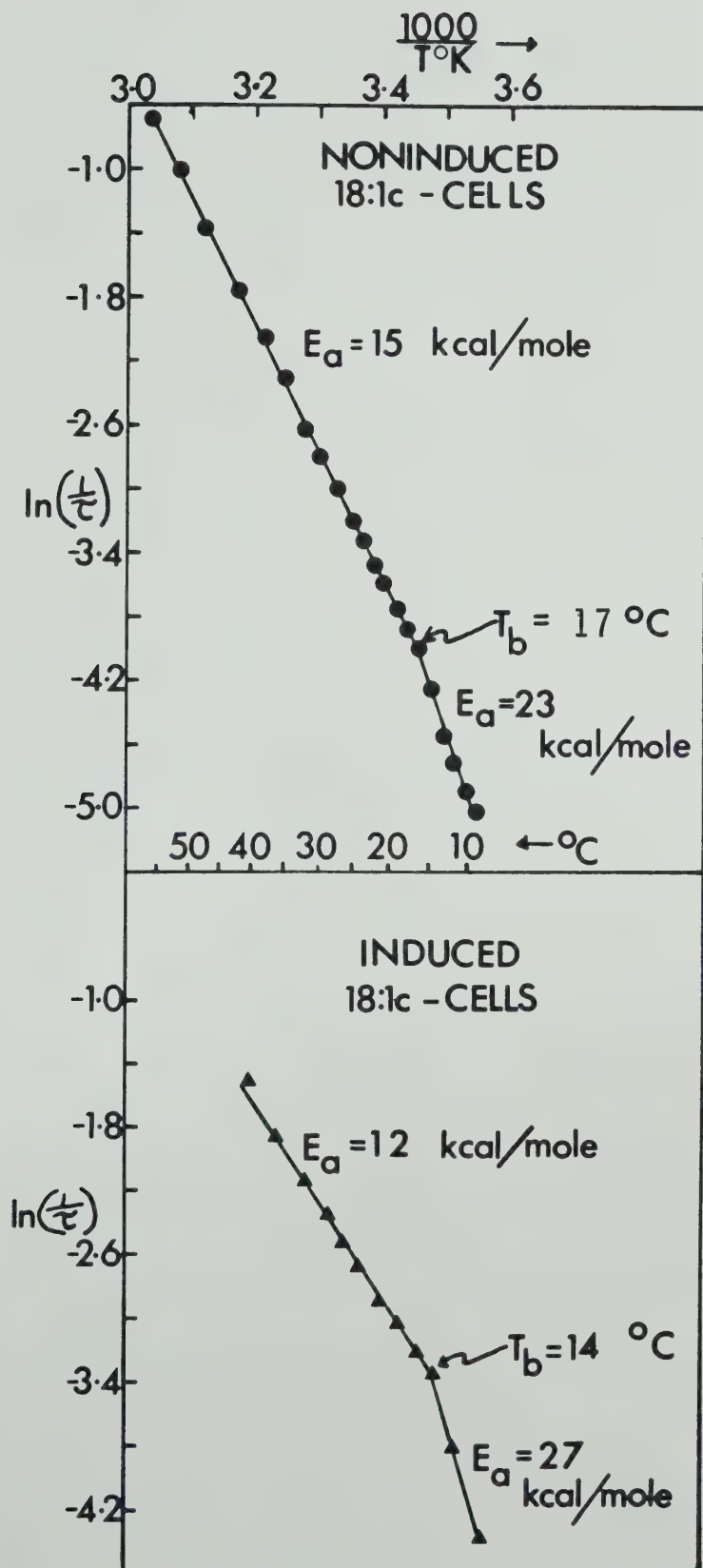






FIGURE 10B. Arrhenius plots of  $1/\tau$  for glycerol passive permeation (top panel) and facilitated diffusion (lower panel) in E. coli K1060 cells enriched in 18:1t. See Fig. 10A.

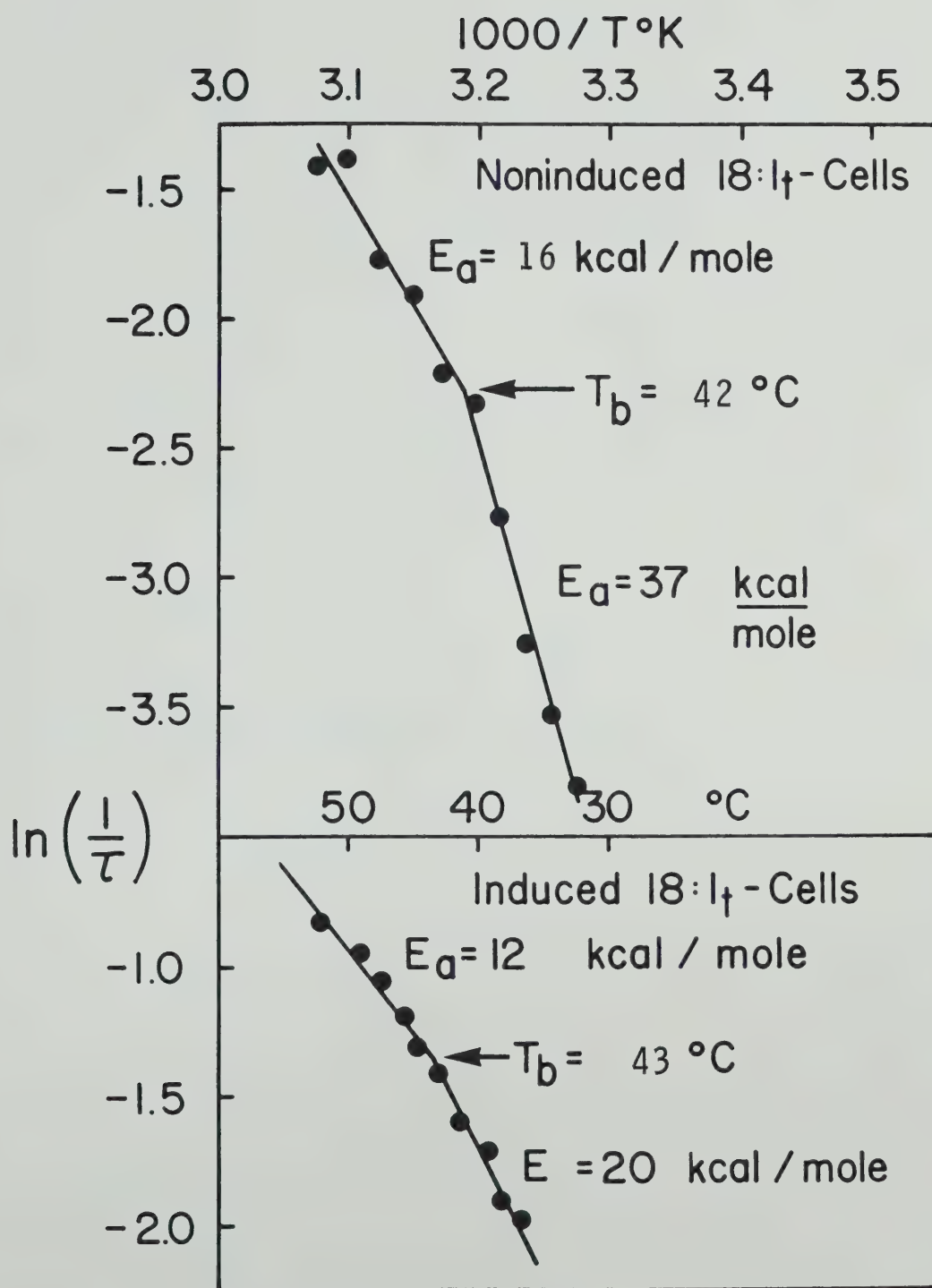








FIGURE 10C. Arrhenius plots of  $1/\tau$  for glycerol passive permeation (top panel) and facilitated diffusion (lower panel) in E. coli K1060 cells enriched in 18:2c,c. See Fig. 10A.

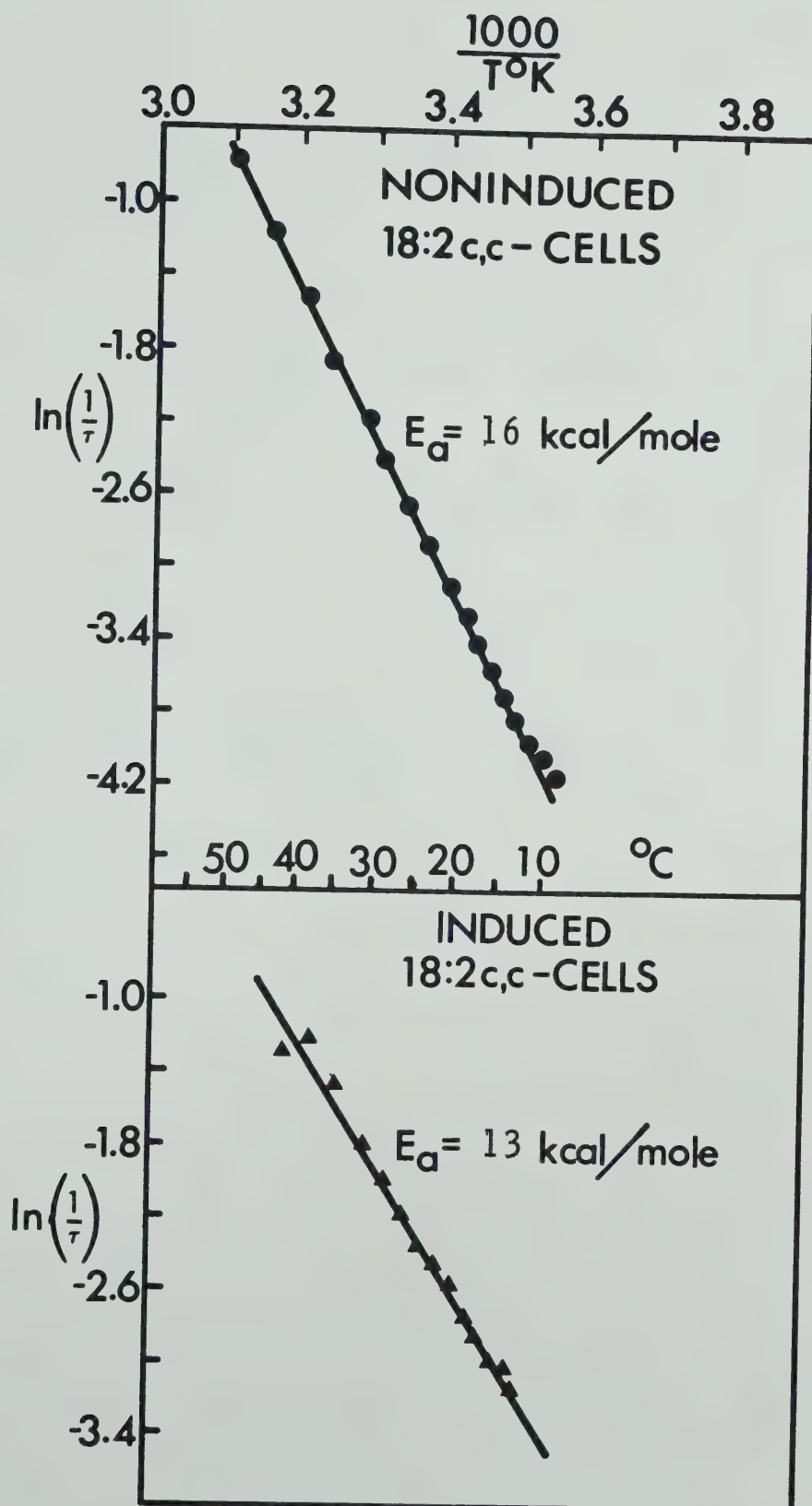
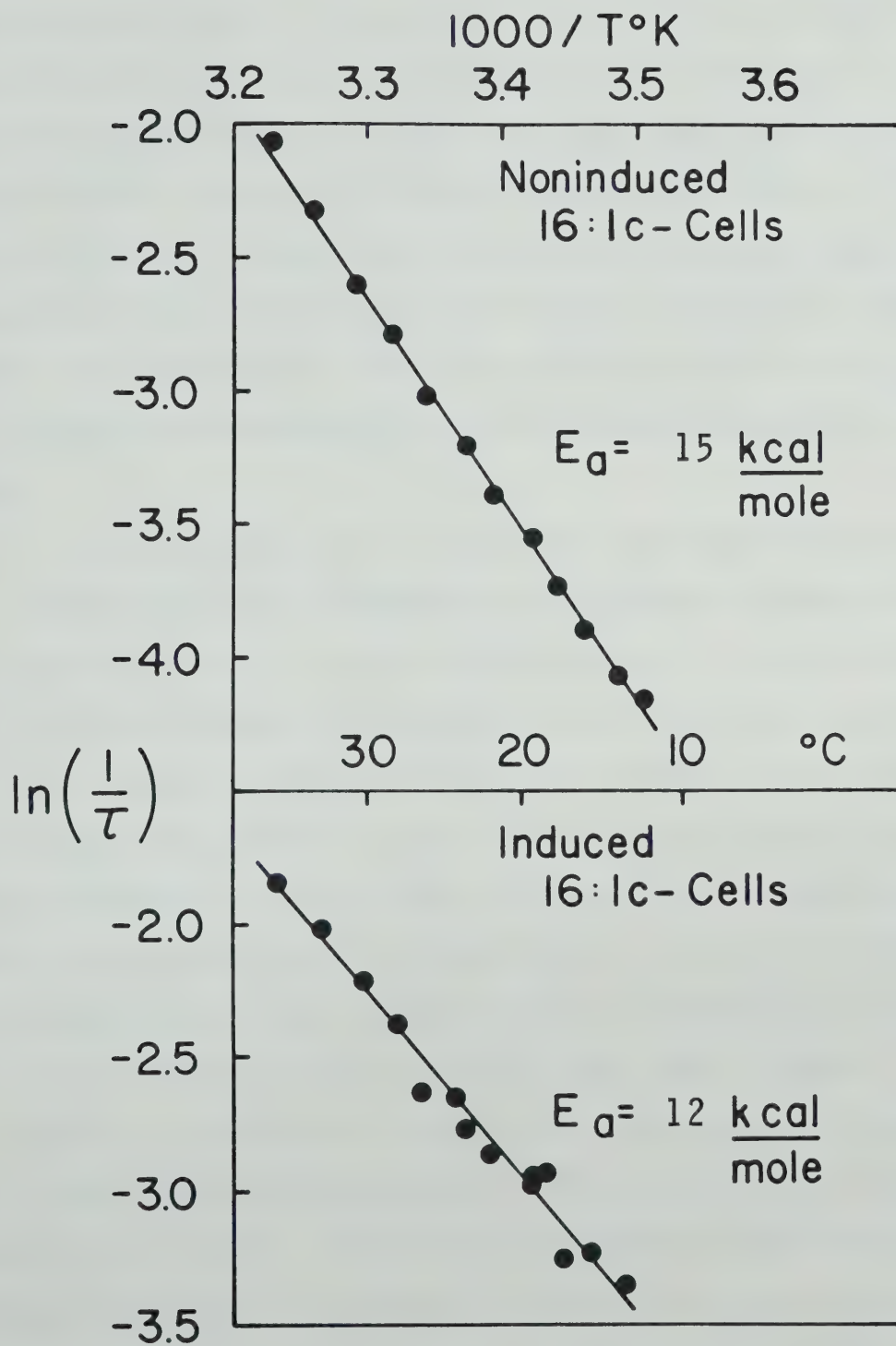






FIGURE 10D. Arrhenius plots of  $1/\tau$  for glycerol passive permeation (top panel) and facilitated diffusion (lower panel) in E. coli K1060 cells enriched in 16:1c. See Fig. 10A.







near the upper boundary, when all the membrane fatty acyl chains should be in the liquid crystalline state as judged from the DSC data in reference 61 (see Table IV). The activation energy,  $E_a$ , has a higher value below  $T_b$  than above it. The  $E_a$  value is constant above  $T_b$  for 18:1c- and 18:1t-cells and it is the same as that calculated from the slopes of the Arrhenius plots for the 18:2c,c- and 16:1c-cell (Table V). Its value is, however, slightly lower than expected for a purely passive permeation process. This observation is further discussed in a later section (see "Discussion"). Unlike the constant  $E_a$  value above  $T_b$ , the  $E_a$  value below this temperature varies with UFA-enrichment of the membrane.

The rate constant for the facilitated diffusion of glycerol in this organism also shows a dependence on the fluidity and phase state of the membrane lipids. As can be seen in Figure 9, the dependence of the facilitated diffusion rate constant on membrane fluidity parallels that for the passive permeation process (lower panel), the  $1/\tau$  versus temperature curves shifting to lower temperatures for 18:2c,c- and to higher temperatures for 18:1t-cells. This constitutes a convincing piece of evidence that this facilitated diffusion process is faster when the fraction of liquid crystalline lipid in the membrane is high and that it is slower when most (or all) of the lipid is gelled. This is, therefore, a demonstration that a rate limiting step in this mediated transport mechanism is a movement of the carrier-substrate complex within the lipid bilayer. Thus, when the fluidity of this bilayer core is high, this movement is enhanced, and inhibition of the movement occurs as the bilayer fluidity decreases. It is noteworthy, in any case, that the rate constant for the facilitated diffusion process at any



TABLE V

Arrhenius Plot Break Temperatures and Activation Energies for  
Glycerol Permeation in E. coli K1060

	UFA Supplement	T <sub>b</sub> (°C)	Ea kcal/mole	
			Above T <sub>b</sub>	Below T <sub>b</sub>
Noninduced cells	18:1c	17	15	23
	18:1t	42	16	37
	18:2c,c	-	16	-
	16:1c	-	15	-
Induced cells *	18:1c	14	12	27
	18:1t	43	12	20
	18:2c,c	-	13	-
	16:1c	-	12	-

The values shown here were taken from Fig. 10A - D.

\* It is possible that the values of Ea above T<sub>b</sub> reported here for glycerol facilitated diffusion have been over-estimated since the facilitated diffusion rate measured is contaminated by a high passive permeation component.



temperature is higher than that for the passive permeation. The ratio  $[(1/\tau)_{\text{induced}} / (1/\tau)_{\text{noninduced}}]$ , however, is only  $\sim 1.5$  to 3, probably due to the relatively large passive permeation contribution to the measured apparent rates of facilitated diffusion.

As was observed for the passive permeation process, the Arrhenius plots for the facilitated diffusion shows only a single straight line for 18:2c,c- and 16:1c-cells (Figure 10C and D), while those for the 18:1t and 18:1c-cells are biphasic, displaying a  $T_b$  value in each of these two latter cases (Figure 10A and B). However, while the  $T_b$  value for induced 18:1t-cells corresponds to that for noninduced 18:1t-cells, the  $T_b$  for 18:1c-cells is lower for the induced than for the non-induced case (Table V). Thus, at  $T_b$  for induced 18:1t-cells, all the membrane lipids are liquid crystalline (Table IV) while at  $T_b$  for induced 18:1c-cells, only 58% liquid crystalline lipid exists, as against 70% in the noninduced 18:1c case. The significance of these observations is further discussed later (see "Discussion").

In addition, these Arrhenius plots for the induced cells differ in other ways from their noninduced counterparts. For instance, even though the  $E_a$  value above the break point ( $T_b$ ) for induced 18:1t- and 18:1c-cells, as well as that for induced 18:2c,c- and 16:1c-cells, is constant, this constant value is significantly lower than that for the passive permeation. This result is consistent with earlier work (71) in which it was observed that the  $E_a$  value for mediated glucose transport in A. laidlawii B is lower than that for the passive permeation of this molecule. The  $E_a$  value below  $T_b$  is higher than above it but again varies with the UFA supplementation.



#### D. DISCUSSION

The data presented clearly show that during the swelling of E. coli in glycerol or erythritol, some as yet undetermined factors influence the parameters measured. Glycerol permeation in glucose-grown E. coli is assumed to occur by a passive permeation process (269) and as such, its  $1/\tau \text{ sec}^{-1}$  (or  $k \text{ sec}^{-1}$ ) should be independent of the permeant concentration. One therefore expects that the initial rate of passive glycerol entry should vary linearly as a function of permeant concentration. These obvious predictions were not borne out by our results. However, for the simple procaryote, Acholeplasma laidlawii B, which lacks a cell wall, initial rates of glycerol (and other non-electrolyte) passive permeation, as measured by spectrophotometric means, have been found to increase linearly with increasing permeant concentration (74).

These artifacts were still obtained after correction for refractive index was effected using Ficoll-400 (Table II) and they were not eliminated by the presence of  $5 \times 10^{-7} \text{ M CuCl}_2$ , an inhibitor of the glycerol facilitated diffusion system. In addition, aerobic glycerol-3-phosphate dehydrogenase activity could not be detected in membranes of cells grown in the presence of glucose or xylose. It was therefore neither differences in refractive index nor some residual level of the glycerol facilitator which caused the artifacts. These complications, together with the irregularities in the results published by Alemohammad and Knowles (274), have been extensively discussed (174).

The data presented on the temperature-dependence of passive permeation and facilitated diffusion of glycerol in E. coli K1060 are in agreement with previous work and seem to show a consistent correlation with the fluidity and physical state of the membrane lipids. This suggests







that the anomalous variation of  $1/\tau$  with glycerol concentration for the passive permeation process does not affect the temperature dependence data, at least to any serious extent. Also, the contribution of passive permeation to the measured facilitated diffusion does not seem to affect the qualitative conclusions derivable from these results in view of the following observations: (i) The facilitated diffusion rate constant at any UFA-enrichment and constant temperature is higher than the corresponding value for the passive permeation. (ii) The activation energy ( $E_a$ ) above  $T_b$  is lower for the facilitated diffusion than for the passive permeation. This is in accord with a published report on the  $E_a$  of the mediated transport of glucose in A. laidlawii B (71).

The lipids from 18:2c,c- and 16:1c-cells display a rather broad gel to liquid crystalline transition ranging from  $-16^\circ\text{C}$  to  $+22^\circ\text{C}$  for 18:2c,c- and from  $-10^\circ\text{C}$  to  $+20^\circ\text{C}$  for 16:1c-cells (Table IV). The minimum temperature at which assays were done fell within the broad transitions of these two membranes, so that at the lowest experimental temperatures more than 50% of the lipids were liquid crystalline (i.e.,  $>T_m$ ). Consequently, the Arrhenius plots for either passive permeation or facilitated diffusion in these cells show no breaks. The activation energy for passive permeation calculated from the slope of each plot was similar to that from the slope above the break point of the Arrhenius plot of glycerol passive permeation in 18:1c- or 18:1t-enriched cells. The  $E_a$  for the facilitated diffusion in 18:2c,c- and 18:1c-enriched cells and, above  $T_b$ , for 18:1c- and 18:1t-cells, was lower than for the passive process and was also independent of UFA-supplementation. However, the  $E_a$  above  $T_b$  for passive permeation ( $\approx 15.5$  kcal/mole) was lower than the value predicted ( $\approx 18$  kcal/mole) from earlier reports (74,



209), considering the number of hydrogen bonds with water to be broken for complete dehydration. The cause of this difference is uncertain. It may be due to either some unexpected effects of the cell wall (174), or to some residual level of the glycerol facilitator present when xylose is used to generate noninduced cells. This second possibility is, however, unlikely considering that, as demonstrated in Table I, G3PDH activity was completely lacking in the membranes of xylose- as well as glucose-grown K1060. Moreover, when noninduced cells were generated by growing mutant K1060 in medium supplemented with xylose and  $\alpha$ -methylglucoside ( $\alpha$ MG), which is a non-metabolizable catabolite repressor of glycerol permeability in Salmonella typhimurium (293), the  $T_b$  and  $E_a$  values obtained from the Arrhenius plot were essentially identical to those obtained with cells grown in xylose (data not presented). It was observed, however, that when cells grown in the presence of glucose and 18:1c were used, the  $E_a$  above  $T_b$  was about 18 kcal/mole. However,  $T_b$  was  $\approx 20^\circ\text{C}$  since (as given in Appendix 2) membrane fluidity is lower due to decreased UFA incorporation. It is therefore difficult to establish what the cause of the low  $E_a$  could be for xylose-grown cells.

The break temperature in the Arrhenius plot for 18:1t-cells corresponds to the point at which all the membrane acyl chains are flexible (see ref. 61) and the temperature is the same for the induced and non-induced cases. However, for 18:1c-cells, the break temperature  $T_b$  is within the phase transition range, as revealed in the DTA data (Fig. 8A and B) and differs for the induced as compared to noninduced case (Table V). The variations in the manifestation of  $T_b$  between 18:1t- and 18:1c-grown cells may be due to the fact that there is more homogeneity in the membrane lipids of 18:1t- than of 18:1c-cells. Considering



the fatty acid compositions of K1060 cells grown on different UFA's (see Appendix 3), the 18:1t-cells would contain a higher percentage of the membrane lipids having two 18:1t moieties per molecule as compared to 18:1c-membrane lipids which contain two 18:1c moieties per molecule. The lipids of 18:1t membranes are thus less heterogeneous (more homogeneous) than lipids of 18:1c-cells. This correlation is consistent with that offered by Esfahani et al. (67), who observed that transition temperatures for L-proline uptake and succinate dehydrogenase activity are relatively close to each other in membranes of 18:1t-cells but not in 18:1c- or 18:3c,c,c-cells. The break temperatures for membranes from cells enriched in 18:1t, 18:1c and 18:3c,c,c were respectively 26°C, 18°C and 14°C for proline transport, while for succinate dehydrogenase activity in these same membranes, they were 22°C, 11°C and 23°C respectively. Thus the glycerol facilitator in 18:1c-cells may be associated with some phospholipid molecules containing two unsaturated acyl chains. These lipid molecules would then be lower-melting than the bulk lipid so that the Arrhenius plot of the activity of the facilitator under these conditions would exhibit a lower  $T_b$  than the passive permeation case, in which the glycerol molecule itself experiences the average state of the bulk membrane lipid. In the case of the 18:1t situation, on the other hand, the high incorporation of 18:1t creates a high degree of homogeneity. This is enhanced by the fact that the melting behavior of these 18:1t acyl chains is close to that of the endogenous saturated fatty acids which are also present in the membrane lipids (67). It may therefore be difficult to discern any subtle differences between the bulk membrane melt and that which could be ascribed to the presence of any lipid closely associated with the facilitator.





The  $E_a$  values below  $T_b$  for 18:1c- and 18:1t-cells are not the same and this variation does not seem to follow any predictable trend. The true significance of this variation is obscure at present.

It is obvious from these results that both the mediated and non-mediated permeation of glycerol in E. coli K1060 are dependent on the fluidity and physical state of the membrane fatty acyl chains. Thus the substrate in the case of passive permeation, and probably the substrate-carrier complex in the mediated case, have, as a common feature, a rate-limiting movement within the lipid bilayer during the translocation step. We then conclude that neither the passive permeation nor the facilitated diffusion of glycerol occurs through a fixed aqueous channel. More experimental evidence is required, however, to be able to differentiate between the mobile carrier and the aggregate rearrangement models. In any case, the thermodynamic arguments of Singer and associates (1, 12, 15) would tend to favour the latter model.

It is interesting to note that this glycerol facilitated diffusion system differs from the facilitated diffusion systems for glucose and uridine, both of which are native to the human erythrocyte membrane. Read and McElhaney (294) demonstrated that these two systems did not respond to alterations in the membrane fluidity and physical state. This is intriguing because these two systems of the human red blood cell membrane appear to operate mechanistically differently from the glycerol facilitated diffusion system in E. coli.

It may be possible, however, that the aggregate rearrangement mechanism is the general (or more common) mechanism for translocation in mediated transport. The fixed pore situation could be envisioned as an extreme case for this general model. For the fixed pore case, the





aggregate exists, but the disposition of the individual subunits would be much more rigidly fixed (than in the classical aggregate rearrangement situation) and an aqueous channel of a fixed (or partially fixed) dimension, traversing the cell membrane, would be enclosed. Substrate specificity of the channel would then depend on the molecular conformation of the binding site and that of the channel. Such a model may exhibit only subtle changes in the conformations and/or topological dispositions of the subunits during the binding and translocation of substrate, and such small changes may not be detectable under certain experimental conditions. Alternatively, such conformation changes may not, in certain systems, depend significantly on the fluidity or phase state of the bulk membrane lipids. This framework completely accommodates the observations of Read and McElhaney (294) mentioned above.



## CHAPTER IV

### ACTIVE AMINO ACID TRANSPORT IN ESCHERICHIA COLI:

#### L-GLUTAMINE TRANSPORT

##### A. INTRODUCTION

Gram-negative bacteria release a number of enzymes (periplasmic enzymes) and low molecular weight (~30,000 daltons) binding proteins (periplasmic binding proteins, PBP) (168, 272, 295) when they are subjected to mild osmotic shock as described by Neu and Heppel (167). These same groups of proteins are also released during the conversion of cells to spheroplasts (173). The PBP's reversibly bind substrates of specific active transport systems and are believed to act as the recognition site for these systems (272, 295). In gram-positive bacteria, enzymes corresponding to the periplasmic enzymes of gram-negative bacteria have been recognized but these are either membrane-bound (e.g. penicillinase of Bacillus licheniformis) or secreted into the medium (e.g., alkaline phosphatase of Bacillus subtilis). Binding proteins have also been obtained from animal tissues and by modifications of the shock procedure, have also been obtained from eucaryotic microorganisms, e.g. Neurospora crassa (272).

In gram-negative bacteria, a variety of PBP-dependent active transport systems have been identified for substrates belonging to different classes of compounds, e.g. amino acids, inorganic ions, sugars and vitamins. A single substrate may, however, be transported via more than one kinetically and genetically distinct system(s) operating simultaneously in the same organism (see 272, 295, 296 for review). Leucine, for instance, can be accumulated in E. coli via a



high affinity leucine-specific PBP-dependent system, a high affinity system (LIV I system) common to all three branched chain amino acids (leucine, isoleucine and valine), as well as via a low affinity (LIV II) system not dependent of a PBP (297, 298). Each of the basic amino acids (arginine, lysine and ornithine) can be transported in E. coli by at least four systems, one high affinity system (LAO system) common to all three and one low affinity system specific for each one (299, 300). The same situation may also exist in Salmonella typhimurium (300, 301). Galactose transport in E. coli (302, 303) and S. typhimurium (304), as well as histidine accumulation in S. typhimurium (305, 306), and aromatic amino acid transport in E. coli (307), also operate via multiple systems. Studies of the translocation step in PBP-dependent transport are thus complicated by this involvement of multiple systems. The L-glutamine system in E. coli, therefore, is most suited for these kinds of studies. This system has been very well characterized; it is highly specific for L-glutamine and no other natural amino acid competes for active transport. The single shock-releasable binding protein for glutamine appears to be homogeneous as judged by several criteria and binds 1 mole of glutamine per mole of protein (169, 272). In addition, this L-glutamine system is suitable for studies with whole cells since it has been found that the kinetic parameters of uptake are the same in the absence or presence of azaserine, an inhibitor of  $\gamma$ -glutamyl transfer reactions. Also, a large excess of glutamate, the immediate metabolic product from glutamine does not change these parameters (169).



## B. METHODS

### 1. Bacterial Strains and Growth Conditions

E. coli K1060 and strain 7 were used for  $^{14}\text{C}$ -glutamine uptake studies. Mutant K1060 was always grown in M63 supplemented with nutrients and glycerol as carbon and energy source plus one of five UFA's (18:1c, 16:1c, 18:1t, 16:1t or 18:2c,c). Strain 7 was cultured in M63 containing 1% succinate (titrated to pH 7.0 with KOH) and nutrients but without UFA/Brij 58. Other growth conditions were as detailed in Chapter II (Materials and Methods).

### 2. Preparation of Cells and $^{14}\text{C}$ -Glutamine Uptake Assays

#### (a) Procedure A

Cells were harvested by centrifugation at room temperature in a Sorvall RC-2B centrifuge at 15,000 x g for 5 min. The pellet was washed two times by resuspension in M63 buffer (without any nutrients or other supplementations) and centrifuged at 15,000 x g for 5 min each time. The final pellet was then resuspended in M63 buffer to a concentration of 1 g wet cells to 20ml M63 buffer (1:20 cell suspension). Graded dilutions (1:40, 1:80, 1:160, 1:320 and 1:640 suspensions) of this stock (1:20) suspension were made and these were stored at room temperature with occasional stirring to prevent clumping.

Immediately before uptake studies, to a 500  $\mu\text{l}$  aliquot of cell suspension were added 10  $\mu\text{l}$  of 1M glucose in M63 buffer and 20  $\mu\text{l}$  of 0.2g% chloramphenicol in M63 buffer. This mixture was then incubated at the desired working temperature for exactly 2 mins. A 20  $\mu\text{l}$  aliquot of this treated cell suspension was then quickly mixed with a rapidly stirr-d 485  $\mu\text{l}$  of  $^{14}\text{C}$ -glutamine solution of the







appropriate concentration in M63, which contained glucose and chloramphenicol at the same level as in the cell suspension, and which had been pre-incubated at the same working temperature. A sample (200  $\mu$ l) of this transport assay mixture (total vol. 505  $\mu$ l) was quickly withdrawn at two appropriate time intervals and filtered by suction through 24 mm nitrocellulose filter (type HA, 0.45  $\mu$  pore diameter, Millipore Corporation, Bedford Massachusetts or Matheson Higgins Incorporated, Woburn, Massachusetts) which had been pre-soaked in M63. The trapped cells were immediately washed by suction with 10 ml of M63. The filter was then dried over a hot plate maintained at  $-40^{\circ}\text{C}$ . The filtration apparatus was a 10-place microfilter assembly equipped with a pressure guage (Hoffer Scientific Instruments, San Francisco, California).

For the determination of the linearity of the time course of uptake, the volume of the transport assay mixture was doubled and 4 time samples were taken at each concentration of glutamine. During studies on the temperature-dependence of glutamine uptake, an appropriate cell suspension and appropriate sampling times were chosen such that not more than 10% (or about 20% in some cases, see Results) of the total available radioactivity was accumulated in the cells in order to ensure against the depletion of substrate. These sampling times ranged from 6.5 sec at high temperatures to 3 mins at low temperatures.

#### (b) Procedure B

Cells were harvested and washed two times with and finally suspended in Tanaka minimal medium (169) to the same concentration as in procedure A. Glucose and chloramphenicol were added to the same



level as in procedure A and these treated cells were stored in an ice-water bath before use.

For the transport assay, 500  $\mu$ l of these treated cells was incubated for 5 min at the desired temperature and an aliquot of 20  $\mu$ l was mixed with 485  $\mu$ l of the appropriate concentration of  $^{14}\text{C}$ -glutamine in transport buffer (308). At an appropriate sampling time, 200  $\mu$ l of this reaction mixture was quickly filtered, as in procedure A, through 24 mm nitrocellulose filter (type HA, 0.45  $\mu$  pore diameter) presoaked in phosphateless (A-P) buffer (308). Washing was immediately effected as in procedure A, but using 10 ml of a buffer containing 10 mM Tris HCl, pH 7.3, 150 mM NaCl and 0.5 mM  $\text{MgCl}_2$  (169).

The other operations were done as detailed in procedure A.

### 3. Liquid Scintillation Counting

These filters were collectively dried further in scintillation vials in an oven at 50° to 60°C for ~1 hr before counting in 5 ml of toluene-based scintillation cocktail (169, see preparation as given in Chapter II) using any of three Beckman Liquid Scintillation System models (LS-200B, LS-230 and LS-330).

Cells poisoned in energy metabolism (see Chapter II) and assayed for transport in the same way as normal cells did not show significantly higher radioactivity (cpm) than control runs. The control runs consisted of filtering and washing 200  $\mu$ l of the  $^{14}\text{C}$ -glutamine solution in the absence of cells. These controls were run routinely and the experimental cpm at the appropriate  $^{14}\text{C}$ -glutamine concentration corrected by subtracting the control value.

The counting efficiency of the liquid scintillation counter was routinely checked by counting in duplicate a known amount of



radioactivity (disintegrations per minute, dpm), usually 10  $\mu$ l of each  $^{14}\text{C}$ -glutamine solution, dried on the nitrocellulose filter. This was used to correct the sample cpm during the calculation of the initial rate of transport, i.e., the nmole glutamine accumulated per minute per mg cell protein. The method used to calculate initial rates of transport from the experimental data is given in Appendix 4.

## C. RESULTS

### 1. Time Course of $^{14}\text{C}$ -Glutamine Uptake

By adequate manipulation of cell concentration and sampling time as temperature was changed, as much as 10% of the total available radioactivity could be accumulated without any appreciable change in the initial rate of uptake measured. This is illustrated in Fig. 11 in which four time samples were taken at each glutamine concentration tested. Subsequently, two sampling times were employed, allowing for less than 10% depletion of radioactivity. However, for mutant K1060 grown in the presence of 18:2c,c or 18:1t, reproducible results were obtained only when as high as 20% of the total available radioactivity was accumulated. Under these condition, samples removed at the two time intervals gave the same initial rate of uptake.

### 2. Concentration Range of L-Glutamine Employed

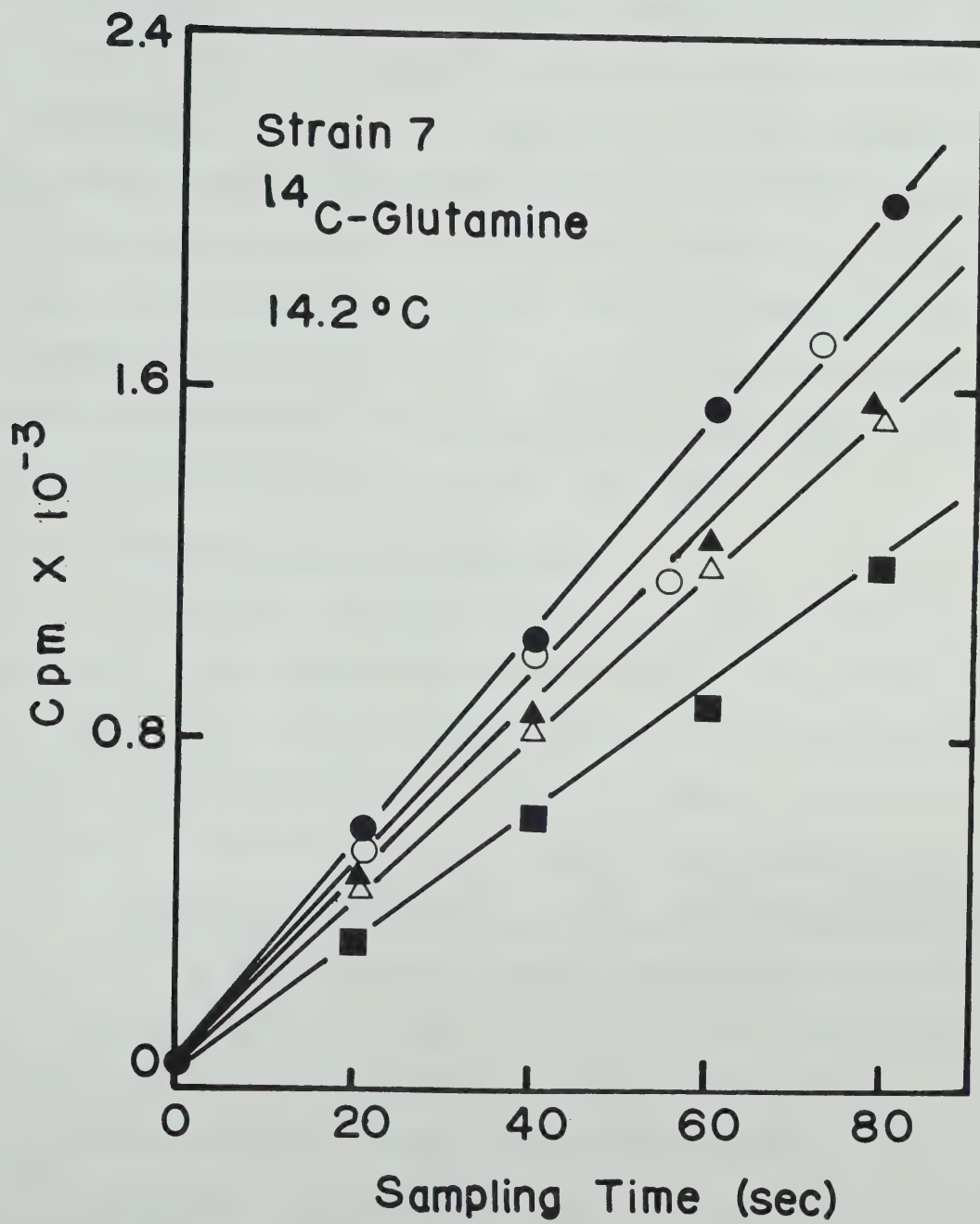
Fig 12 reveals that the  $K_m$  for  $^{14}\text{C}$ -glutamine uptake in E. coli strain 7 is less than 0.1  $\mu\text{M}$ , if substrate concentrations of up to 1.25  $\mu\text{M}$  glutamine are considered. Above this concentration, the Lineweaver-Burk plot displays a rather steep slope. The high  $K_m$  values obtained above 1.25  $\mu\text{M}$  may be due to participation of non-





FIGURE 11. Time course of L-glutamine uptake in E. coli strain 7 at 14.2°C. Cells were prepared and  $^{14}\text{C}$ -glutamine uptake assayed as detailed in Methods. The following  $^{14}\text{C}$ -glutamine concentrations were employed: 0.0574  $\mu\text{M}$  (-■-■-); 0.1158  $\mu\text{M}$  (-Δ-Δ-); 0.1446  $\mu\text{M}$  (-▲-▲-); 0.2307  $\mu\text{M}$  (-o-o-); 0.4614  $\mu\text{M}$  (-●-●-).







specific systems at these high substrate concentrations. The mean  $K_m$  calculated in this experiment considering the range 0.031 - 1.25  $\mu\text{M}$  L-glutamine is  $0.075 \pm 0.015 \mu\text{M}$  at all temperatures assayed. This value is in accord with published results for this strain (169) and shows that  $K_m$  is invariant with temperature. A similar experiment using mutant K1060 supplemented with 18:1c yielded similar values.  $K_m$  is also independent of the UFA enrichment of the cells as demonstrated by subsequent experiments (Fig 13A-C). All experiments on the temperature-dependence of  $K_m$  and  $V_{\max}$  for  $^{14}\text{C}$ -glutamine uptake reported here for these two E. coli strains were performed with a concentration range of 0.05 to 0.5  $\mu\text{M}$   $^{14}\text{C}$ -glutamine.

### 3. Treatment of Data for $K_m$ and $V_{\max}$

The double reciprocal plot of Lineweaver and Burk (186) was used in some experiments while the Hanes' plot (186, 169) was used in others. In the Hanes' plot,  $\frac{[S]}{v}$  is plotted as a function of  $[S]$ , where  $v$  is the initial rate at a particular substrate concentration  $[S]$ . The  $[S]$  intercept is  $-K_m$  while the  $\frac{[S]}{v}$  intercept is  $K_m/V_{\max}$ .

### 4. Temperature-Dependence of $K_m$ and $V_{\max}$ for $^{14}\text{C}$ -Glutamine Uptake

The  $K_m$  for glutamine transport remained constant within the temperature ranges employed. Figure 12 and the Hanes' plots in Fig. 13A - C illustrate this fact. Arrhenius plots of the  $V_{\max}$  values obtained at different temperatures are given in Fig 14A to F. For strain 7,  $V_{\max}$  increases with temperature up to the highest temperature probed ( $40^\circ\text{C}$ ) and the Arrhenius plot (Fig 14A) is clearly biphasic, displaying a characteristic break temperature ( $T_b$ ). The  $V_{\max}$  for the mutant K1060, however, increases with temperature only up to an upper temperature limit (UTL). The value of this UTL is





FIGURE 12. Lineweaver-Burk plot of the variation of initial rates of  $^{14}\text{C}$ -glutamine uptake with glutamine concentration in E. coli strain 7 at 21°C. Cells were grown and prepared, and  $^{14}\text{C}$ -glutamine uptake assay carried out, as given in Methods. Ten concentrations of L-glutamine (in the range 0.03 - 20  $\mu\text{M}$ ) were employed.

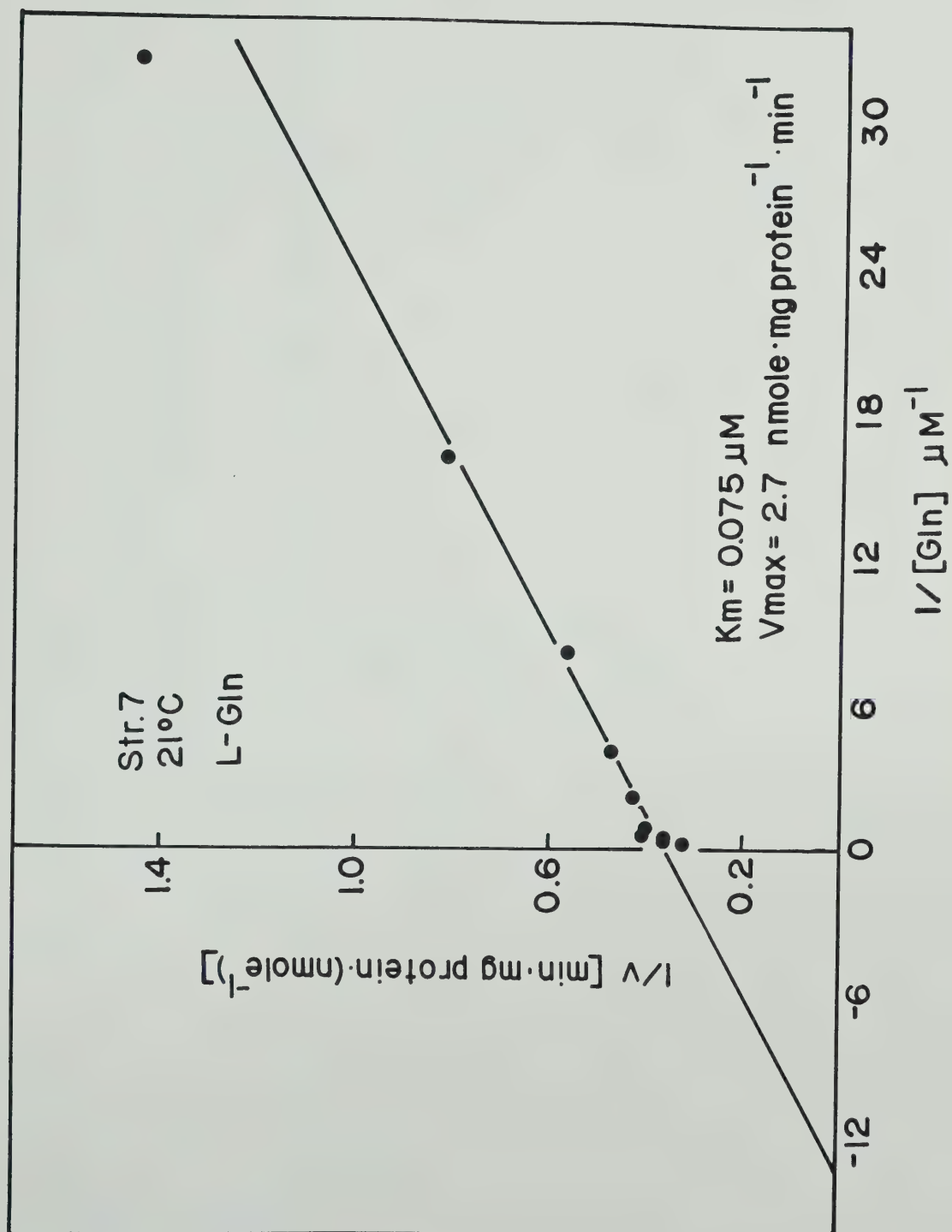








FIGURE 13A. Hanes' treatment of data for the calculation of  $K_m$  and  $V_{max}$  values for  $^{14}C$ -glutamine uptake at various temperatures in 16:1c-enriched K1060 cells. Assays were performed as detailed in Methods. The following  $K_m$  and  $V_{max}$  values were obtained at the indicated temperatures:

Symbol	Temp °C	$K_m$ ( $\mu M$ )	$V_{max}$ (nmole/min/mg protein)
-▲-▲-	11.0	0.063	0.25
-△-△-	13.0	0.053	0.49
-●-●-	15.0	0.078	0.76
-○-○-	17.5	0.048	0.96

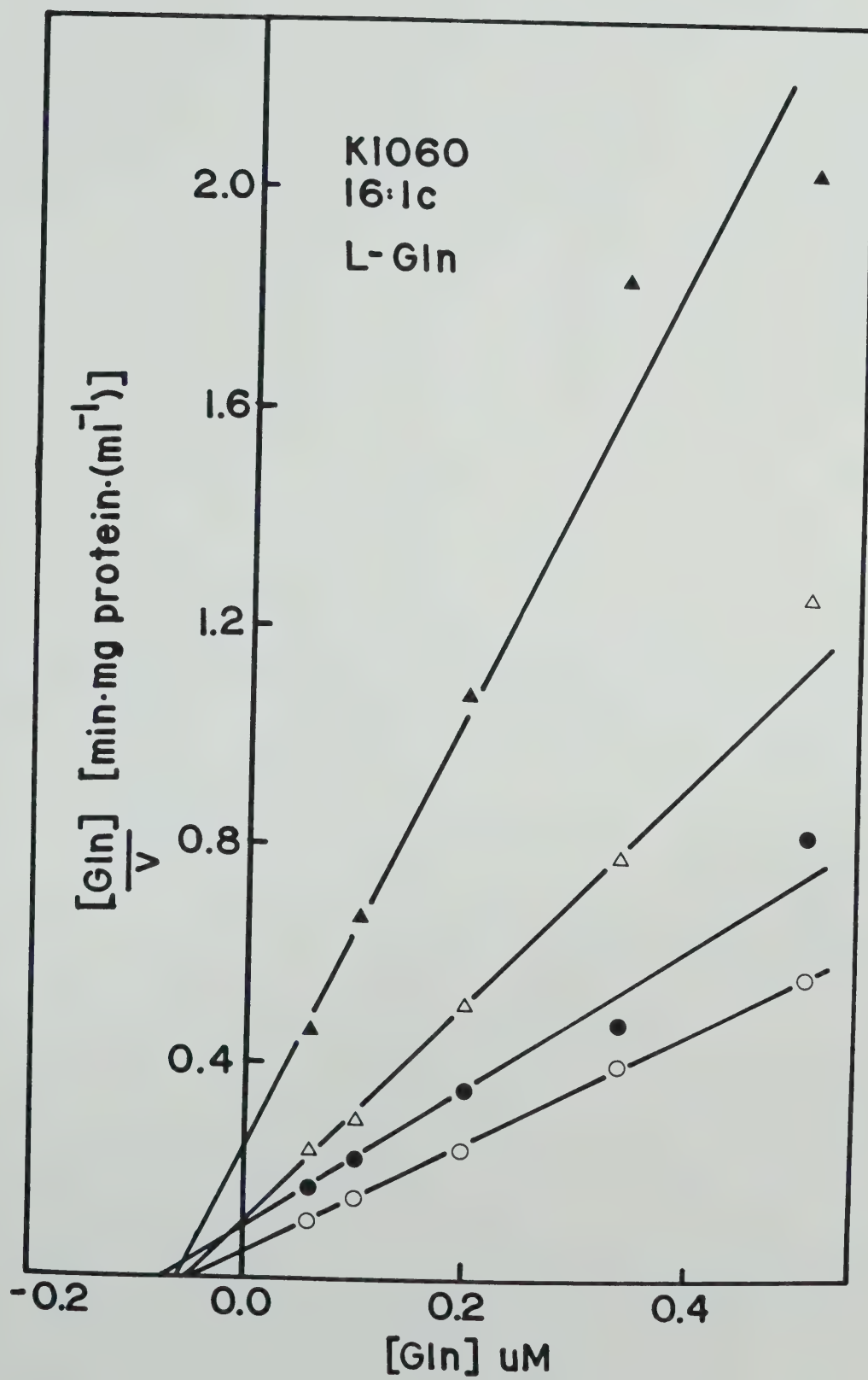






FIGURE 13B. Hanes' treatment of data for the calculation of  $K_m$  and  $V_{max}$  values for  $^{14}C$ -glutamine uptake at various temperatures in 18:2c,c-enriched K1060 cells. Assays were performed as given in Methods. The following  $K_m$  and  $V_{max}$  values were obtained at the indicated temperatures:

Symbol	Temp (°C)	$K_m$ ( $\mu M$ )	$V_{max}$ (nmole/min/mg protein)
-▲-▲-	17.5	0.065	0.59
-△-△-	20.0	0.073	0.91
-●-●-	23.0	0.086	1.4
-○-○-	26.0	0.087	1.7
-■-■-	29.0	0.070	1.8

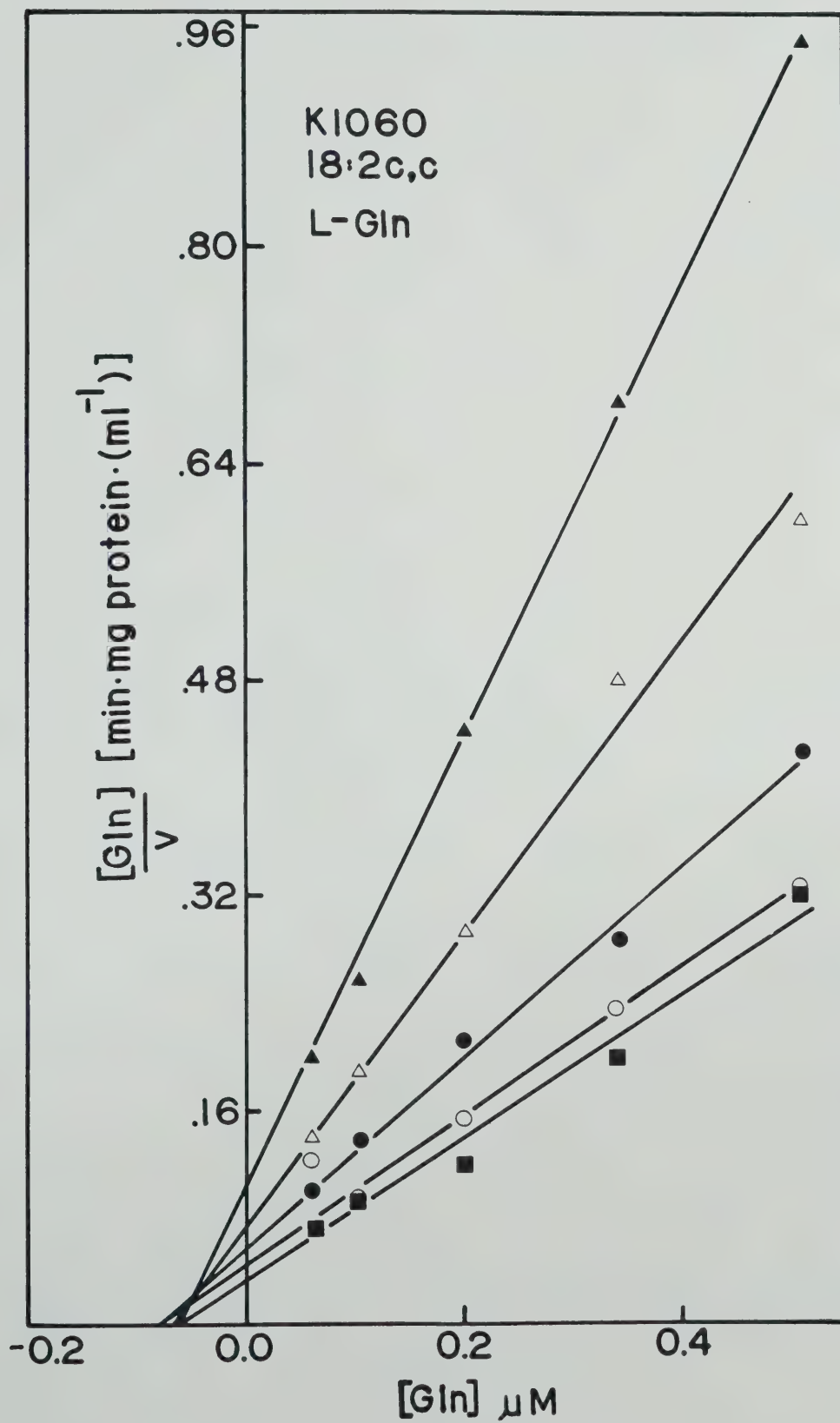


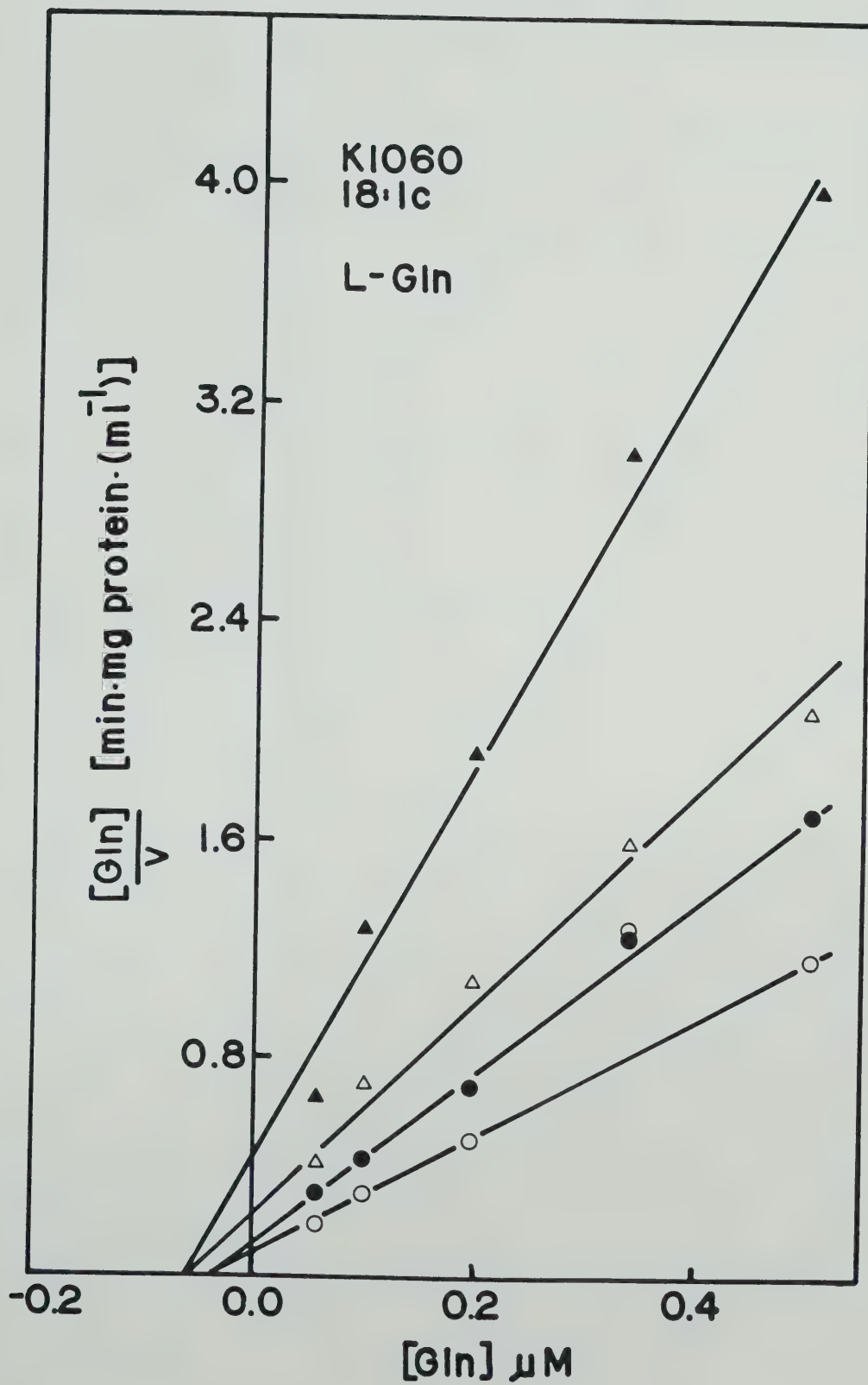




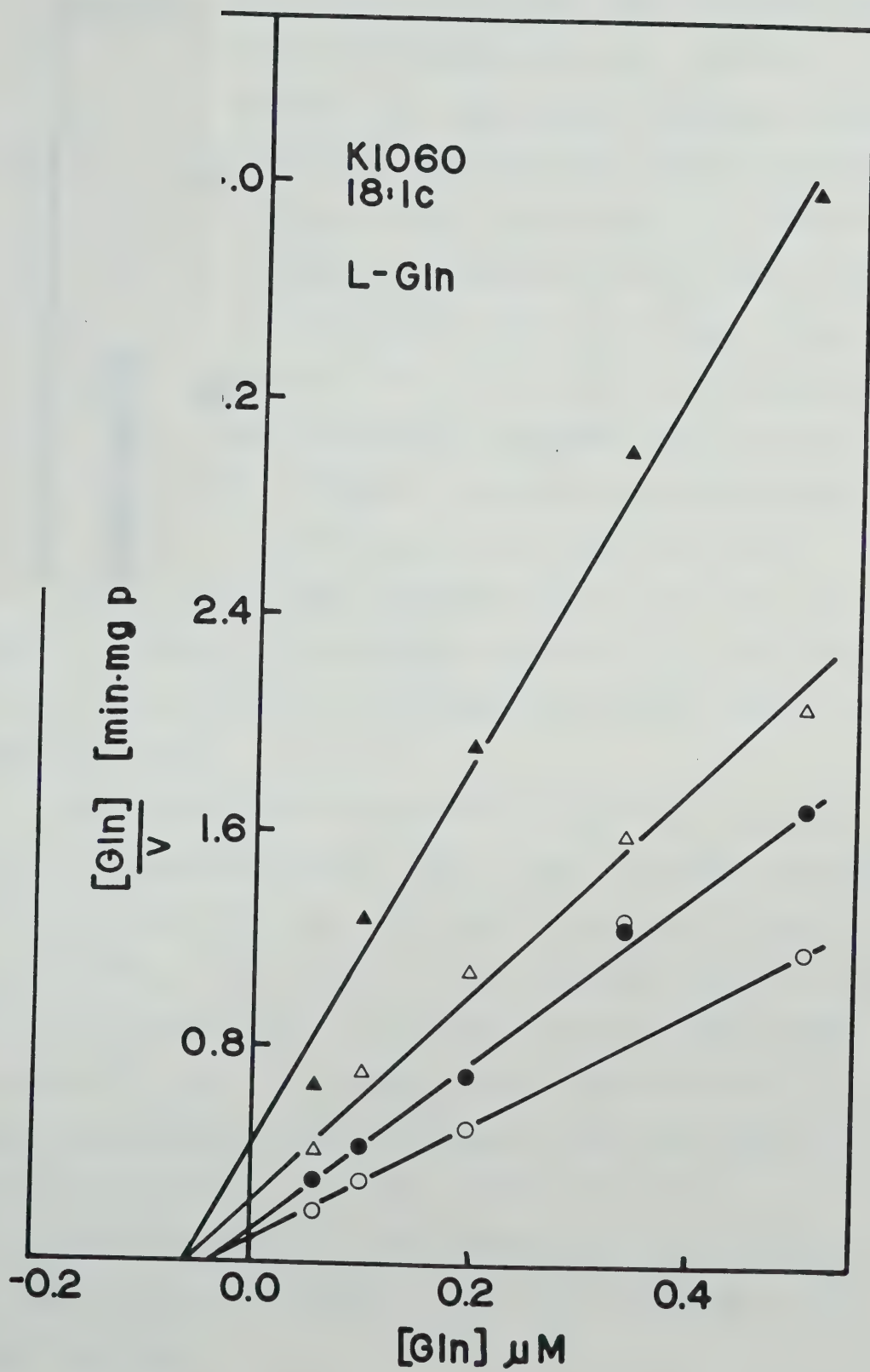


FIGURE 13C. Hanes' treatment of data for the calculation of  $K_m$  and  $V_{max}$  values for  $^{14}C$ -glutamine uptake at various temperatures in 18:1c-enriched K1060 cells. Assays were performed as given in Methods. The following  $K_m$  and  $V_{max}$  values were obtained at the indicated temperatures:

Symbol	Temp (°C)	$K_m$ ( $\mu M$ )	$V_{max}$ (nmole/min/mg protein)
-▲-▲-	9.0	0.063	0.14
-Δ-Δ-	11.0	0.060	0.26
-●-●-	13.0	0.038	0.32
-o-o-	15.0	0.040	0.44









peculiar to each UFA supplement and is always below the growth temperature of 37°C (39°C for 18:1t-supplemented cells). Above the UTL,  $V_{\max}$  starts to decrease with temperature (or otherwise to become aberrant), until at some higher temperature, the transport kinetics no longer follow the Michaelis-Menten equation (186), i.e., the data cannot be treated in conventional fashion to yield  $V_{\max}$  and  $K_m$  values. The absolute amount of radioactivity accumulated per unit time per unit cell protein within the initial rate period, at each glutamine concentration, actually decreases with temperature above the UTL.

Below the UTL, and down to the minimum temperature at which assays were done, data derived from 16:1t-, 18:1c- and 16:1c-cells yield (biphasic) linear Arrhenius plots (Fig 14C - E), each of which has a break at a characteristic temperature ( $T_b$ ). The Arrhenius plot (Fig 14F) of 18:2 c,c-enriched cells, however, shows a smooth curve below the UTL.

Figure 14B is the Arrhenius plot of L-glutamine transport in 18:1t-enriched K1060 cells. The plot shows the general phenomena seen in the other K1060 cases. It should be noted that Fox and associates (58, 64) had earlier reported a similarly shaped Arrhenius plot for the initial rates of  $\beta$ -glucoside transport in another UFA auxotroph of E. coli. They attributed the peculiar behaviour at higher temperatures (UTL here) to changes in the lateral compressibility of the membrane. The data presented here are not in support of the explanation offered by these authors, but suggest instead that the behaviour above the UTL may be due to defects in energy coupling (see "Discussion").







FIGURE 14A. Arrhenius plot of  $V_{\max}$  values for L-glutamine uptake in E. coli strain 7.  $V_{\max}$  values were derived as given in the text (see Methods).

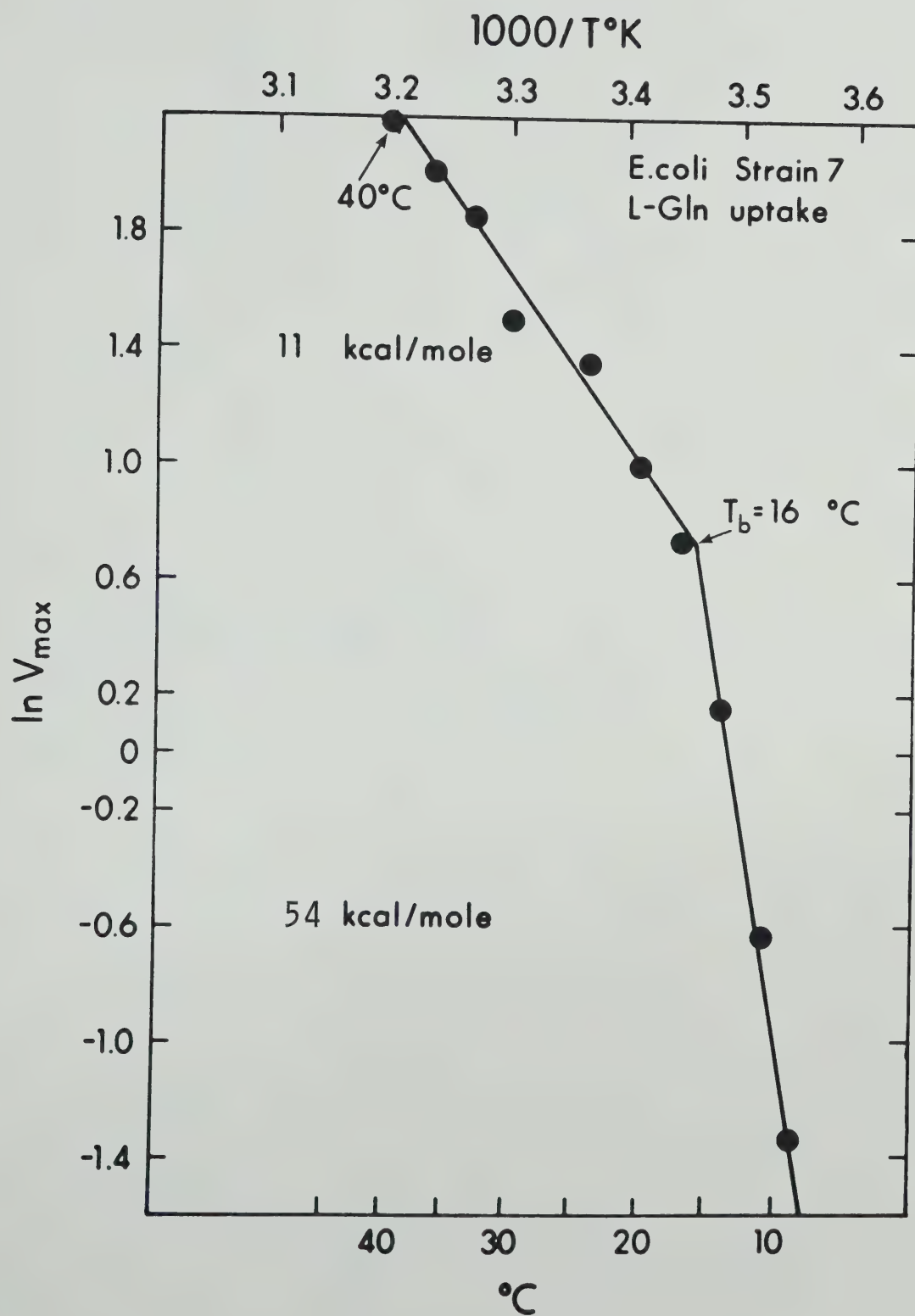






FIGURE 14B. Arrhenius plot of  $V_{\max}$  values for L-glutamine uptake in E. coli K1060 enriched in 18:1t.  $V_{\max}$  values were derived as given in the text (see Methods).

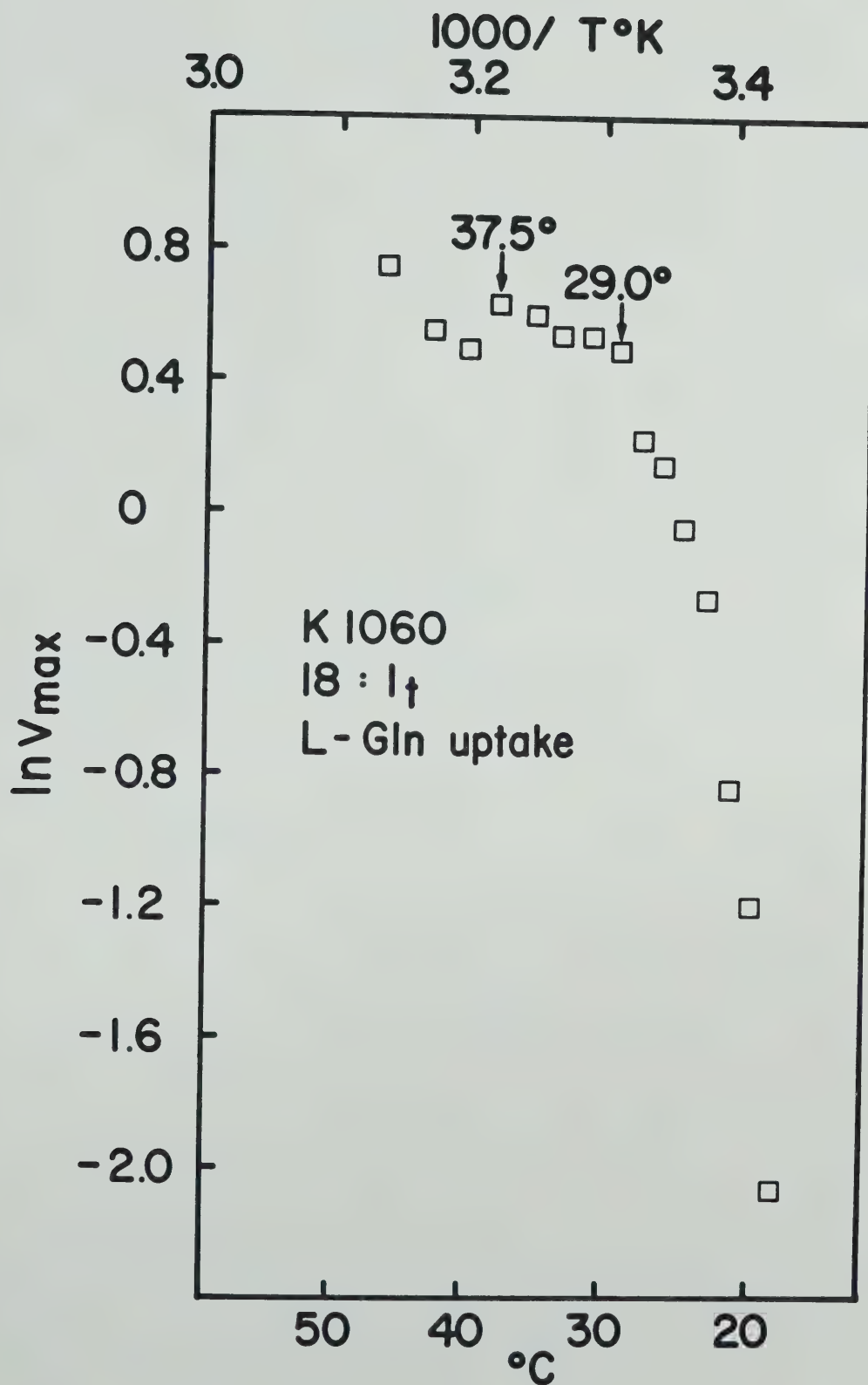








FIGURE 14C. Arrhenius plot of  $V_{\max}$  values for L-glutamine uptake in E. coli K1060 enriched in 16:1t.  $V_{\max}$  values were derived as given in Methods.

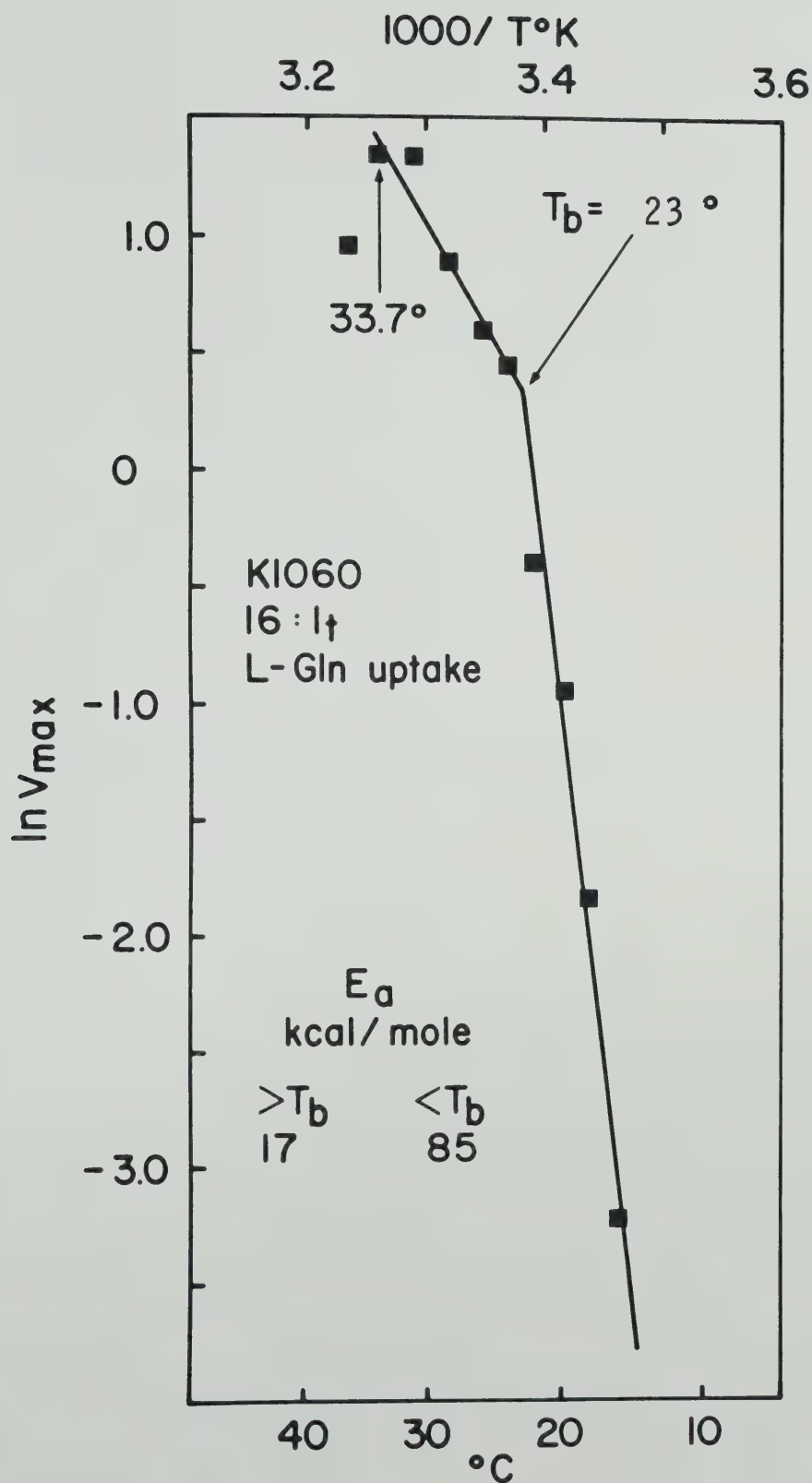






FIGURE 14D. Arrhenius plot of  $V_{\max}$  values for L-glutamine uptake in E. coli K1060 enriched in 18:1c.  $V_{\max}$  values were derived as given in Fig. 13C.

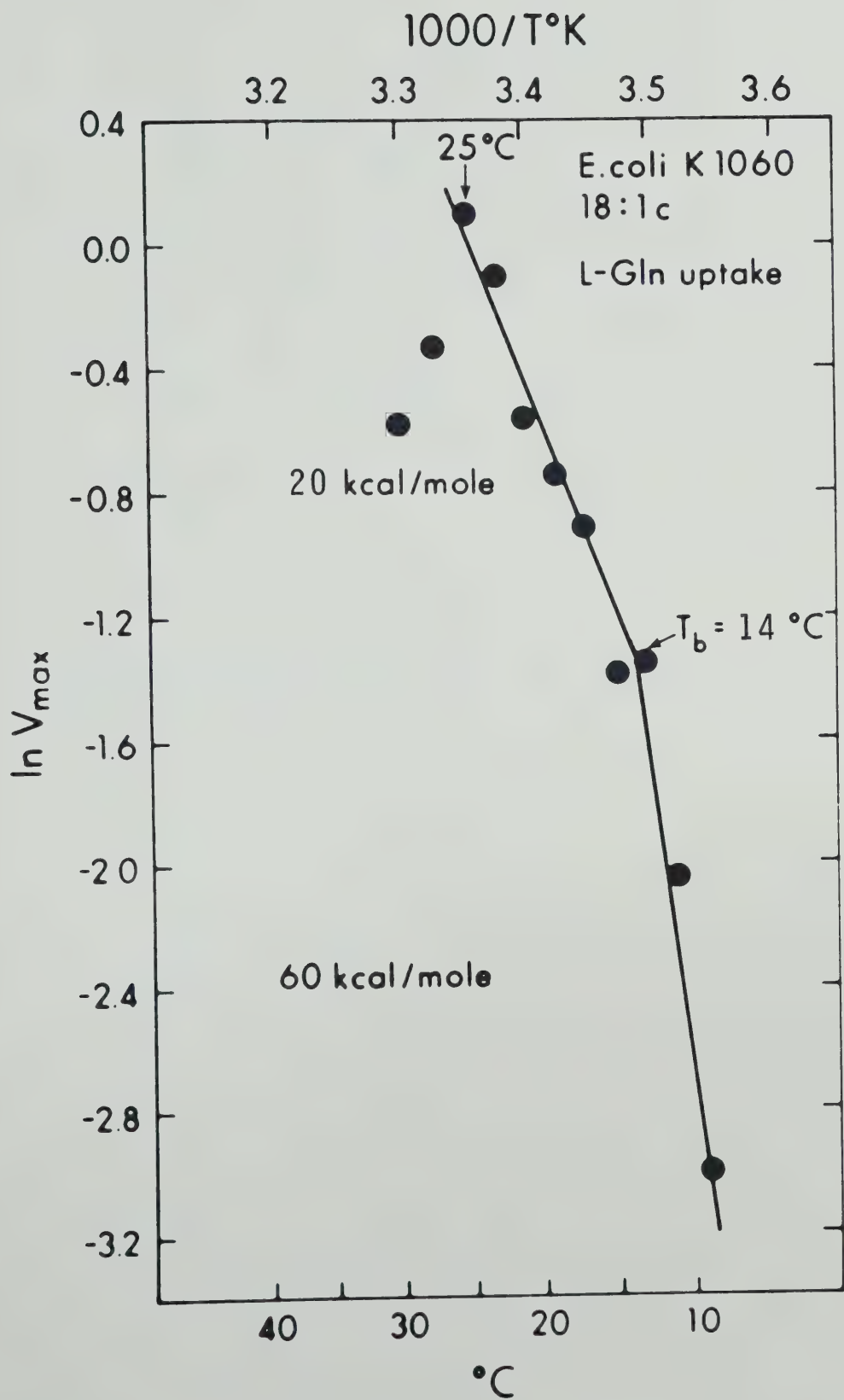








FIGURE 14E. Arrhenius plot of  $V_{\max}$  values for L-glutamine uptake in E. coli K1060 enriched in 16:1c.  $V_{\max}$  values were derived as given in Fig. 13A.

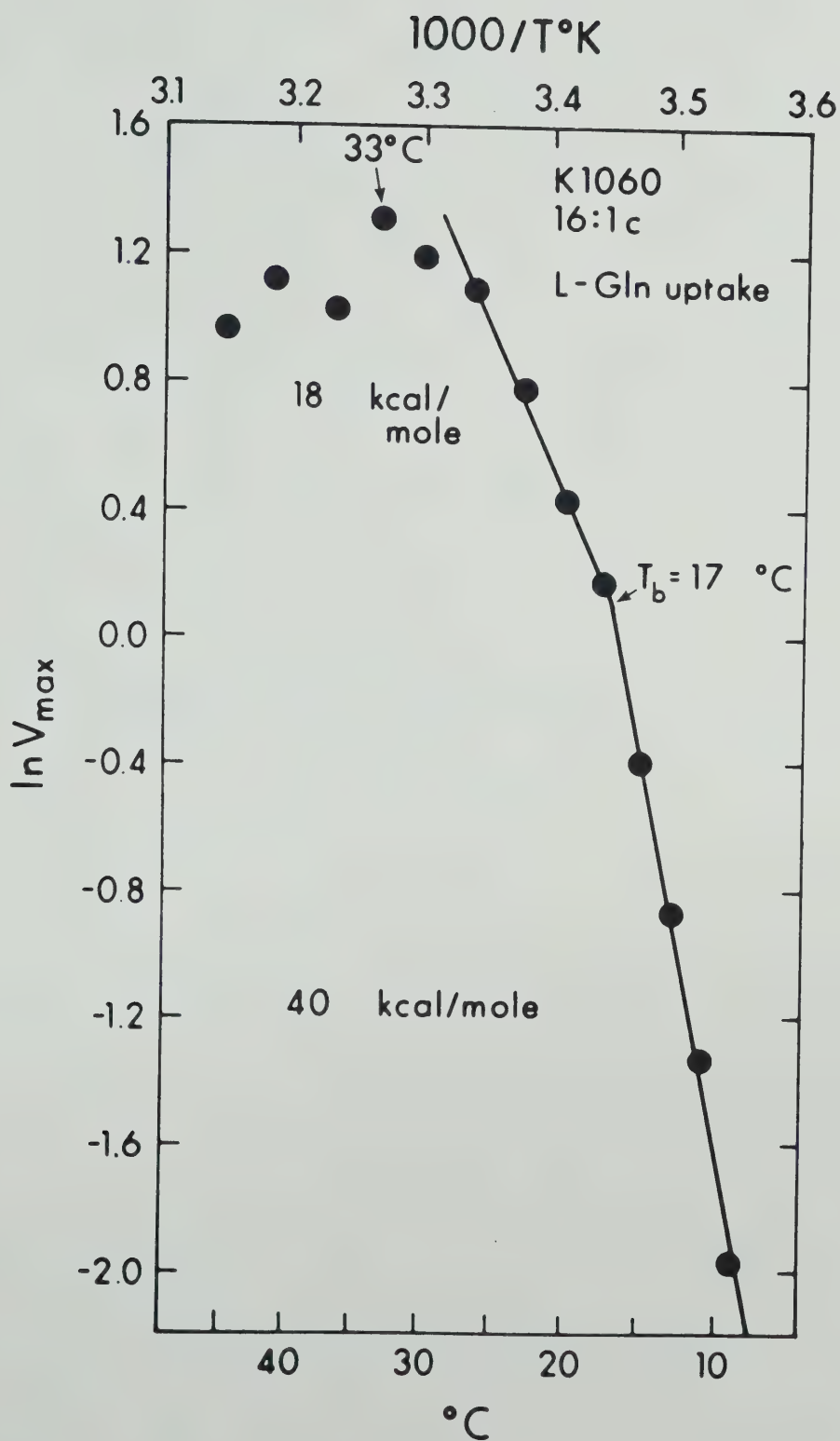
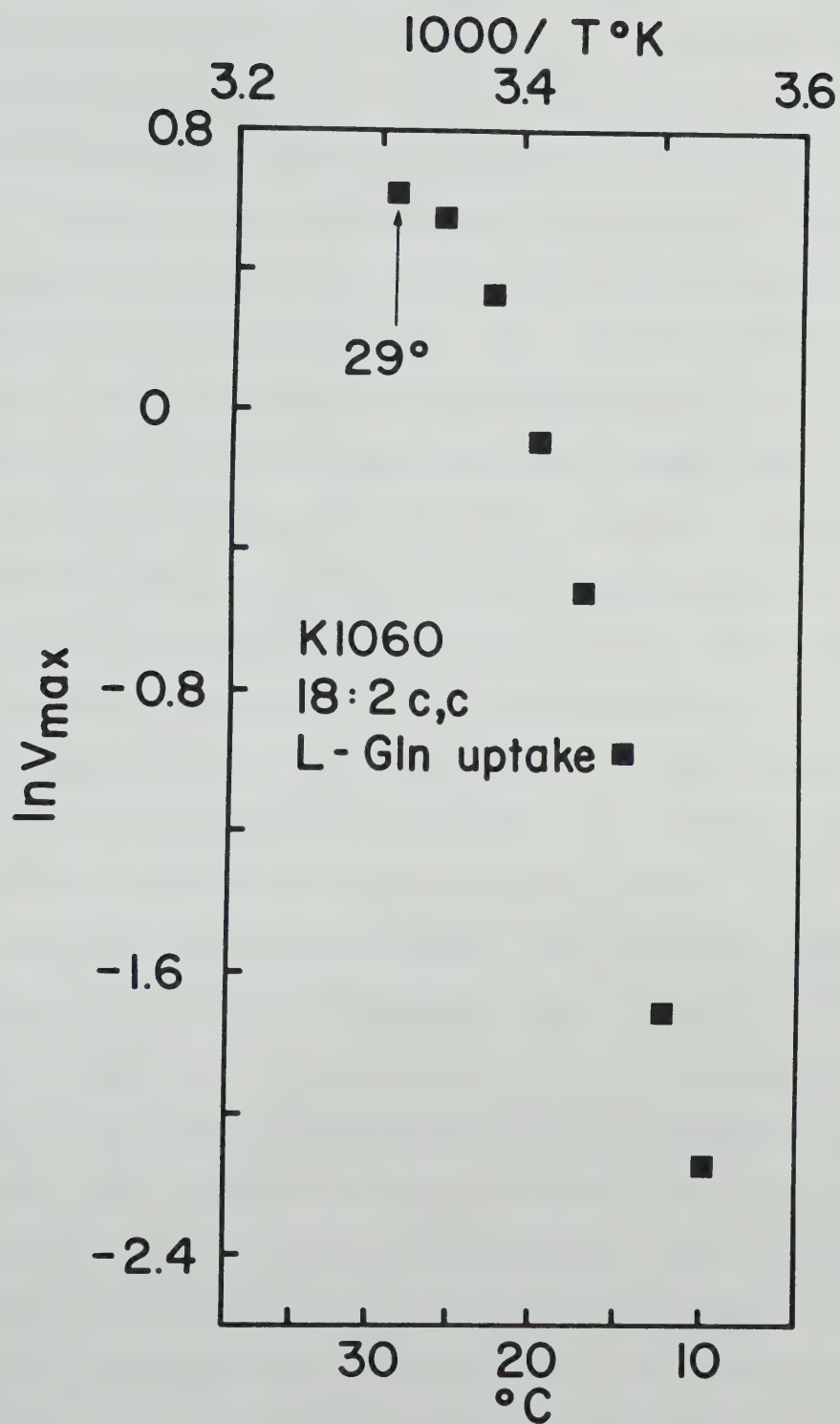






FIGURE 14F. Arrhenius plot of  $V_{\max}$  values for L-glutamine uptake in E. coli K1060 enriched in 18:2c,c.  $V_{\max}$  values were derived as given in Fig. 13B.







#### D. DISCUSSION

The data presented in this chapter clearly demonstrate a profound dependence of L-glutamine transport  $V_{\max}$  on the physical state of the membrane lipids. The  $K_m$  for this process, however, is invariant with either temperature or membrane lipid physical state both in the mutant K1060 grown in various UFA supplements and in strain 7, the mean value obtained in different determinations being close to the 0.08  $\mu\text{M}$  published by Weiner and Heppel (169).  $V_{\max}$  for L-glutamine transport in strain 7 increases with temperature as expected up to the highest temperature (40°C) at which assays were done. However, mutant K1060 displays a peculiar phenomenon in that  $V_{\max}$  increases as expected with temperature only up to a limit (the upper temperature limit, UTL). Beyond this temperature, which is unique for each UFA enrichment,  $V_{\max}$  begins to decrease or otherwise becomes aberrant. In view of this unique behavior, information about the influence of membrane lipid fluidity on these kinetic parameters ( $V_{\max}$  and  $K_m$ ) for this transport system could not be derived from these results.

Every UFA supplementation except 18:2c,c gives an Arrhenius plot of  $V_{\max}$  below the UTL for glutamine transport in K1060 which is biphasic, displaying a  $T_b$  characteristic of the particular UFA. Strain 7 shows no UTL and the Arrhenius plot of  $V_{\max}$  is biphasic,  $V_{\max}$  increasing with temperature as expected up to at least 40°C. Tables IV and VI, Fig. 14A to F, and a comparison of the areas of the DTA thermograms in Fig 8A and B (and see also ref. 61), reveal that the break  $T_b$  in the Arrhenius plot is slightly below  $T_1$  for mutant K1060 grown on 18:1t, but occurs at a point when 21%, ~55% and 97% of the membrane lipids are in the liquid crystalline state for 16:1t-, 18:1c-, and



16:1c-grown K1060 cells, respectively. The  $T_b$  thus follows the trend predictable from the relative fluidities of these membranes as judged by the lipid phase transition midpoints ( $T_m$ ), but differs in how far  $T_b$  lies from  $T_m$  (Tables IV and VI), i.e.,  $T_b - T_m$ . However, this difference ( $T_b - T_m$ ) correlates well with fluidity, being highest for the most fluid membranes (18:2c,c) and lowest for the least fluid (18:1t) membranes. The DTA data thus indicate that relative fluidities decrease in the order, 18:2c,c- > 16:1c- > 18:1c- > 16:1t- > 18:1t-cells, and for the least fluid 18:1t-cells,  $T_b$  is at or slightly below  $T_1$  (i.e.,  $\ll T_m$ ). For 16:1t-, 18:1c- and 16:1c-cells, respectively,  $T_b$  is below  $T_m$ , around  $T_m$  (slightly higher) and above  $T_m$ . It is noteworthy that for the most fluid membranes (18:2c,c) the point at which the Arrhenius plot curves off is around 20° to 23°C and at this point more than 97% of the lipids are liquid crystalline. The data for strain 7, wild-type in fatty acid metabolism, is in accord with this trend. At  $T_b$  (16°C) which is only slightly higher than  $T_m$  (15°C) the liquid crystalline mole fraction is 55% and so, on the basis of fluidity alone, strain 7 would behave approximately similar to 18:1c-grown K1060,  $T_b = 14^\circ$ ,  $T_m = 12.5^\circ$  and liquid crystalline mole fraction at  $T_b = \sim 55\%$ . This is the case here.

Table VI also contains the  $E_a$  values both above and below  $T_b$ .  $E_a$  below  $T_b$  is higher for trans-UFA-enriched- than cis-UFA-enriched K1060 cells and generally,  $E_a$  above  $T_b$  is lower than below it. The physical significance of these  $E_a$  values is as yet unclear.

Above the upper temperature limit (UTL)  $V_{\max}$  begins to decline as mentioned earlier. This decrease in  $V_{\max}$  continues to a certain higher temperature beyond which transport no longer obeys Michaelis-Menten



TABLE VI

Arrhenius Plot Temperature Breaks ( $T_b$ ), Activation Energies ( $E_a$ ) and Temperatures at which  $V_{max}$  Starts to Decrease with Temperature (UTL) for L-Glutamine Transport in Relation to Membrane UFA-Enrichment (mole %) and Phase Transition Midpoint ( $T_m$ ) in E. coli Strain 7 and Strain K1060

Cells	UFA Supplement	UFA supplement incorporated into membrane (mole %)	Temp. at which 50% of membrane lipids are liquid crystal-line (from Table IV)	$T_m$ ( $^{\circ}\text{C}$ )	Arrhenius plot break temperatures $T_b$ ( $^{\circ}\text{C}$ )	UTL ( $^{\circ}\text{C}$ )	Ea kcal/mole	
							Above $T_b$	Below $T_b$
Str 7	None	-	15	16	$\geq 40$		11	54
K1060	16:1t	80 - 85	27	23	33.7		17	85
	16:1c	39 - 44	7	17	33		18	40
	18:1c	52 - 58	12.5	14	25		20	60
	18:1t	66 - 71	38		37.5			
	18:2c,c	48 - 50	(approx.) -2		29			





kinetics (186). The following points are worth noting about transport occurring above the UTL: (i) the radioactivity (cpm) accumulated within the cells per unit time per unit of cell protein (i.e. initial rate) actually decreases with temperature at each substrate concentration. Thus, this increase in temperature mimics the effects of adding increasing amounts of an uncoupler which can uncouple the energy supply for glutamine uptake by causing the dissipation of cellular ATP levels in a futile attempt to maintain a normal  $\Delta\bar{\mu}_{H^+}$ ; (ii) the UTL is below the growth temperature in each case; (iii) it has been established in other studies that there is an upper as well as a lower limit to the degree of fluidity compatible with normal functioning of cellular processes, e.g., the growth of microorganisms (30, 72, 73, 75, 216). When these microorganisms are grown at higher temperatures, there is an increase in the proportion of higher-melting fatty acids in the membrane lipids (30) which would confer stability to the organism by a homeoviscous regulatory mechanism. Organisms unable to regulate the fatty acid composition of their membrane lipids with temperature, exhibit lower optimum and maximum growth temperatures. It has therefore been suggested (30, 75) that an upper limit to the fluidity of the membrane lipids may arise from an excessively "leaky" membrane, a structurally unstable lipid bilayer, or an inability of excessively fluid lipid to stabilize certain membrane proteins in a functional configuration. Considering these experimental findings (30, 72, 73, 75) and arguments (30, 75) together with the DTA data in Fig. 8A and B and Table IV and the DSC data in reference 61, one would have been led to predict that 18:1t-cells should exhibit normal increase in  $V_{\max}$  up to relatively high temperatures, i.e., the UTL should be higher than observed. The





reason for this is that 18:1t-membranes display a phase transition range at high temperatures with a  $T_m$  of about 38°. This should, therefore, confer higher thermal stability to these membranes. The  $T_m$  for lipids from each of the other membranes, as estimated by comparison of areas under these DTA curves according to the method reported by McElhaney (73) reveals that the order of  $T_m$  values (which is also the order of decreasing relative fluidity) is as follows: 18:1t > 16:1t > 18:1c > 16:1c > 18:2c,c. Considering fluidity alone, one would then predict that the tendency for membrane stabilization at high temperatures should decrease in the order given above. However, the actual experimental data presented here are not completely in accord with this prediction. Even though 18:1t-cells exhibit the highest UTL relative to the others, its value (which is  $\sim T_m$ ) is, in fact, much lower than expected. On the other hand, 18:2c,c-cells show a UTL which is much higher than would be expected on the basis of fluidity consideration, the value being higher than  $T_m$  by 31°. In the case of 16:1c- and 18:1c-cells UTL is higher than  $T_m$  by 26° and 12.5° respectively. For 16:1t-cells, the UTL, which is  $\sim T_h$ , is higher than  $T_m$  by 7°. On the basis of the difference between the UTL and  $T_m$  therefore, the order of stability observed is as follows: 18:2c,c- > 16:1c- > 18:1c- > 16:1t- > 18:1t-cells.

It is therefore clear that the value of the UTL is not determined solely by the degree of fluidity conferred by UFA-supplementation. Another possibility is that it is determined by the degree of membrane lipid acyl heterogeneity, as has been postulated for some other UFA auxotrophs (60, 290). For example, progressive inactivation of membrane-bound NADH, L- $\alpha$ -glycerol-3-phosphate, succinate and D-lactate



oxidases have been reported as the mole fraction of phospholipids acylated on the 1- and 2-positions with a single UFA species exceeded that found in normal cells grown under similar conditions (290). The acyl chain heterogeneity (see fatty acid profiles in Appendix 3) would decrease in the order 18:2c,c- > 16:1c- > 18:1c- > 18:1t- > 16:1t-cells. Thus, the correlation between acyl heterogeneity and relative thermal stability holds true if one considers 18:2c,c-, 16:1c-, 18:1c- and either 18:1t- or 16:1t-cells. It, however, breaks down when 18:1t-cells are compared with 16:1t-cells. The UTL is therefore not solely determined by the degree of fatty acyl heterogeneity either, although both the degree of membrane lipid fluidity and acyl heterogeneity acting together could explain these results. However, other factors, such as a differential loss of viability at high temperatures, or some non-specific effects (in this strain) of chloramphenicol present in the transport assay medium, could also be responsible. The effect of the presence of Brij 58 in the growth medium for K1060 should not be overlooked.

This phenomenon was not observed with strain 7 at temperatures of up to 40°C, the highest temperature at which assays were done. Since this strain is wild-type in fatty acid metabolism, it possesses the necessary machinery for fine regulation of its membrane fatty acid composition. It therefore shows a fatty acid profile (Appendix 3) containing presumably the optimum amounts of a variety of fatty acids. This might have contributed to the rather different behavior exhibited by this strain.

The possible involvement of the energy coupling mechanism in these phenomena will be discussed in a later section (see Chapter V).



## CHAPTER V

### ACTIVE AMINO ACID TRANSPORT IN ESCHERICHIA COLI: L-PROLINE TRANSPORT AND GENERAL CONCLUSIONS

#### L-PROLINE TRANSPORT

##### A. INTRODUCTION

In bacteria, chemiosmotic phenomena, as postulated by Mitchell (187, 199, 309, 193-198, 200), are involved in the energization of various membrane-associated processes, such as the osmotic shock-resistant active transport of some neutral and ionic solutes, and also, ATP synthesis via the membrane-bound proton-translocating adenosine triphosphatase,  $(Ca^{2+}, Mg^{2+})$ -ATPase. The driving force, the electrochemical gradient of protons (the proton motive force), can be generated by proton extrusion in E. coli under aerobic conditions by electron transport to oxygen or, under anaerobic conditions, either by anaerobic electron transport with, say, nitrate as terminal electron acceptor and formate as electron donor, or by hydrolysis of ATP (from substrate level phosphorylation) by the  $(Ca^{2+}, Mg^{2+})$ -ATPase. The proton motive force (PMF), designated  $\Delta\bar{\mu}_{H^+}$ , is composed of an electrical and a chemical component as follows:

$$\Delta\bar{\mu}_{H^+} = \Delta\psi - \frac{2.3RT}{F} \Delta pH$$

where  $\Delta\psi$  is the electrical potential difference across the membrane (i.e., the membrane potential);  $\Delta pH$  is the transmembrane pH difference; R, T and F are the gas constant, the absolute temperature and the Faraday respectively; and  $2.3RT/F$  is 58.8 mV at 25°C. Recent investigations (309 - 312) have revealed that the transport of some amino acids





(e.g., proline, serine and glycine) and sugars (e.g., lactose) in E. coli is driven by a combination of  $\Delta\psi$  and  $\Delta$  pH (i.e.,  $\Delta\bar{u}_{H^+}$ ), while the accumulation of the anionic substrates (e.g., glucose-6-phosphate and D-lactate) is driven primarily by  $\Delta$  pH. The transport of the cationic substrates has been postulated to respond to  $\Delta\psi$  alone.

Extensive studies in a number of laboratories have established this requirement of the electrochemical potential of protons as the driving force in the transport of proline in Escherichia coli under aerobic and anaerobic conditions (312, 179, 181, 190-192). The proline transport system is thus the best characterized of all the osmotic shock-resistant amino acid transport systems in E. coli. No naturally occurring compound has so far been found which inhibits the function of the proline carrier and it is not known to transport any other natural amino acid. This system is also highly stereospecific (179, 181, 313). The system is amenable to studies with whole cells since the  $K_m$  obtained with membrane vesicles (179) was quite close to that observed with whole cells (181), indicating that metabolism does not change the transport kinetics to any appreciable extent. This same phenomenon has also been reported for the L-glutamine system (169).

There have been some previous reports on the temperature dependence of proline transport in membrane vesicles of E. coli UFA auxotrophs (67, 68). In these studies, however, initial rates of transport at a fixed proline concentration were measured. As discussed in Chapter I of this report, it has been demonstrated (218, 266) that the use of initial rates measured at a single substrate concentration during studies of the temperature-dependence of membrane-associated processes could lead to artifactual breaks in Arrhenius plots. It was therefore considered





necessary to re-examine this transport system in E. coli K1060 and strain 7 with respect to the dependence of both  $K_m$  and  $V_{max}$  on temperature and on the fluidity and physical state of the membrane lipid fatty acyl chains. The results could then be compared directly with those for L-glutamine given in Chapter IV, in the light of the already established differences in energy-coupling between the two transport systems (179, 190-192). The discrepancies that are apparent in these earlier published reports (67, 68) will be discussed in a later section (see "Discussion" and also "General Conclusions") together with the results presented here.

## B. METHODS

### 1. Bacterial Strains and Growth Conditions

E. coli K1060 and strain 7 used here for  $^{14}\text{C}$ -proline uptake studies were the same ones used for  $^{14}\text{C}$ -glutamine transport reported in the preceding chapter. The growth of these cells was done under identical conditions to those employed for glutamine uptake.

### 2. Preparation of Cells and $^{14}\text{C}$ -Proline Uptake Assays

Cells were prepared and transport assays were done exactly as detailed in "Procedure A" for glutamine transport studies.

### 3. Liquid Scintillation Counting

This was also done exactly as detailed for glutamine uptake. Calculations of the initial rates of uptake from the experimental data were carried out as given in Appendix 4.



## C. RESULTS

### 1. Time Course of $^{14}\text{C}$ -Proline Uptake

By adequate manipulation of cell concentration and sampling time as temperature was changed, very reproducible initial rates were achieved in all instances at any single temperature, at much less than 10% depletion of the total available radioactivity in the reaction mixture. This thus differed from the observation for glutamine transport where more than 10% depletion was necessary in some cases. The reason for this may be the fact that the  $K_m$  for proline uptake and, therefore, the concentrations employed in the assays are 10 times higher than the situation for the glutamine transport system.

### 2. Concentration Range of L-Proline Employed

The data presented in Figure 15 is a Lineweaver-Burk plot of the variation with L-proline concentration of initial rate of L-proline transport in E. coli K1060 grown in the presence of 16:1t. The plot is linear for the whole range from 0.031  $\mu\text{M}$  to 19.50  $\mu\text{M}$  L-proline and the  $K_m$  was constant in this instance as the temperature was varied from 20°C to 29.9°C. The mean  $K_m$  of these three temperatures was  $1.07 \pm 0.12$   $\mu\text{M}$  (see also Table VII). This  $K_m$  agrees reasonably well with the value of 0.60  $\mu\text{M}$  for membrane vesicles (179) and 0.44  $\mu\text{M}$  for whole cells (181) reported for E. coli strain W3092. A second  $K_m$  (high  $K_m$ ) has been reported at very high proline concentrations (181). The studies on the temperature-dependence of proline uptake reported herein employed only the low substrate concentration range, 0.05  $\mu\text{M}$  to 5.0  $\mu\text{M}$ . The  $K_m$  for mutant K1060 was found to be also invariant with UFA enrichment (Figure 16A and B and Table VII).

It should be pointed out at this juncture, however, that the  $K_m$





FIGURE 15. Lineweaver-Burk plot of the variation of initial rates of  $^{14}\text{C}$ -proline uptake with L-proline concentration in E. coli K1060 enriched in 16:1t. Cells were grown and prepared, and  $^{14}\text{C}$ -proline uptake assayed as detailed in Methods. Ten concentrations of L-proline (in the range 0.031 to 19.50  $\mu\text{M}$ ) were employed.

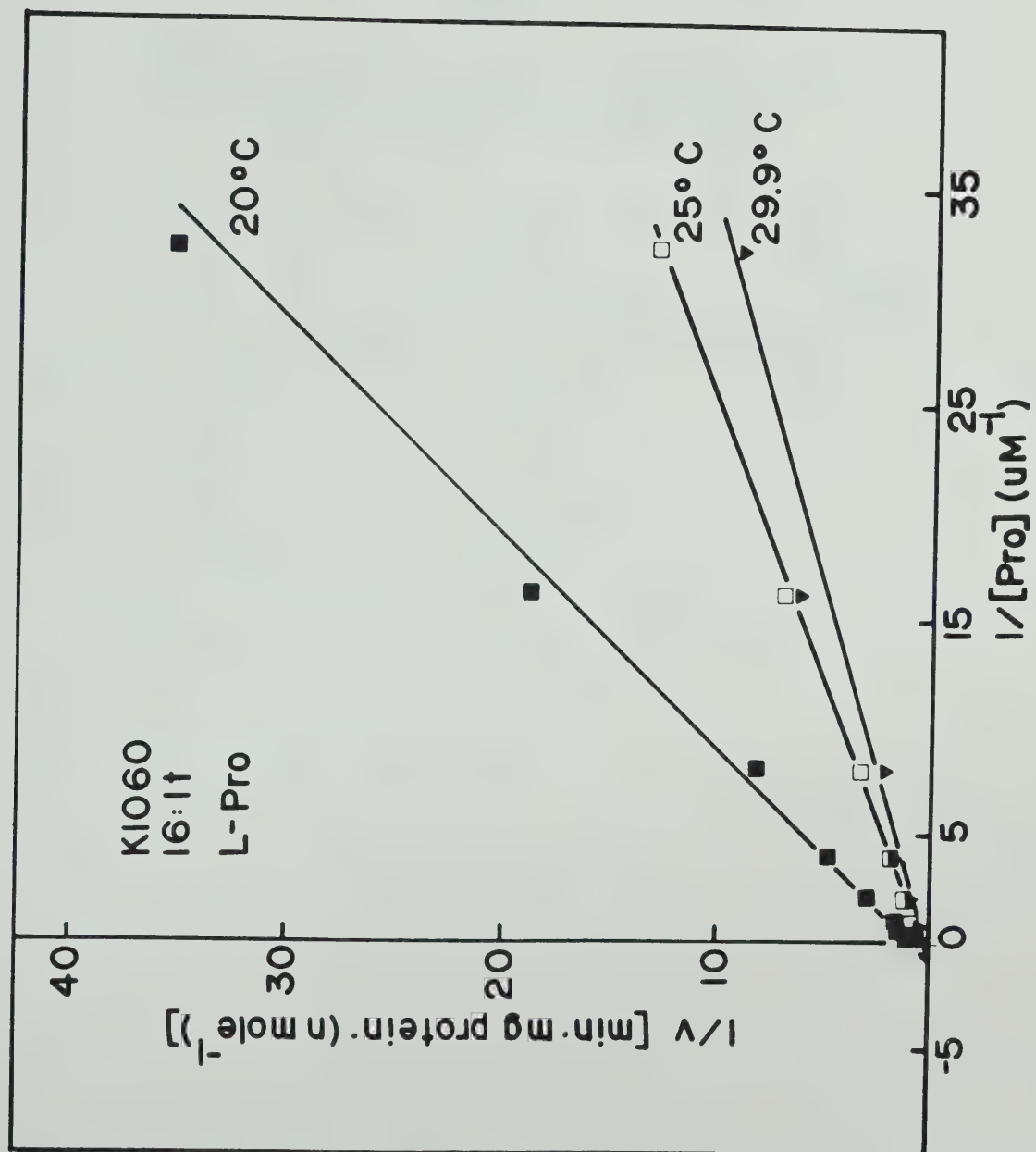






TABLE VII

Mean  $K_m$  Values Over the Assay Temperature Ranges for  
 $^{14}\text{C}$ -Proline Uptake in E. coli K1060  
 Grown with Different UFA Supplements

Cells		$K_m$ (mean $\pm$ S.D.) for proline uptake	Temperature Range
K1060:	16:1t	1.11 $\pm$ 0.33	14.5° - 38°C
	16:1c	1.06 $\pm$ 0.22	7.0° - 41°
	18:1c	0.66 $\pm$ 0.19	3.0° - 38°
	18:2c,c	0.66 $\pm$ 0.12	5.0° - 40°





FIGURE 16A. Hanes' treatment of data for the calculation of  $K_m$  and  $V_{max}$  values for  $^{14}C$ -proline uptake at various temperatures in 18:1c-enriched K1060 cells. Assays were performed as given in Methods. The following values of  $K_m$  and  $V_{max}$  were obtained at the indicated temperatures:

Symbol	Temp (°C)	$K_m$ ( $\mu M$ )	$V_{max}$ (nmole/min/mg protein)
■-■-	13.0	0.83	1.2
□-□-	15.0	0.85	1.5
▼-▼-	17.0	0.84	2.1
▽-▽-	21.0	0.71	2.7
●-●-	29.5	0.90	3.6

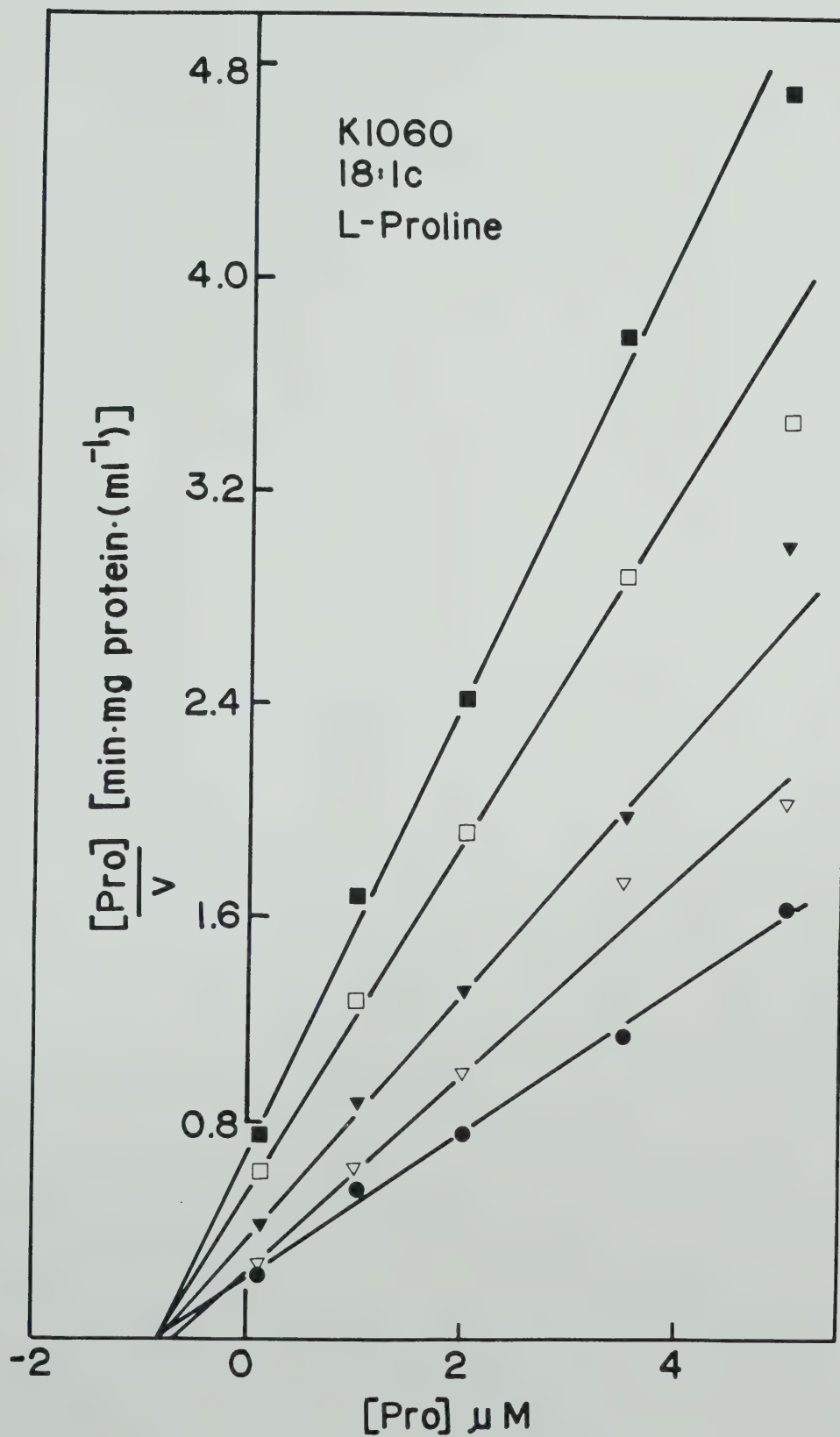


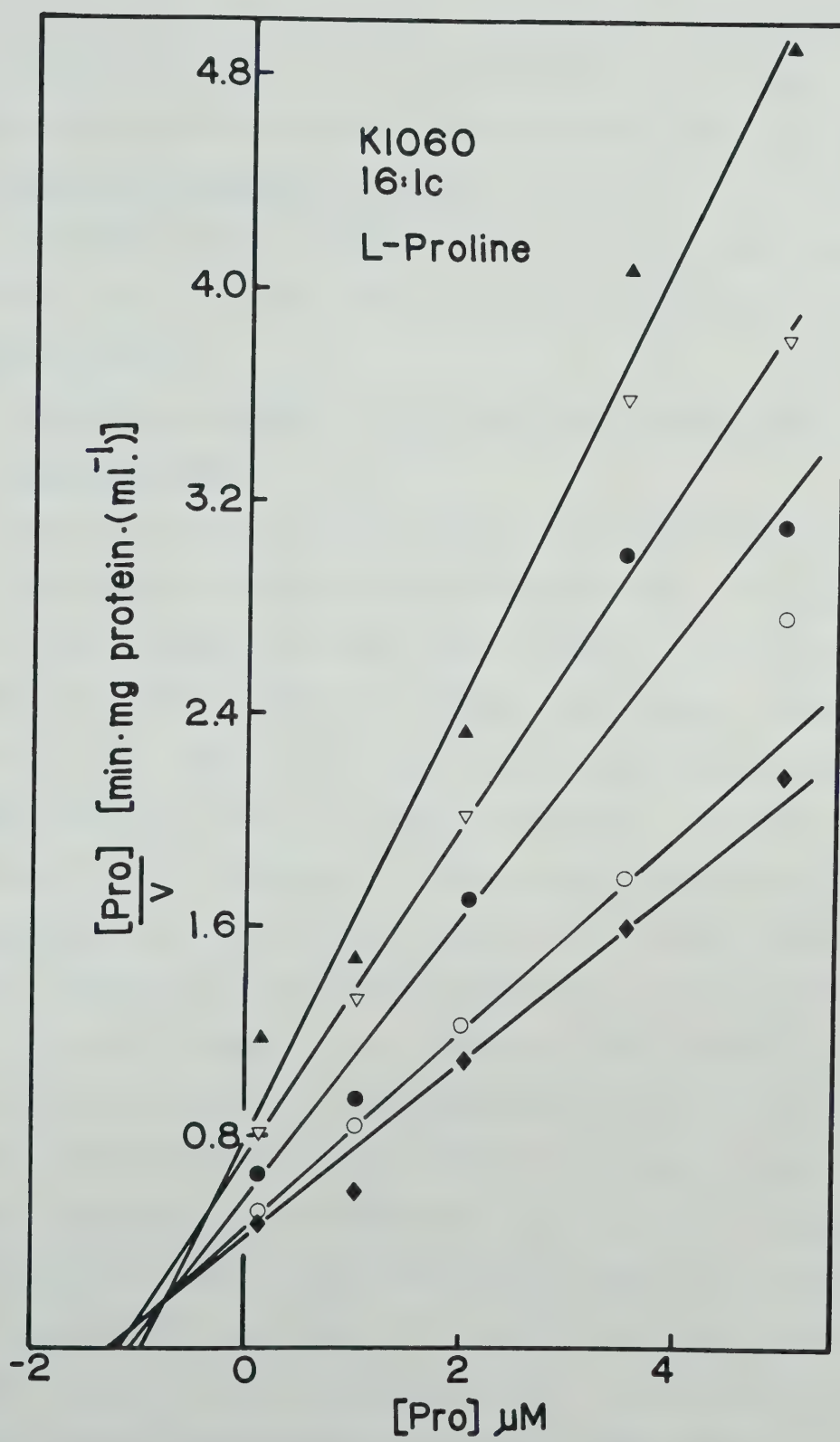




FIGURE 16B. Hanes' treatment of data for the calculation of  $K_m$  and  $V_{max}$  values for  $^{14}C$ -proline uptake at various temperatures in 16:1c-enriched K1060 cells. Assays were done as given in Methods. The following  $K_m$  and  $V_{max}$  values were obtained at the indicated temperatures:

Symbol	Temp (°C)	$K_m$ ( $\mu M$ )	$V_{max}$ (nmole/min/mg protein)
-▲-▲-	15.1	0.98	1.2
-▽-▽-	17.5	1.2	1.6
-●-●-	20.0	1.1	1.9
-○-○-	23.0	1.2	2.6
-◆-◆-	26.0	1.3	3.0







for L-proline uptake in strain 7 decreased ten-fold as temperature was decreased from 45°C to 3°C (Table VIII and Figure 19). Significantly, though, the  $K_m$  at 21°C (i.e., ~ room temperature) was ~0.7 (mean of two determinations) which is close to those reported earlier (179, 181).

### 3. Treatment of Data for $V_{max}$ and $K_m$

Apart from the data presented in Figure 15,  $V_{max}$  and  $K_m$  values were derived from the initial rates by the Hanes' treatment as discussed for glutamine uptake.

### 4. Temperature-Dependence of $V_{max}$ and $K_m$ for L-Proline Uptake

#### (i) Mutant K1060

The  $K_m$  for proline transport remained reasonably constant for mutant K1060 enriched in the various UFA's as portrayed by the mean values and their standard deviations given in Table VII as well as the data presented in Figure 16A and B. However, these data do indicate that the  $K_m$  is ~1.5 times greater for 16:1t- and 16:1c-enriched K1060 cells than for their 18:2c,c- and 18:1c- counterparts. It should also be mentioned that even though the  $K_m$  remained fairly stable below the upper temperature limit (UTL; to be discussed later), there tended to be a slight decrease in  $K_m$  for each UFA-enrichment, a few degrees above the UTL. A slight decrease at lower temperatures also occurred for all except 16:1c-enriched cells, but this could not be related to any particular part of the temperature range. The mean  $K_m$  values in Table VII include all values of  $K_m$  in the temperature range indicated. Considering the fact that at 49.8°C the  $K_m$  for proline transport in strain 7 showed a decrease over the values at 40° to 45°C (see later, and also Table VIII) and that at this temperature (49.8°C) transport  $V_{max}$  obviously indicated aberrant behavior due to excessively high temperature, one



TABLE VIII

Dependence of  $K_m$  and  $V_{max}$  for the Transport of L-Glutamine (L-Gln) and L-Proline (L-Pro) in E. coli Strain 7 on Assay Temperature

L-Gln uptake			L-Pro uptake		
Temp °C	$K_m$ ( $\mu M$ )	$V_{max}$ (nmole/min/ mg protein)	Temp °C	$K_m$ ( $\mu M$ )	$V_{max}$ (nmole/min/ mg protein)
			49.8*	0.90*	7.03 *
			45.0	1.4	20.9
40.0	0.13	8.9	40.0	1.1	20.5
36.4	0.086	7.5	36.0	0.98	19.0
33.1	0.078	6.4	33.0	0.95	18.4
30.0	0.051	4.5	30.0	1.3	19.4
23.9	0.056	3.9	27.0	0.80	13.3
20.1	0.045	2.7	24.0	0.90	11.4
17.0	0.10	2.4	21.0	0.67	8.38
14.2	0.050	1.2	18.0	0.54	6.14
11.2	0.030	0.53	15.0	0.60	4.38
9.0	0.073	0.26	12.0	0.36	2.25
			9.5	0.27	1.17
			7.0	0.22	0.61
			5.0	0.19	0.29
			3.0	0.15	0.14

\*Transport aberrant due to excessively high temperature.



is tempted to speculate that this decrease in  $K_m$  above the UTL in mutant K1060 proline transport is due to some impairment of membrane integrity. The possible significance of this slight decrease in this kinetic parameter above the UTL and at the lower temperatures is uncertain (also see later "Discussion").

The variation with temperature of  $V_{max}$  for proline uptake in K1060 follows the same general trends discussed earlier for the  $V_{max}$  for glutamine uptake in these cells. This parameter increases, as expected, as temperature increases until an upper temperature limit (UTL) is reached. The value of the UTL is unique for K1060 grown with each of the UFA's and above this UTL,  $V_{max}$  starts to decrease. At a certain higher temperature above UTL, transport kinetics no longer obey the Michaelis-Menten equation (186). The Arrhenius plots of these  $V_{max}$  values (Figure 17A - D) show a biphasic linear slope below the UTL for K1060 at all UFA enrichments (except 18:2c,c, which gives a gentle curve) and the break temperature,  $T_b$ , is peculiar to each UFA supplementation. The  $E_a$  below  $T_b$  has a higher value than above it.

The most conspicuous difference between these proline transport data and the glutamine results already discussed (preceding chapter) is that in each case, for K1060 grown with various UFA supplements, both the UTL and the  $T_b$  values observed for proline are shifted to lower temperatures with respect to these same parameters for glutamine transport (Tables VI and XI). The UTL for the two transport systems which is the same value in 18:1c-enriched cells may be the only exception. For strain 7, there is no UTL but rather there are two break temperatures (see following section).







FIGURE 17A. Arrhenius plot of  $V_{\max}$  values for L-proline uptake in E. coli K1060 enriched in 16:1t.  $V_{\max}$  values were derived as given in Methods.

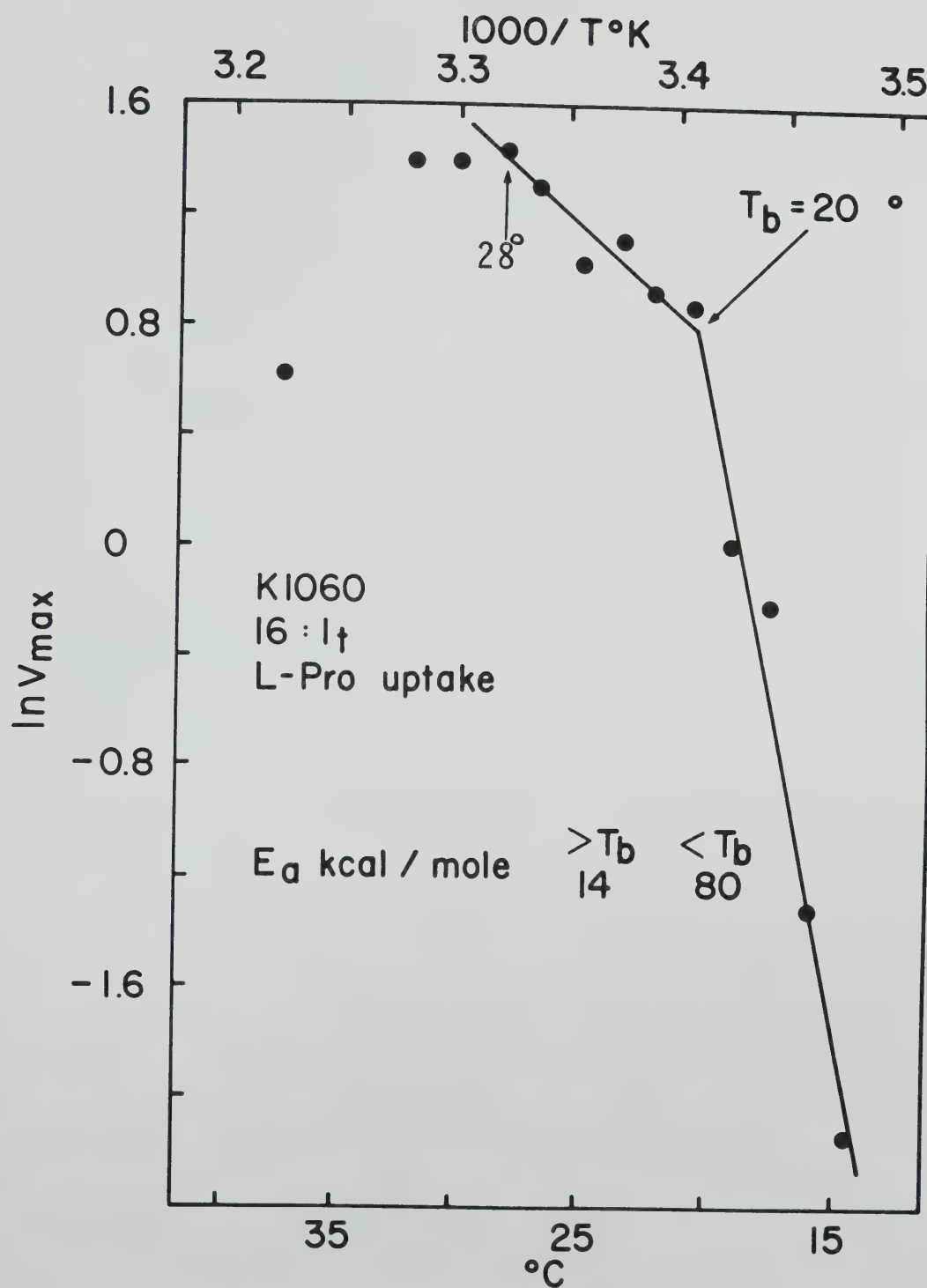






FIGURE 17B. Arrhenius plot of  $V_{\max}$  values for L-proline uptake in E. coli K1060 enriched in 16:1c.  $V_{\max}$  values were derived as given in Fig. 16B.

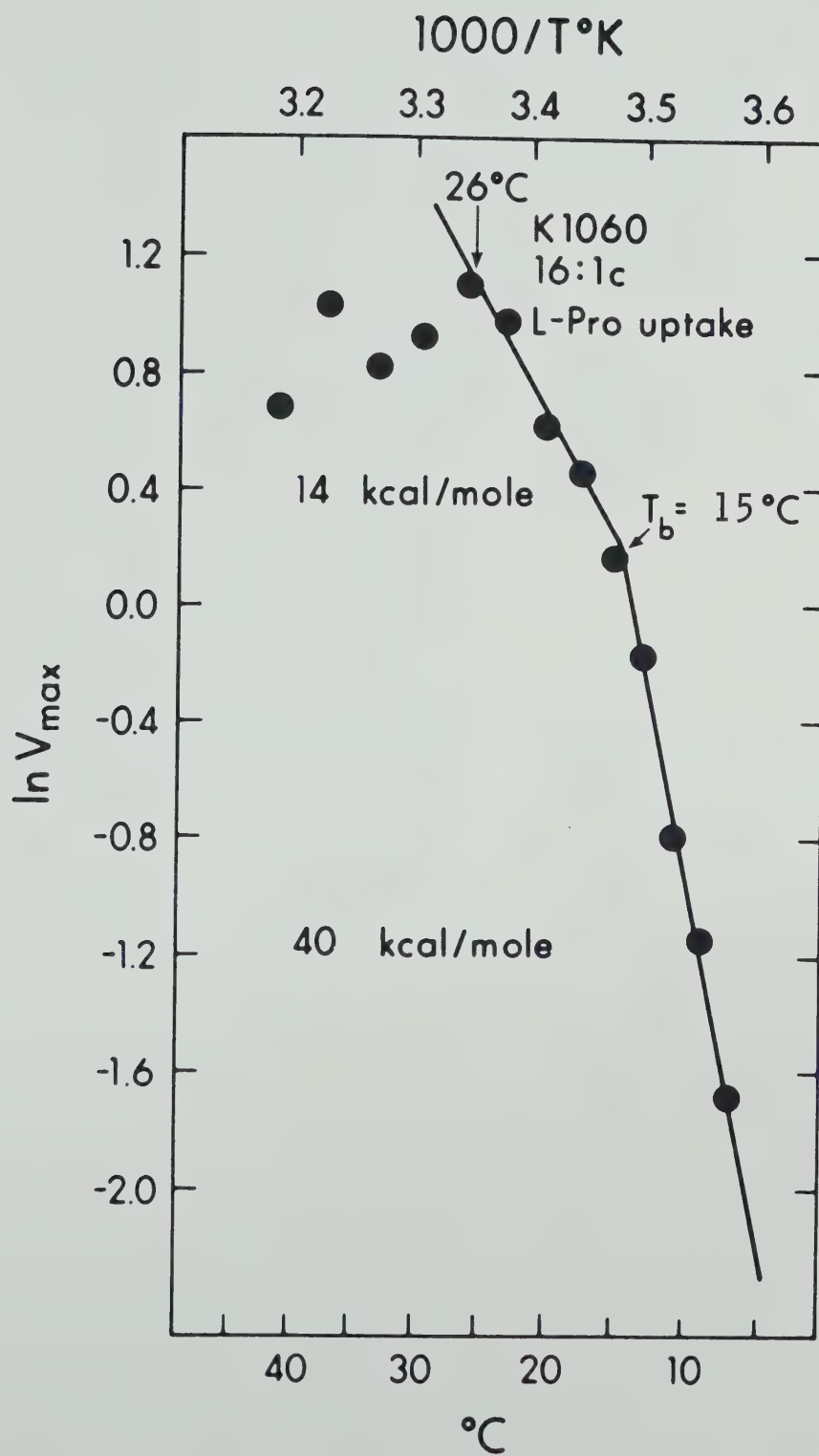








FIGURE 17C. Arrhenius plot of  $V_{\max}$  values for L-proline uptake in E. coli K1060 enriched in 18:1c.  $V_{\max}$  values were derived as given in Fig. 16A.

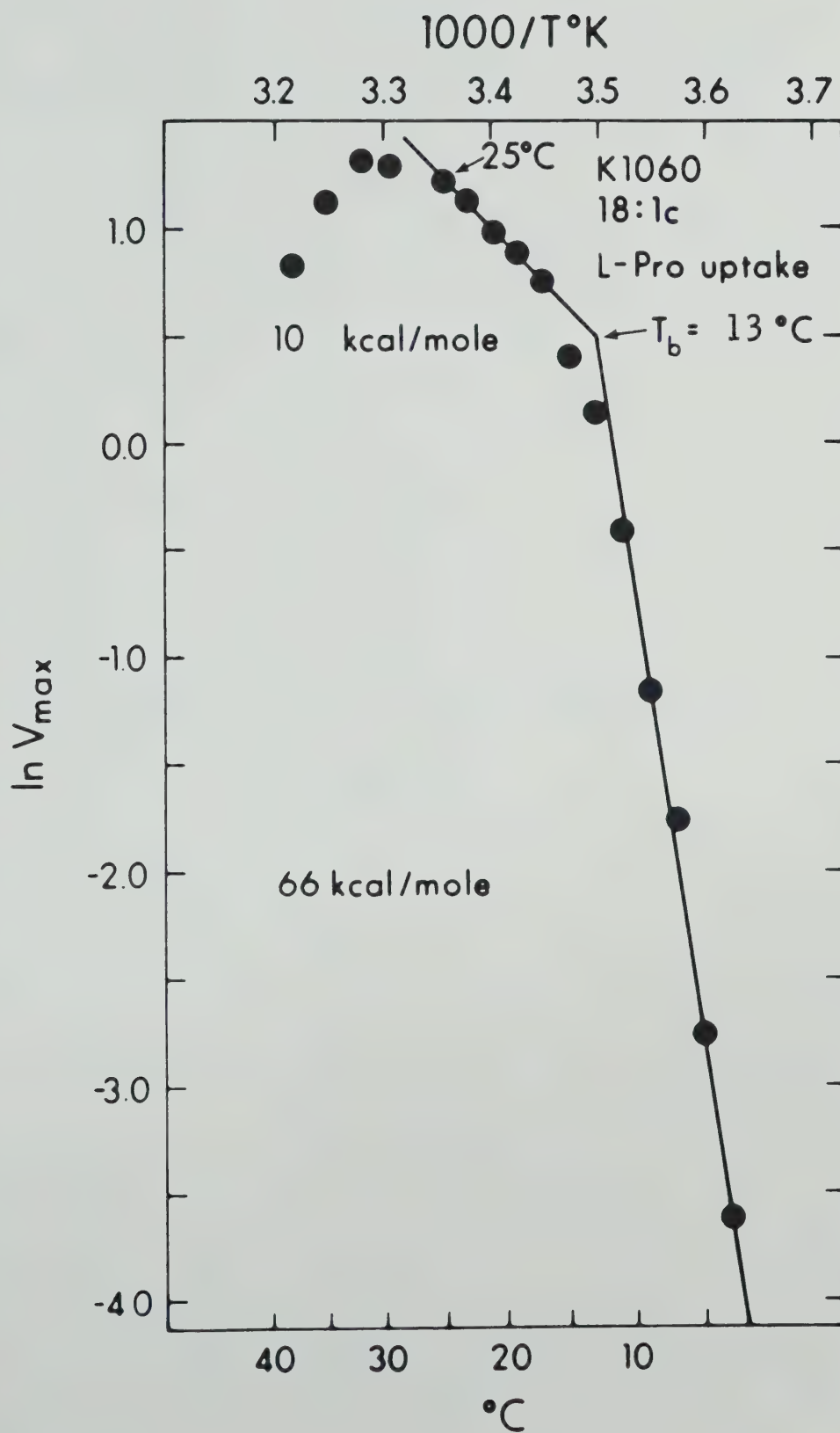






FIGURE 17D. Arrhenius plot of  $V_{\max}$  values for L-proline uptake in E. coli K1060 enriched in 18:2c,c.  $V_{\max}$  values were derived as given in Methods.

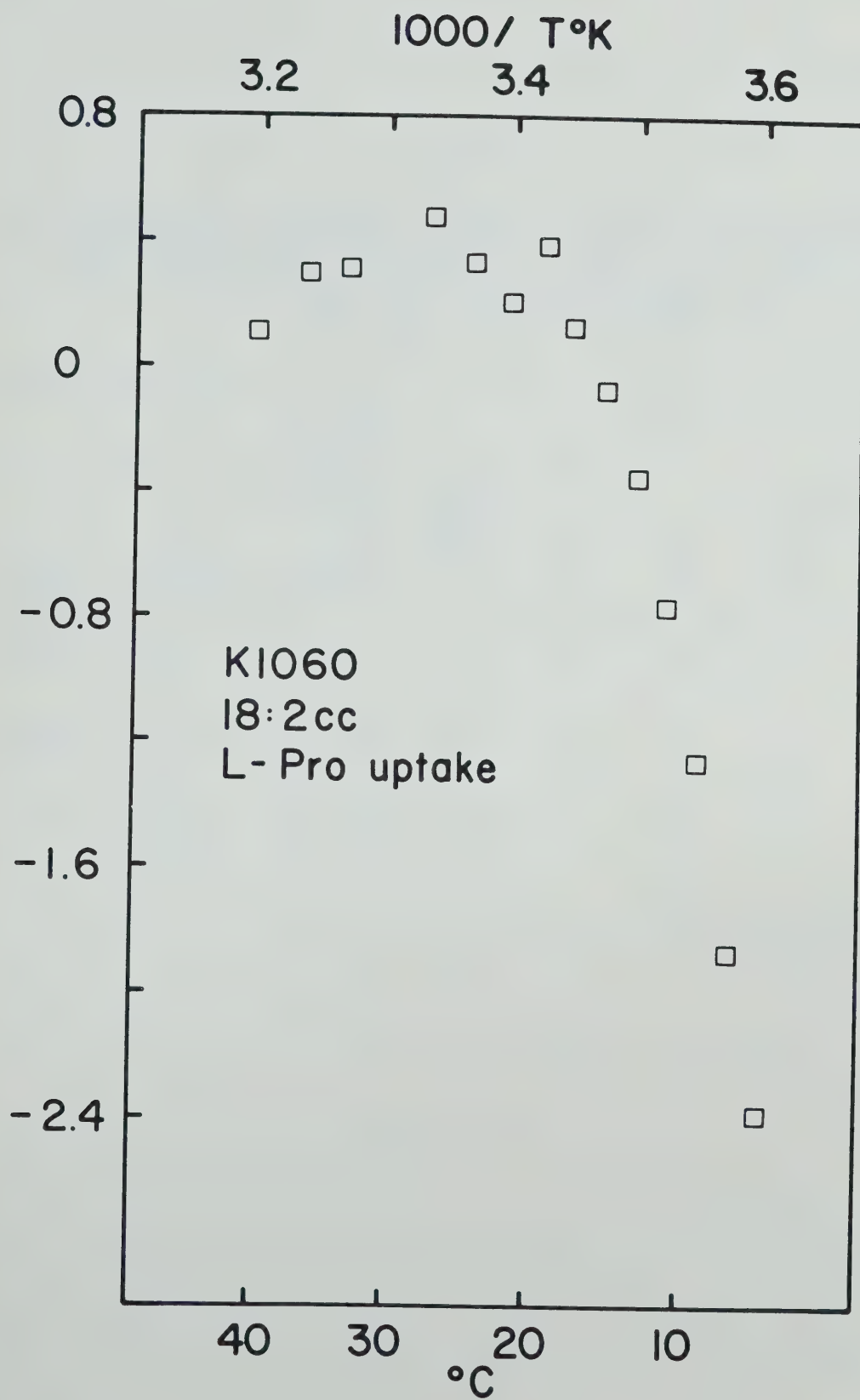






TABLE IX

Arrhenius Plot Temperature Breaks ( $T_b$ ), Activation Energies ( $E_a$ ) and Temperatures at which  $V_{max}$  Starts to Decrease with Temperature (UTL) for L-Proline Transport in Relation to Membrane UFA Enrichment (mole %) and Phase Transition Midpoint ( $T_m$ ) in E. coli K1060 and Strain 7

Cells	UFA Supplement	UFA supplement incorporated into membrane (mole %)	$T_m$ (From Table IV) °C	$T_b$ °C	UTL °C	$E_a$ kcal/mole	
						Above $T_b$	Below $T_b$
Str 7	None	-	15	13	45	17	52
K1060	16:1t	80 - 85	27	20	28	14	80
	16:1c	39 - 44	7	15	26	14	40
	18:1c	52 - 58	12.5	13	25	10	66
	18:2c,c	48 - 50	-2		27		



### (ii) Strain 7

The  $K_m$  for L-proline transport in strain 7 reproducibly varied over a ten-fold range with temperature (Table VIII and Figure 19), decreasing from a value of  $1.40 \mu\text{M}$  at  $45^\circ\text{C}$  to  $0.15 \mu\text{M}$  at  $3^\circ\text{C}$ . This behavior thus differs strikingly from the constant  $K_m$  observed for glutamine transport in both strain 7 (Table VIII) and mutant K1060 (Figures 12 and 13A - C) and the constancy of  $K_m$  for proline uptake in K1060 cells (Table VII and Figures 15 and 16A and B).

$V_{\text{max}}$  for proline transport in strain 7 shows an increase as temperature increases from  $3^\circ\text{C}$  to  $45^\circ\text{C}$ . At  $49.8^\circ$  there is a dramatic decrease, which is indicative of the thermal denaturation of transport proteins and/or a loss of membrane integrity at this rather high temperature. The  $K_m$  also shows a concomitant decrease at  $49.8^\circ\text{C}$ .

Arrhenius treatment of the data (Figure 18) shows a triphasic plot with a break ( $T_b$ ) at  $13^\circ$  and another one ( $T_{30}$ ) at  $30^\circ\text{C}$ . The  $E_a$  below  $T_b$  is higher than above it while that above  $30^\circ$  has the lowest value. Intriguingly,  $T_{30}$  is quite close to the upper boundary  $T_h$  ( $32^\circ\text{C}$ , see Table IV and Figure 8B) of the gel  $\rightleftharpoons$  liquid crystalline phase transition of these membranes. The  $T_b$  value of  $13^\circ\text{C}$  is also lower than its counterpart for glutamine transport in this strain.

### D. DISCUSSION

The data presented here indicate a number of similarities between the response to temperature of the L-proline transport and the L-glutamine transport systems in E. coli. However, they also go further to demonstrate a number of striking differences between these two amino acid transport systems.





FIGURE 18. Arrhenius plot of  $V_{\max}$  values for L-proline uptake in E. coli strain 7.  $V_{\max}$  values were derived as given in Methods.

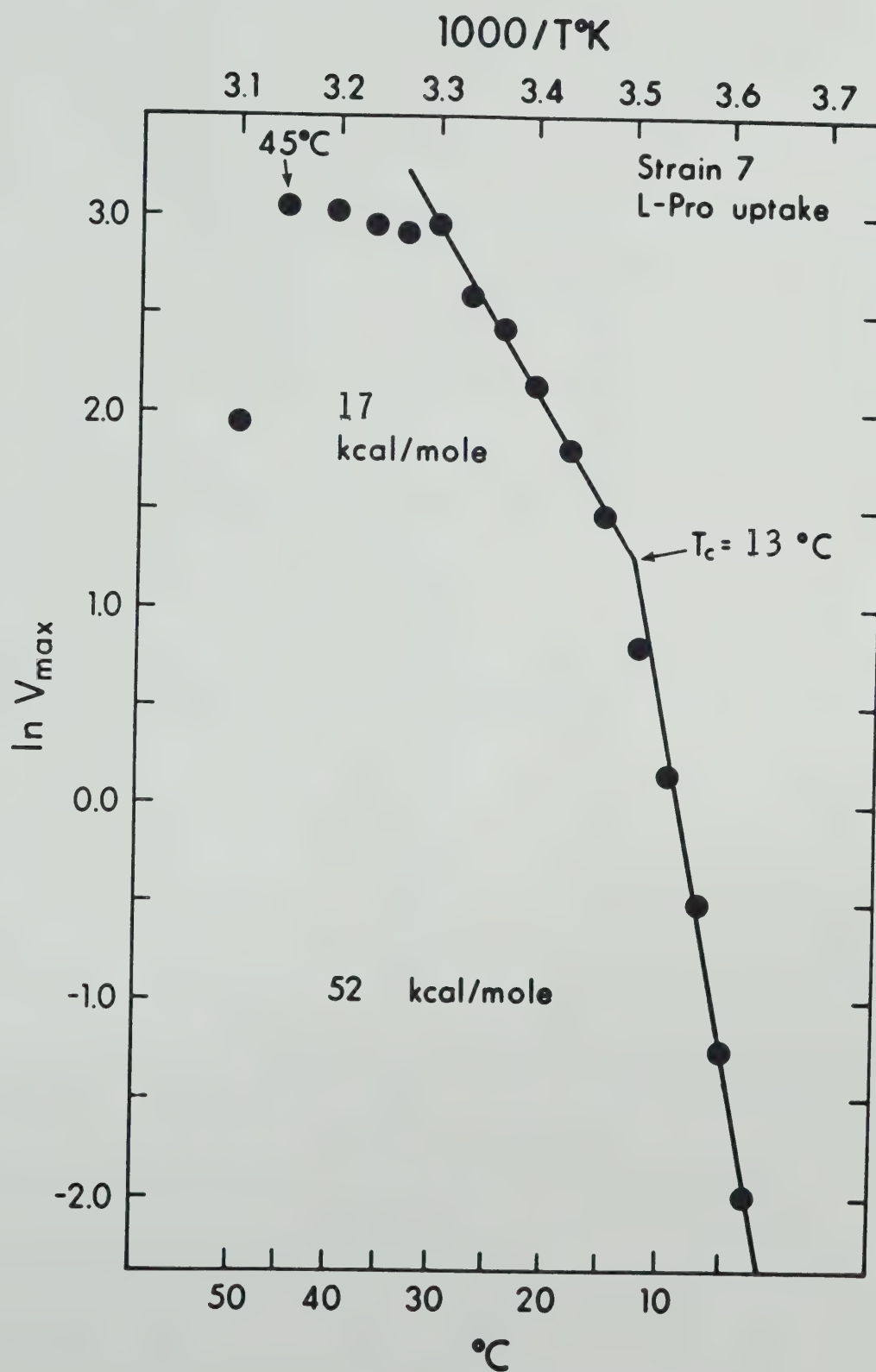
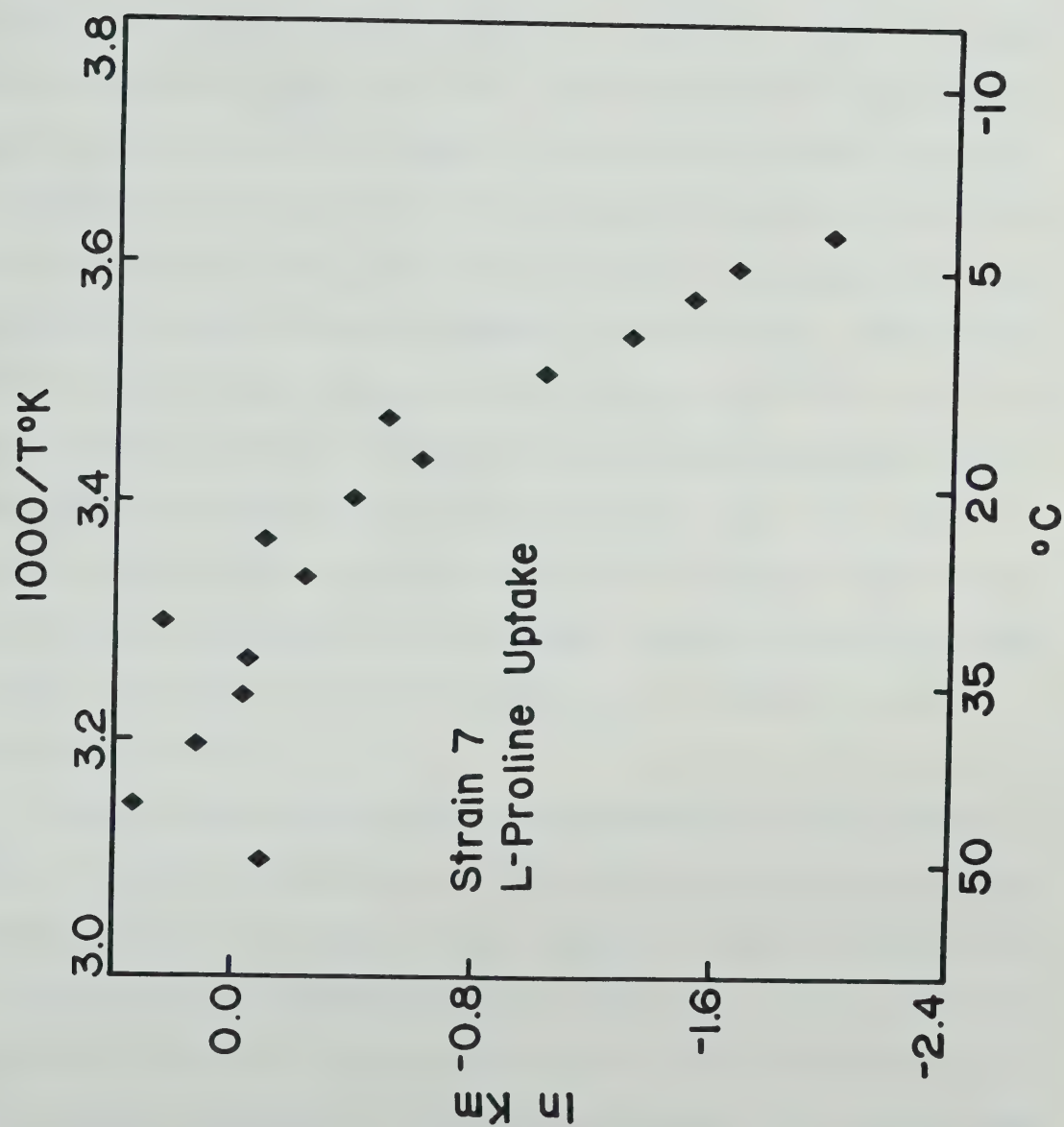








FIGURE 19. Van't Hoff plot of  $K_m$  values for L-proline uptake in E. coli strain 7.  $K_m$  values were derived as given in Methods.





The  $K_m$  for proline transport is reasonably constant in mutant K1060 (Table VII and Figures 15 and 16 A and B) but reproducibly varies over a ten-fold range in strain 7 (Table VIII and Figure 19). It is of interest to note that the  $K_m$  at 21° (i.e., room temperature) is consistently about 0.7  $\mu$ M, which is quite close to published values for a different strain of E. coli (179, 181). The reason for this variation in  $K_m$  for proline transport in strain 7 is not known, but one is tempted to speculate that it may be wild type phenotypic behavior. It has been reported (218) that the  $K_m$  for lactose transport in E. coli ML308 also responds to temperature in a strikingly similar fashion. Since it has now been conclusively demonstrated that these two shock-resistant transport systems are similar with regard to the energetics of their operation (both are driven by the proton motive force  $\Delta\bar{\mu}_{H^+}$ ) (312, 309), it will not be surprising if it is discovered that they have other characteristics in common, which would have some bearing on some common mechanistic attributes of these two systems, e.g., a similar response to temperature changes.

A behavior which reveals an obvious difference between a binding protein dependent transport system (glutamine transport, see preceding chapter) and the non-binding protein dependent transport reported here is the resistance to temperature changes displayed by the  $K_m$  of the former system (Table VIII and Figures 12 and 13A - c). It would then appear that the resistance to changes in temperature of the proline transport system in mutant K1060 could have been acquired during the various mutagenic treatments by which this UFA auxotroph was derived. The slight decrease in  $K_m$  shown by K1060 enriched in some UFA species may then be a manifestation of rudiments of this lost wild type trait. It



would be interesting to determine if other shock-resistant transport systems in these two strains exhibit similar behavior.

As was the case with glutamine uptake, strain 7 shows an increase in  $V_{\max}$  for proline transport from 3°C to 45°C, this kinetic parameter dropping dramatically only at 49.8°C (Table VIII and Figure 18) as previously discussed (see "Results"). The Arrhenius plot of  $V_{\max}$  displays the characteristic break temperature,  $T_b$ , at 13°C as well as a second break temperature,  $T_{30}$ , at 30°C. At 30°C, more than 99% of the strain 7 membrane lipids are in the liquid crystalline state. Thus, the drop in the  $E_a$  value above this temperature demonstrates that, as soon as all the membrane lipids are in the liquid crystalline state, further increase in temperature (i.e., further increase in thermal motion of the fatty acyl chains) above this point does not lead to a significant increase in  $V_{\max}$ . The  $T_b$  of 13° is lower than that displayed in the Arrhenius plot of  $V_{\max}$  for glutamine uptake in this E. coli strain. The UTL is not exhibited for proline transport in this strain.

The  $V_{\max}$  for proline transport in mutant K1060 increases with temperature only up to a UTL which is peculiar for each UFA supplementation. Above the UTL,  $V_{\max}$  decreases with temperature until another higher temperature (less definitive) above which the data can no longer be treated to yield  $K_m$  and  $V_{\max}$  values. Also, above the UTL, the initial rate of uptake at each proline concentration actually decreases as temperature increases. Thus, an increase in temperature above the UTL mimics the effects of adding increasing concentrations of an uncoupler. Below the UTL, the Arrhenius plots are biphasic, displaying a peculiar  $T_b$  value for each UFA supplementation, with the exception of 18:2c,c-grown cells which give a plot curving off between 13° and 15°C (Figure





17A - D). This behavior resembles that displayed by glutamine transport in this *E. coli* auxotroph. An obvious difference, however, is that both the UTL and  $T_b$  are shifted to lower temperatures relative to the situation for glutamine transport.

The  $E_a$  values in Table IX demonstrate that, just like the case for glutamine transport,  $E_a$  below  $T_b$  is higher for mutant K1060 enriched in the trans-UFA, 16:1t, than for this auxotroph enriched in the cis-UFA species, as well as than for strain 7. A similar behavior has been reported for  $\alpha$ -amino isobutyric acid uptake in Ehrlich ascites cells (221) in which  $E_a$  below  $T_b$  was higher the higher the saturated fatty acid content of the membranes. Generally also, for both strain 7 and mutant K1060,  $E_a$  below  $T_b$  is higher than above it; but no definite discernible trend exists in these  $E_a$  values above  $T_b$ . Table X portrays the striking similarity which exists between the  $E_a$  value below  $T_b$  for proline transport and that for glutamine transport in the same cell type. For instance, the  $E_a$  below  $T_b$  for strain 7 is 52 kcal/mole for proline transport and 54 kcal/mole for glutamine transport and, for K1060 enriched in 16:1t, the values are 85 and 80 kcal/mole, respectively, for glutamine and proline uptake. For mutant K1060, the  $E_a$  above  $T_b$  is lower for proline than for glutamine transport at all UFA supplementations, but the order is reversed for these systems in strain 7. No reasonable rationalization has so far been found for these trends in  $E_a$  values.

At their respective break temperatures ( $T_b$ ), for proline transport, the 16:1t-grown K1060 cell membrane lipids are 13% in the liquid crystalline state while the 18:1c-, 16:1c- and 18:2c,c-cell membrane lipids are ~50%, 93% and (82% - 87%), respectively, in the liquid crystalline state. From a consideration of the  $T_m$  values (Tables IV, VI and IX),



TABLE X

Activation Energies (Ea) for L-Glutamine (L-Gln) and L-Proline (L-Pro) Transport in E. coli Strain 7 and E. coli K1060

Cells	UFA Supplement	Ea kcal/mole			
		L-Gln		L-Pro	
		Above T <sub>b</sub>	Below T <sub>b</sub>	Above T <sub>b</sub>	Below T <sub>b</sub>
Str 7	None	11	54	17	52
K1060	16:1t	17	85	14	80
	16:1c	18	40	14	40
	18:1c	20	60	10	66

These values were taken from Tables VI and IX.



TABLE XI

Arrhenius Plot Temperature Breaks ( $T_b$ ) and Temperatures at which  $V_{\max}$  Starts to Decrease with Temperature (UTL) for L-Glutamine (Gln) and L-Proline (Pro) Transport in E. coli Strain 7 and E. coli K1060

Cells	UFA Supplement	$T_b$ (°C)		Upper Temperature Limit (UTL) (°C)	
		Gln	Pro	Gln	Pro
Str 7	None	16	13	≥40	45
K1060	16:1t	23	20	33.7	28
	16:1c	17	15	33	26
	18:1c	14	13	25	25
	18:1t			37.5	
	18:2c,c			29	27

These values were taken from Tables VI and IX.



the order of relative fluidities conferred to these membranes would be 18:2c,c > 16:1c > 18:1c > 16:1t. Thus, it appears that, as was the case with the  $T_b$  values for glutamine transport, the  $T_b$  values for proline transport respond to fluidity alone. In other words, the more positive is the difference  $T_b - T_m$ , the higher is the liquid crystalline fraction at  $T_b$ . This correlation holds for 16:1t- K1060 cells, strain 7, 18:1c- and 16:1c- K1060 cells. For these four,  $T_b - T_m$  values are  $-7^\circ$ ,  $-2^\circ$ ,  $+0.5^\circ$  and  $+8^\circ$  respectively, and the liquid crystalline fraction at their respective  $T_b$  values is 13%, 35%,  $\sim 50\%$  and 93%. However, the correlation breaks down for 16:1c- and 18:2c,c-cells, for which  $T_b - T_m$  are respectively  $+8^\circ$  and  $(+15^\circ \text{ to } +17^\circ)$  but the liquid crystalline fractions at  $T_b$  are, respectively, 93% and (82% to 87%).

Even though the UTL values are shifted to lower temperatures relative to the glutamine values, they are still determined by both membrane lipid fluidity and membrane phospholipid acyl chain heterogeneity. Considering the earlier discussion (see preceding chapter) for the glutamine situation, the order of relative thermal stabilities conferred to the K1060 membranes should decrease in the same order as their decreasing  $T_m$  values, thus, 16:1t > 18:1c > 16:1c > 18:2c,c. However, the stability is higher the more positive is the difference  $UTL - T_m$ , and so the actual order of relative stabilities is 18:2c,c > 16:1c > 18:1c > 16:1t. This therefore means that some other factor operating in concert with fluidity has contributed to such an extent as to reverse the order of relative stabilities conferred by fluidity alone. This factor may be the heterogeneity of the acyl chains of the membrane phospholipids. As was discussed for the glutamine case (Chapter IV), it is possible that the heterogeneity of the 18:2c,c-membrane may contribute





a sufficient stabilizing influence to make it most stable of them all, and the extreme homogeneity of the 16:1t-membranes would militate against stability to a great extent and so make them rather unstable to temperature. This same line of argument places 16:1c and 18:1c-membranes respectively next to 18:2c,c-membranes. Strain 7 is much more thermally stable than K1060 grown on 18:2c,c. This is therefore suggestive of the influence of fine regulatory effects on the fatty acid metabolism of this wild type strain. The fatty acid profile of this strain presumably contains an optimum amount of each of a variety of fatty acids, and these confer a higher heterogeneity to its membrane lipids than is the case with K1060 grown with any UFA supplement.

It is tempting to speculate that the cause of the display of the UTL is some defect of energy-coupling in these K1060 cells under these conditions. It should be mentioned again that strain 7 behaves normally up till 45°C. The main difference which is experimentally detectable between glutamine transport and proline transport in E. coli is the mode of energy coupling.

As was discussed in the preceding chapter, it has been reported that leakage of ions from E. coli cells (60) and inactivation of energy coupling enzymes (290) may result from a high degree of homogeneity in the membrane phospholipid acyl chains. The apparent degree of heterogeneity in the membranes of the cells employed in these studies has been discussed earlier (preceding chapter). If there is leakage of protons from these cells (inversely related to the extent of heterogeneity), it then follows that the energy status of the membrane would be adversely affected. The magnitude of  $\Delta\bar{\mu}_{H^+}$  across the membrane



would be diminished to the same extent as the proton leak. Thus, proline transport would be inhibited as soon as this phenomenon starts. Further increase in temperature leads to the formation of more liquid crystalline lipid and creates increased flexibility of the acyl chains of the other lipids already in the liquid crystalline state. Thus, the leakage of protons is enhanced. This would account for the further drop in  $V_{\max}$  (and initial rates at each proline concentration) with increase in temperature.

In the glutamine transport, the energy coupling is linked to ATP or its derivative. Since ATP supply from glycolysis is available to these cells during the transport assay, the effects of the  $H^+$  leakage should not be obvious until at such a temperature when the dissipation of  $\Delta\bar{\mu}_{H^+}$  is enough to start to lead to the depletion of glycolytically derived ATP. It is at this temperature, therefore, that  $V_{\max}$  for glutamine transport should start to decrease. Thus, this explains why the UTL is higher for glutamine transport than for proline transport in mutant K1060 enriched in any UFA (except perhaps 18:1c). In the case of strain 7 [wild type, with an optimally heterogeneous membrane (see Chapter IV)] the membrane remains thermally stable up to 45°C. Moreover, for the different UFA enrichments of mutant K1060 considered, the most heterogeneous (18:2c,c-cells) exhibits the most thermally stable membrane and the converse is also the case, i.e., the least heterogeneous (18:1t- and 16:1t-cells) have the least stable membranes. Thus, this correlates with the experimental findings.

Comparison of the results on the temperature-dependence of L-glutamine transport (given in the preceding chapter) with those reported here, shows up a number of similarities between these two transport



systems, while at the same time high-lighting a number of interesting differences. (i) The different trends in the  $K_m$  with change in temperature (invariant in K1060 and strain 7 for glutamine transport and varying for proline transport in strain 7 but not in K1060) suggest some mechanistic difference in the two amino acid transport systems. (ii) A  $T_b$  is exhibited in each E. coli type for both transport systems, indicating a response to membrane lipid physical state. However, the lower value of  $T_b$  for proline transport is suggestive of differing preferential interactions with (specific) lipid types in the rate limiting step of the two transport systems. (iii) Only one break temperature is obtained for glutamine transport  $V_{max}$  in strain 7 up to 40°C (the highest assay temperature employed). However, the  $V_{max}$  values for proline transport yield two break temperatures, the one at 30°C ( $T_{30}$ ) being close to the point of completion of the broad gel  $\rightleftharpoons$  liquid crystalline phase transition of these membranes. This, of course, reinforces the earlier suggestion that there is preferential lipid association in the operation of each of these two systems. The break at 30°C also tends to indicate that some degree of order is required in the lipids around the rate limiting protein in proline transport in order for a large increase in  $V_{max}$  to be observed with increasing temperature. (iv) The UTL phenomenon is exhibited by K1060 for both glutamine and proline transport. However, this temperature parameter has a lower value for proline transport than for glutamine transport in K1060 cells enriched in any particular UFA. This therefore bears on the difference in energetics between the two systems since, as discussed earlier, the proline system would be adversely affected at a lower temperature than the glutamine system, if the UTL is created as a result of proton leak, thus





decreasing  $\Delta pH$ .

It is however possible that other factors are responsible for the UTL phenomenon as discussed in the preceding chapter. It is also worthy of note that some recent studies of the inhibition of proline and glutamine transport in E. coli by colicin K (318) tend to show that these two transport systems have some features in common. This notwithstanding, these transport systems do differ in a number of ways as earlier discussed.

A great part of the results reported here on proline transport differs from those already reported (67, 68) for this transport system operating in membrane vesicles derived from other UFA auxotrophs (Tables XII and XIII). It should be also mentioned that many discrepancies do exist even between these already published data for strain OL<sub>2</sub><sup>-</sup> (67) and those published for strain K1059 (68). These differences are perhaps not surprising, however, for a number of reasons. In the first place, strain differences are known to introduce discrepancies in results obtained in some studies (271). Secondly, these earlier studies on the temperature dependence of proline uptake utilized membrane vesicles, and thirdly, these investigations relied on initial uptake rates at single purportedly "saturating" levels of proline. It is thus clear that since the data herein presented demonstrate that for proline transport,  $K_m$  increases with temperature for strain 7 (i.e., wild type), if such a situation existed for any of these earlier studies reported in references 67 and 68, an artifactual break in Arrhenius plots would be obtained, as already demonstrated in other systems (218, 266). The activation energies derived together with these false breaks would therefore be very prone to serious errors.





TABLE XII

Arrhenius Plot Break Temperatures ( $T_b$ ) for L-Proline Uptake  
 $V_{max}$  Values in E. coli K1060 Compared with the Same Parameter  
 for L-Proline "Initial Rate" of Uptake in Other  
E. coli UFA Auxotrophs Reported in References 67 and 68

UFA Supplement	$T_b$ °C for Proline Uptake		
	Esfahani <u>et al.</u> (reference 67)	Schechter <u>et al.</u> (reference 68)	This study
	<u>E. coli</u> strain OL <sub>2</sub> <sup>-</sup> membrane vesicles Initial Rates	<u>E. coli</u> K1059 membrane vesicles Initial Rates	<u>E. coli</u> K1060 whole cells $V_{max}$
18:1c	19°	22°	13°
18:1t	26°	38°	N.D.
18:3c,c,c	14°	19°	N.D.
18:2c,c	N.D.	No break	~13° - 15°



TABLE XIII

Activation Energies ( $E_a$ ) Below and Above  $T_b$  for L-Proline Uptake  
 $V_{max}$  in K1060 Compared with the Same Parameter for L-Proline  
 "Initial Rate" of Uptake Reported in Reference 68 for  
 Another E. coli UFA Auxotroph

UFA Supplement	Ea kcal/mole from Arrhenius plots			
	<u>Schechter et al.</u> (reference 68)		This study	
	<u>E. coli</u> K1059 membrane vesicles Initial Rates		<u>E. coli</u> K1060 whole cells $V_{max}$	
	Above $T_b$	Below $T_b$	Above $T_b$	Below $T_b$
18:1c	18	29	10	66
18:1t	10	55	N.D.	N.D.
18:3c,c,c	14	35	N.D.	N.D.
18:2c,c		26	?	44



## GENERAL CONCLUSIONS

A comparison of the data presented here on the amino acid transport systems with those for the facilitated diffusion of glycerol (see Chapter III) reveals a number of differences. (i) The UTL is not exhibited by the glycerol facilitated diffusion system. (ii) The  $T_b$  for 18:1t-grown K1060 cells occurs at  $\sim 42^\circ\text{C}$  (i.e., above  $T_h$ ) for glycerol facilitated diffusion, while for glutamine uptake it occurs at  $\sim T_1$ . (iii) For 18:1c-grown cells, the  $T_b$  for facilitated diffusion of glycerol is higher than that for either glutamine or proline transport. (iv) No breaks are obtained in the Arrhenius plots for glycerol facilitated diffusion in 16:1c- and 18:2c,c-cells of K1060. For both glutamine and proline transport, however, 16:1c-K1060 cells yield a biphasic linear Arrhenius plot while 18:2c,c-cells yield a gentle curve. (v) Considering the mutant K1060, the  $E_a$  values above  $T_b$  for facilitated diffusion in 18:1t- and 18:1c-cells and those from the 18:2c,c- and 16:1c-cells are equal and are generally lower than that for glutamine or proline transport. (vi) The  $E_a$  below  $T_b$  is generally lower for glycerol facilitated diffusion than for proline or glutamine uptake. All these observations can be rationalized on the basis of one or both of two possibilities. In the first place, each of the transport systems studied involves the operation of a different kind of protein or proteins. Each of these systems could have, therefore, a unique temperature dependence, related to membrane lipid fluidity and phase state in somewhat different ways. Another possibility is that at least a part of the observed differences are due to a differential response of the energy coupling machinery to the physical state of the membrane lipids. The glycerol facilitated diffusion, in this regard, involves no input of energy. The effects



observed in this system are therefore pertinent to the translocation step alone. Glutamine and proline transport are energy coupled in different ways (as previously discussed). The differences observed between these two may therefore be due to these energy coupling differences.

A number of other studies have implicated the energy coupling reaction as an intimate component of the active transport process, and suggest that the interpretation of data obtained from experiments on the temperature-dependence of active transport should not treat the translocation step in isolation of the energy coupling step. In this regard, a report by Hutson (314) on the steady state kinetics of mitochondrial  $\text{Ca}^{2+}$  uptake focuses attention on the driving force for  $\text{Ca}^{2+}$  uptake and the limitations of treating the  $\text{Ca}^{2+}$  transport system as an isolated enzyme system. The author implies that the rate-limiting step is probably at the level of the electron transport chain rather than at the calcium carrier. In addition, Sprott et al. (210) (as discussed earlier) observed that in E. coli energized submaximally, a rate-limiting step in the uptake of amino acids belonging to various transport system types the transfer from an aqueous to a hydrophobic environment. However, this hydrophobic effect is not manifested when transport under aerobic conditions is considered. The authors suggest that the reason for this could be that differing numbers of carriers are involved. Another possible reason, emanating from these experiments reported here, would be the differential involvement of the energy coupling reactions in each of the amino acid transport types.

In an earlier publication, Shechter and associates (68) concluded, from data derived from Arrhenius plots of initial rates of active amino acid and sugar transport in membrane vesicles of a UFA auxotroph of E.





coli, that the membrane physical state was affecting the translocation step of the active transport of proline. Surprisingly, these same investigators have recently presented new data on the temperature-dependence of initial rates of  $\beta$ -galactoside transport and the binding of fluorescent dansylgalactoside to the lac carrier in E. coli membrane vesicles, which they interpret to be consistent with a change in the number of functional lac carriers in response to the gel  $\rightleftharpoons$  liquid crystalline phase transition of these membranes (260, 261). They reported that the binding of the dansylgalactoside was independent of temperature. Nonetheless, they did not address the fact that the  $K_m$  for  $\beta$ -galactoside transport increases with increases in temperature (218), nor did they consider the possible contribution to their observations by the energy link to the overall transport process. Thus, these phenomena might have contributed to the rather equivocal interpretations that have emanated from their various reports (68, 260, 261).

It is known that the different membrane-bound enzymes which are involved in energy-coupling reactions do respond to the composition and physical state of the membrane lipids (14, 67, 290, 315). In some instances, however, these enzymes respond in remarkably different ways. This is illustrated by the observation by Van Heerikhuizen et al. (315), who reported that when membrane vesicles are formed at 0°C, NADH oxidase and succinate dehydrogenase activities are found mainly in the protein-rich (particulate) portions of the membrane while D-lactate dehydrogenase activity is found in both parts of the membrane. This therefore means that an added complication is introduced in the interpretation of results on membrane phase state effects on an active transport process. This would result from the fact that a break in an Arrhenius



plot may thus be due to a physical separation of some (or all) of the energy-coupling proteins from the carrier proteins by the preferential segregation of any of these sets of proteins to a different domain of the membrane at low temperatures, thus abruptly creating a new rate-limiting step in the overall process.

The final conclusion to be drawn from these studies presented here is that, in a purely facilitated diffusion system, the response of the system to the fluidity and physical state of the membrane lipids reflects the interaction of the carrier protein(s) with the membrane lipid phase. In an active transport system, however, the response observed is a complex one possibly involving the response of the carrier protein(s) superimposed on that of the proteins which constitute the energy-coupling machinery of the active transport system as a whole.

#### SUGGESTIONS FOR FURTHER INVESTIGATIONS:

Lancaster and Hinkle have very recently reported an elegant demonstration of a purely facilitated diffusion system derived, without the use of energy poisons, from the  $\beta$ -galactoside transport system in E. coli. These authors studied this system in inverted membrane vesicles and characterized it by a number of criteria (316). Since the proline transport system in E. coli is a shock-resistant system as is the lactose system, very useful information can be derived by first characterizing an equivalent facilitated diffusion system for proline in the E. coli strains used here, and then studying the temperature-dependence of  $V_{\max}$  and  $K_m$  for this facilitated diffusion system in these strains under the same conditions reported here, using the same techniques devised by these authors (316). The results derived from these studies would



yield direct information with respect to the influence of the membrane lipid phase state on the translocation step of this process. In addition, by comparison with results reported here, it would then be possible to find out whether the UTL is a characteristic of one or both of the translocation step and energy-coupling step of the active transport of this amino acid. Thus, if the UTL is caused by proton leak, no such phenomenon would be observed with this purely facilitated component of the proline system.

Secondly, according to Mitchell's chemiosmotic theory, uptake of such neutral substrates as lactose and proline occurs by co-transport with protons (i.e., symport) (<sup>309</sup>~~141~~). This has been experimentally demonstrated for the lactose system of E. coli (280). Thus, if the same is true for the proline system, it will be of great significance to study the rate of alkalization of the medium as a function of temperature during proline transport in whole cells of these E. coli strains used here. If the UTL is a result of proton leak, it therefore means that the  $V_{\max}$  for alkalization of the medium would increase as temperature increases until the UTL, when this  $V_{\max}$  for alkalization should start to decrease. This trend in the  $V_{\max}$  for alkalization is expected to be in parallel with the change in  $V_{\max}$  for proline uptake over the entire temperature range studied.

In order to be able to characterize the glycerol facilitated diffusion system in E. coli adequately, a suitable radio-labelled substrate analog is required, since efforts in other directions have so far proved futile. In this regard, it is necessary to synthesize a glycerol analog which would have a bulky hydrophilic moiety attached to one of the three carbon atoms of this triol while still retaining high specificity



for the glycerol facilitator protein. With such an analog, whose efflux from the cell would thus be minimized, fresh efforts should be put into investigating the kinetic parameters for this transport system.







## BIBLIOGRAPHY

1. Singer, S.J. and Nicolson, G.L.: *Science* 175 (1972) 720-731.
2. Hackenbrock, C.R., Höchli, M. and Chau, R.M.: *Biochim. Biophys. Acta* 455 (1976) 466-484.
3. Gulik-Krzywicki, T.: *Biochim. Biophys. Acta* 415 (1975) 1-28.
4. Nicolson, G.L.: *Biochim. Biophys. Acta* 457 (1976) 57-108.
5. Höchli, M. and Hackenbrock, C.R.: *Proc. Nat. Acad. Sci. (USA)* 73 (1976) 1636-1640.
6. Nicolson, G.L.: *Series Haematologica*, Vol. VI (1973) 275-291.
7. Edidin, M.: *Ann. Rev. Biophys. Bioeng.* 3 (1974) 179-201.
8. Gorter, E. and Grendel, F.: *J. Exptl. Med.* 41 (1925) 439-443.
9. Danielli, J.F. and Davson, H.: *J. Cell. Comp. Physiol.* 5 (1935) 495-508.
10. Robertson, J.D.: *Biochem. Soc. Symposia* 16 (1959) 3-43.
11. Benson, A.A.: *J. Amer. Oil Chem. Soc.* 43 (1966) 265-270.
12. Singer, S.J.: In "Structure and Function of Biological Membranes" L.I. Rothfield, Ed. (Academic Press, New York, 1971), pp 145-222.
13. Read, B.D.: Ph.D. Thesis, University of Alberta (1975).
14. Overath, P. and Träuble, H.: *Biochemistry* 12 (1973) 2625-2634.
15. Singer, S.J.: *Ann. Rev. Biochem.* 43 (1974) 805-833.
16. Benson, A.A. and Singer, S.J.: *Abstr. 150th Nat. Meet. Amer. Chem. Soc.* (1965), p 8c.
17. Singer, S.J.: *Advan. Protein Chem.* 17 (1962) 1-68.
18. Jost, P.C., Capaldi, R.A., Vanderkooi, G. and Griffith, O.H.: *J. Supramol. Struct.* 1 (1973) 269-280.
19. Marchesi, V.T. and Steers, Jr., E.: *Science* 159 (1968) 203-204.
20. Staros, J.V., Richards, F.M. and Haley, B.E.: *J. Biol. Chem.* 250 (1975) 8174-8178.
21. Steck, T.L.: *J. Mol. Biol.* 66 (1972) 295-305.
22. Kyte, J.: *J. Biol. Chem.* 247 (1972) 7642-7649.



23. Tanford, C.: "The Hydrophobic Effect: Formation of Micelles and Biological Membranes" (John Wiley & Sons, New York, 1973).
24. Bangham, A.D., Standish, M.M. and Watkins, J.C.: J. Mol. Biol. 13 (1965) 238-252.
25. Haydon, D.A. and Taylor, J.: J. Theoret. Biol. 4 (1963) 281-296.
26. Chapman, D., Williams, R.M. and Ladbroke, B.D.: Chem. Phys. Lipids 1 (1967) 445-475.
27. Melchior, D.L. and Steim, J.M.: Ann. Rev. Biophys. Bioeng. 5 (1976) 205-238.
28. Engelman, D.: J. Mol. Biol. 58 (1971) 153-165.
29. Steim, J.M., Tourtellotte, M.E., Reinert, J.C., McElhaney, R.N. and Rader, R.L.: Proc. Nat. Acad. Sci. (USA) 63 (1969) 104-109.
30. McElhaney, R.N.: In "Extreme Environments: Mechanisms of Microbial Adaptation", Heinrich, M.R., Ed. (Academic Press, 1976), pp 255-281.
31. Jacobson, K. and Papahadjopoulos, D.: Biochemistry 14 (1975) 152-161.
32. Träuble, H.: In "Biomembranes, Vol. 3", L.A. Manson, Series Ed. (Plenum Press, New York & London, 1972), pp 197-227.
33. Thilo, L. and Overath, P.: Biochemistry 15 (1976) 328-334.
34. Schroeder, F., Holland, J.F. and Vagelos, P.R.: J. Biol. Chem. 251 (1976) 6739-6746.
35. Schroeder, F., Holland, J.F. and Vagelos, P.R.: J. Biol. Chem. 251 (1976) 6747-6756.
36. Schlessinger, J., Barak, L.S., Hammes, G.G., Yamada, K.M., Pastan, I., Webb, W.W. and Elson, E.L.: Proc. Nat. Acad. Sci. (USA) 74 (1977) 2909-2913.
37. Schlessinger, J., Axelrod, D., Koppel, D.E., Webb, W.W. and Elson, E.L.: Science 195 (1977) 307-309.
38. Edidin, M. and Fambrough, D.: J. Cell Biol. 57 (1973) 27-37.
39. Poo, M. and Cone, R.A.: Nature 247 (1974) 438-441.
40. Poste, G., Papahadjopoulos, D., Jacobson, K. and Vail, W.J.: Nature 253 (1975) 552-554.
41. Kehry, M., Yguerabide, J. and Singer, S.J.: Science 195 (1977) 486-487.



42. Hinz, H-J. and Sturtevant, J.M.: J. Biol. Chem. 247 (1972) 6071-6075.
43. McElhaney, R.N.: PAABS Revista 3 (1974) 753-767.
44. Engelman, D.M.: J. Mol. Biol. 47 (1970) 115-117.
45. Spiker, Jr., R.C. and Levin, I.W.: Biochim. Biophys. Acta 433 (1976) 457-468.
46. Verma, S.P. and Wallach, D.F.H.: Biochim. Biophys. Acta 426 (1976) 616-623.
47. Gottlieb, M.H. and Eanes, E.D.: Biochim. Biophys. Acta 373 (1974) 519-522.
48. Ladbrooke, B.D., Williams, R.M. and Chapman, D.: Biochim. Biophys. Acta 150 (1968) 333-340.
49. Hinz, H-J. and Sturtevant, J.M.: J. Biol. Chem. 247 (1972) 3697-3700.
50. Demel, R.A., Jansen, J.W.C.M., Van Dijck, P.W.M. and Van Deenen, L.L.M.: Biochim. Biophys. Acta 465 (1977) 1-10.
51. Stockton, G.W., Polnaszek, C.F., Tulloch, A.P., Hasan, F. and Smith, I.C.P.: Biochemistry 15 (1976) 954-966.
52. Lucy, J.A.: FEBS Letters 40 (Supplement) (1974) S105-S111.
53. Chapman, D. and Penkett, S.A.: Nature 211 (1966) 1304-1305.
54. Trudell, J.R., Payan, D.G., Chin, J.H. and Cohen, E.N.: Proc. Nat. Acad. Sci. (USA) 72 (1975) 210-213.
55. Papahadjopoulos, D., Vail, W.J. and Moscarello, M.: J. Membrane Biol. 22 (1975) 143-164.
56. Chapman, D.: In "Biological Membranes", Chapman, D. and Wallach, D.F.H., Eds. (Academic Press, 1973), pp 91-144.
57. Ladbrooke, B.D. and Chapman, D.: Chem. Phys. Lipids 3 (1969) 304-367.
58. Linden, C.D. and Fox, C.F.: Accounts Chem. Res. 8 (1975) 321-327.
59. Seelig, J.: Seperatum Experientia 29 (1973) 509-516.
60. Baldassare, J.J., Rhinehart, K.B. and Silbert, D.F.: Biochemistry 15 (1976) 2986-2994.
61. Jackson, M.B. and Sturtevant, J.M.: J. Biol. Chem. 252 (1977) 4749-4751.





62. Overath, P., Brenner, M., Gulik-Krzywicki, T., Shechter, E. and Letellier, L.: *Biochim. Biophys. Acta* 389 (1975) 358-369.
63. Rottem, S. and Leive, L.: *J. Biol. Chem.* 252 (1977) 2077-2081.
64. Linden, C.D., Wright, K.L., McConnell, H.M. and Fox, C.F.: *Proc. Nat. Acad. Sci. (USA)* 70 (1973) 2271-2275.
65. Linden, C.D. and Fox, C.F.: *J. Supramol. Struct.* 1 (1973) 535-544.
66. Kleeman, W. and McConnell, H.M.: *Biochim. Biophys. Acta* 345 (1974) 220-230.
67. Esfahani, M., Limbrick, A.R., Knotton, S., Oka, T. and Wakil, S.J.: *Proc. Nat. Acad. Sci. (USA)* 68 (1971) 3180-3184.
68. Shechter, E., Letellier, L. and Gulik-Krzywicki, T.: *Eur. J. Biochem.* 49 (1974) 61-76.
69. Chapman, D. and Urbina, J.: *FEBS Letters* 12 (1971) 169-172.
70. Reinert, J.C. and Steim, J.M.: *Science* 168 (1970) 1580-1582.
71. Read, B.D. and McElhaney, R.N.: *J. Bacteriol.* 123 (1975) 47-55.
72. McElhaney, R.N.: *J. Supramol. Struct.* 2 (1974) 617-628.
73. McElhaney, R.N.: *J. Mol. Biol.* 84 (1974) 145-157.
74. McElhaney, R.N., De Gier, J., Van Der Neut-Kok, E.C.M.: *Biochim. Biophys. Acta* 298 (1973) 500-512.
75. McElhaney, R.N. and Souza, K.A.: *Biochim. Biophys. Acta* 443 (1976) 348-359.
76. Blazyk, J.F. and Steim, J.M.: *Biochim. Biophys. Acta* 266 (1972) 737-741.
77. Feo, F., Canuto, R.A., Garcea, R., Avogadro, A., Villa, M. and Celasco, M.: *FEBS Letters* 72 (1976) 262-266.
78. Davis, D.G., Inesi, G. and Gulik-Krzywicki, T.: *Biochemistry* 15 (1976) 1271-1276.
79. Blaurock, A.E.: *J. Mol. Biol.* 56 (1971) 35-52.
80. Stamatoff, J.B., Krimm, S. and Harvie, N.R.: *Proc. Nat. Acad. Sci. (USA)* 72 (1975) 531-534.
81. Wilkins, M.H.F., Blaurock, A.E. and Engelman, D.M.: *Nature New Biology* 230 (1971) 72-76.





82. Tourtellotte, M.E., Branton, D. and Keith, A.: Proc. Nat. Acad. Sci. (USA) 66 (1970) 909-916.
83. Metcalfe, J.C., Birdsall, N.J.M. and Lee, A.G.: FEBS Letters 21 (1972) 335-340.
84. Hubbell, W.L. and McConnell, H.M.: J. Amer. Chem. Soc. 93 (1971) 314-326.
85. Linden, C.D., Keith, A.D. and Fox, C.F.: J. Supramol. Struct. 1 (1973) 523-534.
86. Esser, A.F. and Souza, K.A.: Proc. Nat. Acad. Sci. (USA) 71 (1974) 4111-4115.
87. Raison, J.K., Lyons, J.M., Mehlhorn, R.J. and Keith, A.D.: J. Biol. Chem. 246 (1971) 4036-4040.
88. Rousselet, A., Colbeau, A., Vignais, P.M. and Devaux, P.F.: Biochim. Biophys. Acta 426 (1976) 372-384.
89. James, R. and Branton, D.: Biochim. Biophys. Acta 323 (1973) 378-390.
90. Rottem, S. and Samuni, A.: Biochim. Biophys. Acta 298 (1973) 32-38.
91. Tsukagoshi, N., Petersen, M.H., Huber, U., Franklin, R.M. and Seelig, J.: Eur. J. Biochem. 62 (1976) 257-262.
92. Finne, G. and Matches, J.R.: J. Bacteriol. 125 (1976) 211-219.
93. Pontus, M. and Delmelle, M.: Biochim. Biophys. Acta 401 (1975) 221-230.
94. Wisnieski, B.J., Iwata, K.K.: Biochemistry 16 (1977) 1321-1326.
95. Plachy, W.Z., Lanyi, J.K. and Kates, M.: Biochemistry 13 (1974) 4906-4913.
96. Lanyi, J.K., Plachy, W.Z. and Kates, M.: Biochemistry 13 (1974) 4914-4920.
97. Jost, P.C., Griffith, O.H., Capaldi, R.A. and Vanderkooi, G.: Proc. Nat. Acad. Sci. (USA) 70 (1973) 480-484.
98. Milanovich, F.P., Yeh, Y., Baskin, R.J. and Harney, R.C.: Biochem. Biophys. Acta 419 (1976) 243-250.
99. Träuble, H. and Overath, P.: Biochim. Biophys. Acta 307 (1973) 491-512.
100. Levine, Y.K., Birdsall, N.J.M., Lee, A.G. and Metcalfe, J.C.: Biochemistry 11 (1972) 1416-1421.



101. Hesketh, T.R., Smith, G.A., Houslay, M.D., McGill, K.A., Birdall, N.J.M., Metcalfe, J.C. and Warren, G.B.: *Biochemistry* 15 (1976) 4145-4151.
102. Moor, H. and Mühlethaler, K.: *J. Cell Biol.* 17 (1963) 609-628.
103. Pinto da Silva, P. and Branton, D.: *J. Cell Biol.* 45 (1970) 598-605.
104. Hong, K. and Hubbell, W.L.: *Proc. Nat. Acad. Sci. (USA)* 69 (1972) 2617-2621.
105. Bayer, M.E., Dolack, M. and Houser, E.: *J. Bacteriol.* 129 (1977) 1563-1573.
106. Mitranic, M., Sturgess, J.M. and Moscarello, M.A.: *Biochim. Biophys. Acta* 443 (1976) 190-197.
107. Duppel, W. and Dahl, G.: *Biochim. Biophys. Acta* 426 (1976) 408-417.
108. Brown, P.K.: *Nature New Biology* 236 (1972) 35-38.
109. Cone, R.A.: *Nature New Biology* 236 (1972) 39-43.
110. Tsai, K-H. and Lenard, J.: *Nature* 253 (1975) 554-555.
111. Lenard, J. and Rothman, J.E.: *Proc. Nat. Acad. Sci. (USA)* 73 (1976) 391-395.
112. Bloj, B. and Zilversmit, D.B.: *Biochemistry* 15 (1976) 1277-1283.
113. Steck, T.L. and Dawson, G.: *J. Biol. Chem.* 249 (1974) 2135-2142.
114. Rousselet, A., Guthmann, C., Matricon, J., Bienvenue, A. and Devaux, P.F.: *Biochim. Biophys. Acta* 426 (1976) 357-371.
115. Nicolson, G.L. and Singer, S.J.: *Proc. Nat. Acad. Sci. (USA)* 68 (1971) 942-945.
116. Nicolson, G.L. and Singer, S.J.: *J. Cell Biol.* 60 (1974) 236-248.
117. Marinetti, G.V. and Love, R.: *Chem. Phys. Lipids* 16 (1976) 239-254.
118. Sheetz, M.P. and Singer, S.J.: *Proc. Nat. Acad. Sci. (USA)* 71 (1974) 4457-4461.
119. Zwaal, R.F.A., Roelofsen, B. and Colley, C.M.: *Biochim. Biophys. Acta* 300 (1973) 159-182.
120. Shin, B.C. and Carraway, K.L.: *Biochim. Biophys. Acta* 345 (1974) 141-153.



121. Tinberg, H.M., Melnick, R.L., Maguire, J. and Packer, L.: Biochim. Biophys. Acta 345 (1974) 118-128.
122. Kyte, J.: J. Biol. Chem. 249 (1974) 3652-3660.
123. Kyte, J.: J. Biol. Chem. 250 (1975) 7443-7449.
124. Clarke, S.: J. Biol. Chem. 251 (1976) 1354-1363.
125. Dutton, A., Rees, E.D. and Singer, S.J.: Proc. Nat. Acad. Sci. (USA) 73 (1976) 1532-1536.
126. Fisher, K.A.: Proc. Nat. Acad. Sci. (USA) 73 (1976) 173-177.
127. Tomich, J.M., Mather, I.H. and Keenan, T.W.: Biochim. Biophys. Acta 433 (1976) 357-364.
128. Christensen, H.: "Biological Transport" (2nd Edition, 1975, W.A. Benjamin, Inc., Advanced Book Program, Reading, Massachusetts).
129. Coleman, R.: Biochim. Biophys. Acta 300 (1973) 1-30.
130. Bretscher, M.S.: Science 181 (1973) 622-629.
131. Salton, M.R.J. and Owen, P.: Ann. Rev. Microbiol. 30 (1976) 451-482.
132. Machtiger, N.A. and Fox, C.F.: Ann. Rev. Biochem. 42 (1973) 575-600.
133. Costerton, J.W.: Microbiology (1977) (Amer. Soc. for Microbiol., Washington, D.C.) Editor, Schlessinger, D., p. 151-157.
134. Costerton, J.W. and Cheng, K-J.: J. Antimicrob. Chemother. 1 (1975) 363-377.
135. Costerton, J.W., Ingram, J.M. and Cheng, K-J.: Bacteriol. Rev. 38 (1974) 87-110.
136. Braun, V. and Hantke, K.: Ann. Rev. Biochem. 43 (1974) 89-121.
137. Mitchell, P.: In "Biological Structure and Function", Vol. II, Goodwin, T.W. and Lindberg, O., Eds. (Academic Press, 1961), pp. 581-603.
138. Kulpa, Jr., C.F. and Leive, L.: J. Bacteriol. 126 (1976) 467-477.
139. Osborn, M.J. and Munson, R.: In "Methods in Enzymology" Vol. XXXI, Fleischer, S. and Packer, L., Eds. (Academic Press, 1974), pp 642-653.
140. Osborn, M.J., Gander, J.E., Parisi, E. and Carson, J.: J. Biol. Chem. 247 (1972) 3962-3972.





141. Schnaitman, C.A.: J. Bacteriol. 104 (1970) 882-889.
142. Schnaitman, C.A.: J. Bacteriol. 104 (1970) 890-901.
143. Salton, M.R.J.: In "Methods in Membrane Biology" Vol 6, Korn, E.D., Ed. (Plenum Press, New York and London, 1976), pp 101-150.
144. Cronan, Jr., J.E. and Gelmann, E.P.: Bacteriol. Rev. 39 (1975) 232-256.
145. Osborn, M.J., Gander, J.E. and Parisi, E.: J. Biol. Chem. 247 (1972) 3973-3986.
146. Bell, R.M., Mavis, R.D., Osborn, M.J. and Vagelos, P.R.: Biochim. Biophys. Acta 249 (1971) 628-635.
147. White, D.A., Albright, F.R., Lennarz, W.J. and Schnaitman, C.A.: Biochim. Biophys. Acta 249 (1971) 636-642.
148. Salton, M.R.J.: "The Bacterial Cell Wall" (Elsevier, Amsterdam, 1964).
149. MacAlister, T.J., Irvin, R.T. and Costerton, J.W.: J. Bacteriol. 130 (1977) 318-328.
150. MacAlister, T.J., Irvin, R.T. and Costerton, J.W.: J. Bacteriol. 130 (1977) 329-338.
151. MacAlister, T.J., Irvin, R.T. and Costerton, J.W.: J. Bacteriol. 130 (1977) 339-346.
152. Nguyen-Huy, H., Nanciel, C. and Wermuth, C.-G.: Eur. J. Biochem. 66 (1976) 79-84.
153. Formanek, H., Schleifer, K.H., Seidl, H.P., Lindemann, R. and Zundel, G.: FEBS Letters 70 (1976) 150-154.
154. Metzler, D.E.: "Biochemistry: The Chemical Reactions of Living Cells" (Academic Press, New York, 1977).
155. Cleveland, R.F., Wicken, A.J., Daneo-Moore, L. and Shockman, G.D.: J. Bacteriol. 126 (1976) 192-197.
156. Knox, K.W. and Wicken, A.J.: Bacteriol. Rev. 37 (1973) 215-257.
157. Millward, G.R. and Reaveley, D.A.: J. Ultrastructure Res. 46 (1974) 309-326.
158. Inouye, M.: Proc. Nat. Acad. Sci. (USA) 71 (1974) 2396-2400.
159. Wong, M., Kulpa, C.F. and Thomas, J.K.: Biochim. Biophys. Acta 426 (1976) 711-722.





160. Nelson, Jr., J.D. and MacLeod, R.A.: J. Bacteriol. 129 (1977) 1059-1065.
161. Nakae, T.: J. Bioch. Chem. 251 (1976) 2176-2178.
162. Nakae, T. and Nikaido, H.: J. Biol. Chem. 250 (1975) 7359-7365.
163. Beacham, I.R., Haas, D. and Yagil, E.: J. Bacteriol. 129 (1977) 1034-1044.
164. Unemoto, T. and MacLeod, R.A.: J. Bacteriol. 121 (1975) 800-806.
165. Witholt, B., Van Heerikhuizen, H. and De Leij, L.: Biochim. Biophys. Acta 443 (1976) 534-544.
166. Hasin, M., Razin, S. and Rottem, S.: Biochim. Biophys. Acta 433 (1976) 229-239.
167. Neu, H.C. and Heppel, L.A.: J. Biol. Chem. 240 (1965) 3685-3692.
168. Heppel, L.A.: In "Structure and Function of Biological Membranes" Rothfield, L.I., Ed. (Academic Press, 1971), pp 223-247.
169. Weiner, J.H. and Heppel, L.A.: J. Biol. Chem. 246 (1971) 6933-6941.
170. Nakamura, K., Ostrovsky, D.N., Miyazawa, T. and Mizushima, S.: Biochim. Biophys. Acta 332 (1974) 329-335.
171. Miura, T. and Mizushima, S.: Biochim. Biophys. Acta 150 (1968) 159-161.
172. Birdsell, D.C. and Cota-Robles, E.H.: J. Bacteriol. 93 (1967) 427-437.
173. Repaske, R.: Biochim. Biophys. Acta 30 (1958) 225-232.
174. Eze, M.O. and McElhaney, R.N.: J. Gen. Microbiol., in press.
175. Rosenthal, K.S., Swanson, P.E. and Storn, D.R.: Biochemistry 15 (1976) 5783-5792.
176. Lugtenberg, B., Bronstein, H., Van Selm, N. and Peters, R.: Biochim. Biophys. Acta 465 (1977) 571-578.
177. Schweizer, M. and Henning, U.: J. Bacteriol. 129 (1977) 1651-1652.
178. Maloney, P.C., Kashket, E.R. and Wilson, T.H.: In "Methods in Membrane Biology" Vol. 5, Korn, E.D., Ed. (Plenum Press, New York and London, 1975), pp 1-49.
179. Kasahara, M. and Anraku, Y.: J. Biochem. (Japan) 76 (1974) 977-983.



180. Kaback, H.R.: *Biochim. Biophys. Acta* 265 (1972) 367-416.
181. Morikawa, A., Suzuki, H. and Anraku, Y.: *J. Biochem. (Japan)* 75 (1974) 229-241.
182. Kaback, H.R., Rudnick, G., Schuldiner, S. and Short, S.A.: In "Carriers and Channels in Biological Systems", *Ann. N.Y. Acad. Sci.* 264 (1975) 350-357.
183. Stryer, L.: *Biochemistry* (W.H. Freeman & Co., San Francisco, 1975).
184. Stein, W.D.: "The Movement of Molecules Across Cell Membranes" (Academic Press, New York, San Francisco and London, 1967).
185. Kotyk, A. and Janáček, K.: "Cell Membrane Transport: Principles and Techniques", 2nd Edition (Plenum Press, 1975).
186. Dixon, M. and Webb, E.C.: "Enzymes" (Longmans, 2nd Edition, 1967).
187. Simoni, R.D. and Postma, P.W.: *Ann. Rev. Biochem.* 44 (1975) 523-554.
188. Winkler, H.H. and Wilson, T.H.: *J. Biol. Chem.* 241 (1966) 2200-2211.
189. Berger, E.A.: *Proc. Nat. Acad. Sci. (USA)* 70 (1973) 1514-1518.
190. Berger, E.A. and Heppel, L.A.: *J. Biol. Chem.* 249 (1974) 7747-7755.
191. Kobayashi, H., Kin, E. and Anraku, Y.: *J. Biochem. (Japan)* 76 (1974) 251-261.
192. Gutowski, S.J. and Rosenberg, H.: *Biochem. J.* 154 (1976) 731-734.
193. Mitchell, P.: *Biol. Rev. (Cambridge)* 41 (1966) 445-502.
194. Mitchell, P.: In "Organization and Control in Prokaryotic and Eukaryotic Cells" (Twentieth Symposium of the Society for General Microbiology, Imperial College, London) (1970) pp 121-166.
195. Mitchell, P.: *J. Theor. Biol.* 62 (1976) 327-367.
196. Mitchell, P.: *Bioch. Soc. (London) Trans.* 4 (1976) 399-430.
197. Harold, F.M.: *Bacteriol. Rev.* 36 (1972) 172-230.
198. Hirata, H., Altendorf, K. and Harold, F.M.: *J. Biol. Chem.* 249 (1974) 2939-2945.
199. Haddock, B.A. and Jones, C.W.: *Bacteriol. Rev.* 41 (1977) 47-99.



200. Harold, F.M.: *Ann. Rev. Microbiol.* 31 (1977) 181-203.
201. Lanyi, J.K.: *J. Supramol. Struct.* 6 (1977) 169-177.
202. MacDonald, R.E. and Lanyi, J.K.: *Feder. Proceed.* 36 (1977) 1828-1832.
203. MacDonald, R.E., Greene, R.V. and Lanyi, J.K.: *Biochemistry* 16 (1977) 3227-3235.
204. Tsuchiya, T., Hasan, S.M. and Raven, J.: *J. Bacteriol.* 131 (1977) 848-853.
205. Miner, K.M. and Frank, L.: *J. Bacteriol.* 117 (1974) 1093-1098.
206. MacDonald, R.E., Lanyi, J.K. and Greene, R.V.: *Proc. Nat. Acad. Sci. (USA)* 74 (1977) 3167-3170.
207. Kundig, W., Ghosh, S. and Roseman, S.: *Proc. Nat. Acad. Sci. (USA)* 52 (1964) 1067-1074.
208. Postma, P.W. and Roseman, S.: *Biochim. Biophys. Acta* 457 (1976) 213-257.
209. De Gier, J., Mandersloot, J.G., Hupkes, J.V., McElhaney, R.N. and Van Beek, W.P.: *Biochim. Biophys. Acta* 233 (1971) 610-618.
210. Sprott, G.D., Wood, J.M., Martin, W.G. and Schneider, H.: *Biochem. Biophys. Res. Comm.* 76 (1977) 1099-1106.
211. McElhaney, R.N., De Gier, J. and Van Deenen, L.L.M.: *Biochim. Biophys. Acta* 219 (1970) 245-247.
212. Deuticke, B. and Ruska, C.: *Biochim. Biophys. Acta* 433 (1976) 638-653.
213. Stein, W.D.: *Biochim. Biophys. Acta* 59 (1962) 47-65.
214. Bruckdorfer, K.R., Demel, R.A., De Gier, J. and Van Deenen, L.L.M.: *Biochim. Biophys. Acta* 183 (1969) 334-345.
215. Shairer, H.U. and Overath, P.: *J. Mol. Biol.* 44 (1969) 209-214.
216. Overath, P., Shairer, H.U. and Stoffel, W.: *Proc. Nat. Acad. Sci. (USA)* 67 (1970) 606-612.
217. Wilson, G. and Fox, C.F.: *J. Mol. Biol.* 55 (1971) 49-60.
218. Sullivan, K.H., Jain, M.K. and Koch, A.L.: *Biochim. Biophys. Acta* 352 (1974) 287-297.
219. Wunderlich, F., Ronai, A., Speth, V., Seelig, J. and Blume, A.: *Biochemistry* 14 (1975) 3730-3735.





220. Fox, C.F.: In "Biochemistry of Cell Walls and Membranes" (MTP International Review of Science, Biochemistry Series One, Vol. 2), Fox, C.F., Vol. Ed. (Butterworths, London; University Park Press, Baltimore, 1975), pp 279-306.
221. Kaduce, T.L., Awad, A.B., Fontenelle, L.J. and Spector, A.A.: J. Biol. Chem. 252 (1977) 6624-6630.
222. Mavis, R.D. and Vagelos, P.R.: J. Biol. Chem. 247 (1972) 652-659.
223. Singh, A.P. and Bragg, P.D.: J. Bioenergetics 7 (1975) 175-188.
224. Kimelberg, H.K. and Papahadjopoulos, D.: Biochim. Biophys. Acta 282 (1972) 277-292.
225. Grisham, G.M. and Barnett, R.E.: Biochemistry 12 (1973) 2635-2637.
226. Keirns, J.J., Kreiner, P.W. and Bitensky, M.W.: J. Supramol. Struct. 1 (1973) 368-379.
227. Lee, A.G., Birdsall, N.J.M., Metcalfe, J.C., Toon, P.A. and Warren, G.B.: Biochemistry 13 (1974) 3699-3705.
228. Lee, M.P. and Gear, A.R.L.: J. Biol. Chem. 249 (1974) 7541-7549.
229. Duppel, W. and Ullrich, V.: Biochim. Biophys. Acta 426 (1976) 399-407.
230. Solomonson, L.P., Liepkalns, V.A. and Spector, A.A.: Biochemistry 15 (1976) 892-897.
231. Enoch, H.G., Catalá, A. and Strittmatter, P.: J. Biol. Chem. 251 (1976) 5095-5103.
232. Yang, C.S., Strickhart, F.S. and Kicha, L.P.: Biochim. Biophys. Acta 465 (1977) 362-370.
233. Watson, K., Houghton, R.L., Bertoli, E. and Griffiths, D.E.: Biochem. J. 146 (1975) 409-416.
234. Tanaka, R. and Strickland, K.P.: Arch. Biochem. Biophys. 111 (1965) 583-592.
235. Martonosi, A., Donley, J.R., Pucell, A.G. and Halpin, R.A.: Arch. Biochem. Biophys. 144 (1971) 529-540.
236. Slack, J.R., Anderton, B.H. and Day, W.A.: Biochim. Biophys. Acta 323 (1973) 547-559.
237. Stahl, W.L.: Arch. Biochem. Biophys. 154 (1973) 56-67.





238. Wheeler, K.P. and Walker, J.A.: Biochem. J. 146 (1975) 723-727.
239. Gennis, R.B. and Strominger, J.L.: J. Biol. Chem. 251 (1976) 1264-1269.
240. Gennis, R.B., Sinensky, M. and Strominger, J.L.: J. Biol. Chem. 251 (1976) 1270-1276.
241. Gennis, R.B. and Strominger, J.L.: J. Biol. Chem. 251 (1976) 1277-1282.
242. Sandermann, Jr., H.: Eur. J. Biochem. 62 (1976) 479-484.
243. Sihotang, K.: Eur. J. Biochem. 63 (1976) 519-524.
244. Schryvers, A., Lohmeier, H. and Weiner, J.H.: J. Biol. Chem., in press.
245. Racker, E.: J. Supramol. Struct. 6 (1977) 215-228.
246. Knowles, A.F., Kandrach, A. and Racker, E.: J. Biol. Chem. 250 (1975) 1809-1813.
247. Knowles, A.F., Eytan, E. and Racker, E.: J. Biol. Chem. 251 (1976) 5161-5165.
248. Goldman, S.S. and Alberts, R.W.: J. Biol. Chem. 248 (1973) 867-874.
249. Wheeler, K.P.: Biochem. J. 146 (1975) 729-738.
250. Wheeler, K.P., Walker, J.A. and Barker, D.M.: Biochem. J. 146 (1975) 713-722.
251. Walker, J.A. and Wheeler, K.P.: Biochim. Biophys. Acta 394 (1975) 135-144.
252. Yu, C., Yu, L. and King, T.E.: J. Biol. Chem. 250 (1975) 1383-1392.
253. Ishinaga, M., Nishihara, M., Kato, M. and Kito, M.: Biochim. Biophys. Acta 431 (1976) 426-432.
254. Dancey, G.F. and Shapiro, B.M.: Biochim. Biophys. Acta 487 (1977) 368-377.
255. Graham, A.B., Pechey, D.T., Toogood, K.C., Thomas, S.B. and Wood, G.C.: Biochem. J. 163 (1977) 117-124.
256. Haydon, D.A.: In "Carriers and Channels in Biological Systems", Ann. N.Y. Acad. Sci. 264 (1975) 2-16.
257. McLaughlin, S. and Eisenberg, M.: Ann. Rev. Biophys. Bioeng. 4 (1975) 335-366.



258. Krasne, S., Eisenman, G. and Szabo, G.: *Science* 174 (1971) 412-415.
259. Van Der Neut-Kok, E.C.M., De Gier, J., Middelbeek, E.J. and Van Deenen, L.L.M.: *Biochim. Biophys. Acta* 332 (1974) 97-103.
260. Therisod, H., Letellier, L., Weil, R. and Schechter, E.: *Biochemistry* 16 (1977) 3772-3776.
261. Letellier, L., Weil, R. and Schechter, E.: *Biochemistry* 16 (1977) 3777-3780.
262. Thilo, L., Träuble, H. and Overath, P.: *Biochemistry* 16 (1977) 1283-1290.
263. Wilson, G., Rose, S.P. and Fox, C.F.: *Biochem. Biophys. Res. Comm.* 38 (1970) 617-623.
264. Tsukagoshi, N. and Fox, C.F.: *Biochemistry* 12 (1973) 2822-2829.
265. Rosen, B.P. and Hackette, S.L.: *J. Bacteriol.* 110 (1972) 1181-1189.
266. Silvius, J.R., Read, B.D. and McElhaney, R.N.: *Science* 199 (1978) 902-903.
267. Dobler, M.: *Biochem. Soc. Trans.* 1 (538th Meet. Birmingham) (1973) 828-832.
268. Madeira, V.M.C., Antunes-Madeira, M.C. and Carvalho, A.P.: *Biochem. Biophys. Res. Comm.* 58 (1974) 897-904.
269. Sanno, Y., Wilson, T.H. and Lin, E.C.C.: *Biochem. Biophys. Res. Comm.* 32 (1968) 344-349.
270. Richey, D.P. and Lin, E.C.C.: *J. Bacteriol.* 112 (1972) 784-790.
271. Lin, E.C.C.: *Ann. Rev. Microbiol.* 30 (1976) 535-578.
272. Rosen, B.P. and Heppel, L.A.: In "Bacterial Membranes and Walls" Leive, L., Ed. (Marcel Dekker Inc., New York, 1973), pp 209-239.
273. Miller, J.: In "Experiments in Molecular Genetics" (Cold Spring Harbour Laboratory, New York, 1972), p 353 and p 431.
274. Alemohammad, M.M. and Knowles, C.J.: *J. Gen. Microbiol.* 82 (1974) 125-142.
275. Bligh, E.G. and Dyer, W.J.: *Can. J. Biochem. Physiol.* 37 (1959) 911-917.
276. Lowry, O.H., Rosenbrough, N.J., Farr, A.L. and Randall, R.J.: *J. Biol. Chem.* 193 (1951) 265-275.



277. Zweig, G. and Whitaker, J.R.: In "Paper Chromatography and Electrophoresis, Vol. II, Paper Chromatography", Sherma, J. and Zweig, G., Eds. (Academic Press, 1971).
278. Purdy, D.R. and Koch, A.L.: J. Bacteriol. 127 (1976) 1188-1196.
279. Stein, W.D.: Biochim. Biophys. Acta 59 (1962) 35-46.
280. West, I.C.: Biochem. Biophys. Res. Comm. 41 (1970) 655-661.
281. Mitchell, P. and Moyle, J.: In "Bacterial Anatomy", Symposia of the Society for General Microbiology, Vol. 6 (1956) 150-180.
282. Bangham, A.D., De Gier, J. and Greville, G.D.: Chem. Phys. Lipids 1 (1967) 225-246.
283. De Gier, J. Mandersloot, J.G. and Van Deenen, L.L.M.: Biochim. Biophys. Acta 150 (1968) 666-675.
284. Van Zoelen, E.J.J., Van Der Neut-Kok, E.C.M., De Gier, J. and Van Deenen, L.L.M.: Biochim. Biophys. Acta 394 (1975) 463-469.
285. Netter, H.: In "Theoretical Biochemistry: Physico-chemical Principles of Vital Processes", English translation (John Wiley & Sons Inc., New York, 1969), pp 102-103.
286. Gibson, Q.H. and Milnes, L.: Biochem. J. 91 (1964) 161-171.
287. Daniels, F. and Alberty, R.A.: In "Physical Chemistry", 3rd Edition (John Wiley & Sons, Inc., 1966), pp 325-330.
288. Hague, D.N.: In "Comprehensive Chemical Kinetics, Vol. 1: The Practice of Kinetics", Bamford, C.H. and Tipper, C.F.H., Eds. (Elsevier, Amsterdam, London and New York, 1969), pp 112-133.
289. Langdon, R.G.: In "Methods in Enzymology", Vol. IX, Wood, W. Ed. (Academic Press, 1966), pp 126-127.
290. Baldassare, J.J., Brenckle, G.M., Hoffman, M. and Silbert, D.F.: J. Biol. Chem. 252 (1977) 8797-8803.
291. Stein, W.D.: Nature 181 (1958) 1662-1663.
292. Cozzarelli, N.R., Freedberg, W.B. and Lin, E.F.C.: J. Mol. Biol. 31 (1968) 371-387.
293. Saier, Jr., M.H. and Roseman, S.: J. Biol. Chem. 251 (1976) 6606-6615.
294. Read, B.D. and McElhaney, R.N.: Biochim. Biophys. Acta 419 (1976) 331-341.





295. Oxender, D.L. and Quay, S.C.: In "Methods in Membrane Biology", Vol. 6, Korn, E., Ed. (Plenum Press, New York and London, 1976), pp 183-242.
296. Oxender, D.L.: Ann. Rev. Biochem. 41 (1972) 777-814.
297. Furlong, C.E. and Weiner, J.H.: Biochem. Biophys. Res. Comm. 38 (1970) 1076-1083.
298. Anderson, J.J., Quay, S.C. and Oxender, D.L.: J. Bacteriol. 126 (1976) 80-90.
299. Rosen, B.P.: J. Biol. Chem. 246 (1971) 3653-3662.
300. Celis, T.F.R.: J. Bacteriol. 130 (1977) 1234-1243.
301. Quay, S. and Christensen, H.N.: J. Biol. Chem. 249 (1974) 7011-7017.
302. Ganesan, A.K. and Rotman, B.: J. Mol. Biol. 16 (1966) 42-50.
303. Wilson, D.B.: J. Biol. Chem. 249 (1974) 553-558.
304. Postma, P.W.: J. Bacteriol. 129 (1977) 630-639.
305. Ames, G.F.-L. and Lever, J.: Proc. Nat. Acad. Sci. (USA) 66 (1970) 1096-1103.
306. Ames, G.F.-L. and Spudich, E.H.: Proc. Nat. Acad. Sci. (USA) 73 (1976) 1877-1881.
307. Whipp, M.J. and Pittard, A.J.: J. Bacteriol. 132 (1977) 453-461.
308. Weiner, J.H., Lohmeier, E. and Schryvers, A.: Can. J. Biochem. in press.
309. Kaback, H.R.: J. Cell. Physiol. 89 (1976) 575-593.
310. Lagarde, A.E. and Haddock, B.A.: Biochem. J. 162 (1977) 183-187.
311. Boonstra, J. and Konings, W.N.: Eur. J. Biochem. 78 (1977) 361-368.
312. Ramos, S. and Kaback, H.R.: Biochemistry 16 (1977) 854-859.
313. Rowland, I. and Tristram, H.: J. Bacteriol. 123 (1975) 871-877.
314. Hutson, S.M.: J. Biol. Chem. 252 (1977) 4539-4545.
315. Van Heerikhuzien, H., Kwak, E., Van Bruggen, E.F.J. and Witholt, B.: Biochim. Biophys. Acta 413 (1975) 177-191.





316. Lancaster, Jr., J.R. and Hinkle, P.C.: J. Biol. Chem. 252 (1977) 7657-7661.
317. Silbert, D.F., Cohen, M. and Harder, M.E.: J. Biol. Chem. 247 (1972) 1699-1707.
318. Plate, C.A., Suit, J.L. , Jetten, A.M. and Luria, S.E.: J. Biol. Chem. 249 (1974) 6138-6143.
319. Bachmann, B.J., Low, K.B. and Taylor, A.L.: Bacteriol. Rev. 40 (1976) 116-167.
320. Jenkinson, T.J., Kamat, V.B. and Chapman, D.: Biochim. Biophys. Acta 183 (1969) 427-433.



# APPENDIX 1

## E. coli Strains Employed in this Study

All the four strains listed below are descendants from the ancestral K12 stock (271, 317).

Strain	Relevant Phenotype	Relevant Genotype	Derived from Strain:	Other Information	Reference	Donated by:
K1060	Unsaturated fatty acid auxotroph, <u>fabB</u> genetic locus (see <u>List of Abbreviations</u> ); defective in $\beta$ -oxidation, <u>oldE</u> genetic class (see <u>List of Abbreviations</u> )	$F^-$ <u>B<sub>1</sub></u> <sup>-</sup> <u>lac</u> <sup>C</sup> <u>fabB</u> <sup>-</sup> <u>oldE</u> <sup>-</sup>	K-12Y <sub>mel</sub>		317	Dr. D. Silbert, Washington Univ. School of Med., St. Louis, Missouri, U.S.A.
E15	Prototrophic for fatty acid metabolism; alkaline phosphatase deficient; inducible in <u>glp</u> regulon.	<u>phoA</u> <sup>-</sup> <u>glpF</u> <sup>+</sup> <u>glpK</u> <sup>+</sup> <u>glpT</u> <sup>+</sup> <u>glpA</u> <sup>+</sup> <u>glpD</u> <sup>+</sup> <u>glpR</u> <sup>+</sup>	K12	Re-named Strain 1	271	Dr. J. Weiner, Dept. of Biochemistry, Univ. of Alberta.
7	Prototrophic for fatty acid metabolism; alkaline phosphatase deficient; constitutive in <u>glp</u> regulon.	<u>phoA</u> <sup>-</sup> <u>glpF</u> <sup>+</sup> <u>glpK</u> <sup>+</sup> <u>glpT</u> <sup>+</sup> <u>glpA</u> <sup>+</sup> <u>glpD</u> <sup>+</sup> <u>glpR</u> <sup>-</sup>	E15 (i.e., strain 1)		271	"
K12F <sup>-</sup>	Prototrophic for fatty acid metabolism.	$F^-$	K12			Dr. W. Paranchych, Dept. of Biochem., Univ. of Alberta.



## APPENDIX 2A

Fatty Acid Profiles at Various Growth Phases of Mutant K1060 Cells  
Grown with 18:1c and Glycerol

# of Generations		2.17	3.04	3.91	5.0	
Harvest A <sub>600</sub> *		0.205	≈0.30	0.52	0.90	1.14
16:1c	mole %	1.7	Trace	2.4	Trace	-
18:1c	"	55.8	55.2	49.2	53.5	51.2
Total UFA	"	57.5	55.2	51.6	53.5	51.2
Cp17	"	Trace	-	-	-	-
Cp19	"	1.5	1.2	1.2	1.5	3.1
12:0	"	2.4	2.5	4.0	2.6	2.1
14:0	"	11.0	9.8	10.8	11.4	13.5
16:0	"	22.3	25.5	23.6	26.1	26.3
18:0	"	3.0	3.6	4.8	3.3	2.4
Total Saturates	"	38.7	41.4	43.2	43.4	44.3
16:0/14:0		2.02	2.61	2.19	2.30	1.95
18:1c + Cp19	"	57.3	56.4	50.4	55.0	54.3

\* A<sub>550</sub> ≈ 1.15 × A<sub>600</sub>

Cells of *E. coli* K1060 were grown (as given in Chapter II) in M63 supplemented with 18:1c together with glycerol as carbon and energy source. Cells were harvested at the optical densities (A<sub>600</sub>) indicated. Fatty acid extraction and analysis were carried out as detailed in Chapter II.



## APPENDIX 2B

Fatty Acid Profiles at Various Growth Phases of Mutant  
K1060 Cells Grown with 18:1c and Glucose

# of Generations		2.33	3.49	4.65			
Harvest A <sub>600</sub> *		0.123	0.28	0.62	1.33	1.90	2.42
16:1c	mole %	2.6	-	-	-	-	-
18:1c	"	34.6	31.3	28.0	24.9	23.4	18.3
Total UFA	"	37.2	31.3	28.0	24.9	23.4	18.3
Cp17	"	0.6	0.7	1.0	1.0	1.2	1.3
Cp19	"	0.8	0.7	0.9	0.8	1.8	2.3
12:0	"	2.8	3.3	3.3	4.2	6.3	5.8
14:0	"	16.3	18.1	19.7	21.3	21.6	24.6
16:0	"	38.7	42.1	44.5	44.8	44.8	47.0
18:0	"	2.9	3.0	2.3	2.3	1.0	1.1
Total Saturates	"	60.7	66.5	69.8	72.6	73.7	78.1
16:0/14:0		2.38	2.33	2.26	2.11	2.08	1.94
18:1c + Cp19	"	35.4	32.0	28.9	25.7	25.2	20.6

\*  $A_{550} \approx 1.15 \times A_{600}$

Same as for Appendix 2A except that glucose was used here as carbon and energy source.





## APPENDIX 2C

Fatty Acid Profiles at Various Growth Phases of E. coli  
K1060 Cells Grown with 18:1c and Xylose

Harvest A <sub>600</sub> *		0.103	0.207	0.376	0.70	1.39
16:1c	mole %	-	-	-	Trace	Trace
18:1c	"	57.1	52.6	51.9	48.9	47.8
Total UFA	"	57.1	52.6	51.9	48.9	47.8
Cp17	"	-	-	-	-	0.4
Cp19	"	1.0	-	0.9	1.5	2.9
12:0	"	1.9	1.9	1.3	1.0	0.6
14:0	"	10.1	8.8	7.3	8.0	7.8
16:0	"	26.0	31.1	36.2	38.6	40.2
18:0	"	1.6	2.3	1.1	0.9	-
Total Saturates	"	39.6	44.1	45.9	48.5	48.6
Others (i)	"	-	2.5	1.4	1.2	0.3
(ii)	"	2.7	0.6	-	-	-

\* A<sub>550</sub>  $\approx$  1.15 x A<sub>600</sub>

Same as for Appendix 2A except that xylose was used here as carbon and energy source.



## APPENDIX 2D

Fatty Acid Profiles at Various Growth Phases of Mutant K1060  
Cells Grown with 18:1c and Succinate

Harvest A <sub>600</sub> <sup>*</sup>		0.09	0.117	0.38	0.81	1.23
16:1c	mole %	-	-	-	-	-
18:1c	"	56.5	53.3	50.9	48.5	45.4
Total UFA	"	56.5	53.3	50.9	48.5	45.4
Cp17	"	3.1	2.8	0.5	0.5	0.6
Cp19	"	3.8	4.1	4.7	5.4	7.6
12:0	"	2.0	2.1	1.1	0.7	-
14:0	"	7.1	6.4	5.4	5.3	5.6
16:0	"	27.6	31.4	37.4	39.6	40.7
18:0	"	-	-	-	-	-
Total Saturates	"	36.7	39.9	43.9	45.6	46.3
16:0/14:0		3.91	4.95	6.97	7.52	7.25

<sup>\*</sup>  
A<sub>550</sub> ≈ 1.15 x A<sub>600</sub>

Same as for Appendix 2A except that succinate was used here as carbon and energy source.



## APPENDIX 3

Typical Fatty Acid Profiles of E. coli Strain 7 and Mutant K1060 Used for the Various Experiments

Fatty Acid Composition of Cells (mole %)*													
Culture in M63	UFA supple- ment	Saturated fatty acids				Total satu- rated fatty acids	Unsaturated fatty acids			Cyclo- propane fatty acids			Total UFA + Cp
		12:0	14:0	16:0	18:0		16:1	18:1	18:2	Cp17	Cp19		
K1060/glycerol	18:1t	1.9	19.7	7.8	1.9	31.3	0.1	68.6					68.7
	16:1t	0.4	4.4	10.1	0.3	15.2	83.8	0.8		0.2			84.8
	18:1c	0.5	12.2	25.7	0.4	38.8		57.4			3.9		61.3
	16:1c	0.3	8.9	37.2	0.3	46.7	43.7	0.2		9.5			53.4
	18:2c,c	0.4	10.9	36.7	0.3	48.3	1.1	1.3	48.4	1.0			51.8
Str 7/succinate		0.2	1.8	45.3	1.4	48.7	19.3	26.6		5.1	0.4		51.4

\*K1060 grown on xylose under the same conditions yields similar fatty acid profiles.

Cultures of K1060 with the UFA supplementations indicated and strain 7 without any supplementation were grown in M63. Cells were harvested in the exponential phase and washed and prepared as detailed under Materials and Methods (Chapter II).



## APPENDIX 4

## Calculation of Initial Rate of Transport

(i) The concentration of protein in cells used in any transport experiment was routinely determined with the 1:40 cell suspension, without prior treatment with glucose and chloramphenicol. For transport assay, 500  $\mu$ l of the suspension was first treated with 10  $\mu$ l of 1 M glucose and 20  $\mu$ l of chloramphenicol (2 mg/ml), i.e., a dilution to 500/530 of the protein concentration in the original suspension.

$$\begin{aligned} &\therefore \text{Effective protein concentration of 1:40 suspension used} \\ &\quad \text{for transport assay}^* \\ &= (500/530 \times \text{mg protein/ml of untreated 1:40} \\ &\quad \text{suspension}) \text{mg/ml treated cell suspension} \quad [x] \end{aligned}$$

\* N.B. When a different concentration of cells was used, n had to be multiplied by an appropriate factor to compensate for the dilution.

(ii) 20  $\mu$ l of these treated cells was added to 485  $\mu$ l of radioactive substrate to make a total of 505  $\mu$ l transport assay mixture, out of which a 200  $\mu$ l aliquot was taken and filtered, and radioactivity in the trapped cells counted.

$$\begin{aligned} &\text{Protein concentration in the 200 } \mu\text{l filtered} \\ &= (x/1 \times 20/1000 \times 200/505) \text{mg} \quad [y] \end{aligned}$$

$$\begin{aligned} &\text{(iii) Initial transport rate} \\ &= \left[ \frac{(\text{cpm on LSC}^* \text{ print-out}) - (\text{appropriate control cpm})}{\text{sampling time (sec)}} \right] \text{cpm/sec} \end{aligned}$$





$$= \left[ (\text{cpm/sec}) \times 60 \right] \text{cpm/min}$$

$$= (\text{cpm/sec} \times 60/1 \times 1/y) \text{cpm/mg protein/min}$$

\*LSC = liquid scintillation counter.

If (a) the specific activity of the starting radioisotope solution [assuming 100% counting efficiency (CE), i.e., dpm = cpm] = SA cpm/nmole, and (b) mean counting efficiency for the run calculated from all the substrate concentrations used = (CE)%, then

$$\text{Specific Activity at (CE)\%} = \frac{\text{SA} \times (\text{CE})\%}{100} \text{cpm/nmole}$$

$$\text{Transport initial rate} = \left[ \frac{\text{cpm} \times 60}{\text{sec} \times y} \times \frac{100}{\text{SA} \times (\text{CE})\%} \right] \text{nmole/min/mg of protein.}$$



## APPENDIX 5

Temperature Programs and Instrument Settings Used  
for GLC Analyses of Fatty Acid Methyl Esters

	GLC PROGRAM*	
	1	2
Detector Temperature (°C)	300	300
Injection Port Temperature (°C)	300	300
Range	1000	1000
Attenuation (Not functioning)	1	∞
Noise Suppression	Max	Max
Recorder Presentation	On	On
mV at input for full scale (Log)	1	1
Slope Sensitivity (mv/min)		
Up	0.03	0.01
Down	0.03	0.01
Baseline Reset Delay (sec)	6	4
Area Threshold	100	10
Shoulder Control (mv)		
Front	Off	On
Rear	10	10
Temperature Program		
Temperature 1 (°C)	160	170
Time T <sub>1</sub> (min)	4	4
Rate (degrees/min)	2	2
Temperature 2 (°C)	190	190
Time T <sub>2</sub> (min)	∞	∞

\*Program 1 was used for most of the analyses.

















**B30206**